THE UNIVERSITY OF CHICAGO

CLIMATE CHANGE IMPACTS ON CROP PRODUCTION: ADVANCEMENTS IN FUTURE PROJECTIONS FOR U.S. CORN

A DISSERTATION SUBMITTED TO
THE FACULTY OF THE DIVISION OF THE PHYSICAL SCIENCES
IN CANDIDACY FOR THE DEGREE OF
DOCTOR OF PHILOSOPHY

DEPARTMENT OF THE GEOPHYSICAL SCIENCES

BY
HAYNES FOREST STEPHENS

CHICAGO, ILLINOIS
JUNE 2024

This work is dedicated to Andrea Forest, William H. Stephens, and Amy L. Young

“Who you Move4?” — Nef The Pharoah

TABLE OF CONTENTS

LIST OF FIGURES

LIST OF TABLES

ACKNOWLEDGMENTS

This work was supported by:

- The University of Chicago Center for Robust Decision-making on Climate and Energy Policy (RDCEP) which is funded by NSF grant SES-1463644 through the Decision Making Under Uncertainty program
- The NSF National Research Traineeship program (grant DGE-1735359)

STATEMENT OF ORIGINALITY AND COPYRIGHT ATTRIBUTION

All text and analysis in Chapters 2, 3, 4, and 5 was produced in collaboration with the authors listed at the beginning of each chapter with Haynes Stephens serving as the lead author in each case.

In Chapter 2, Haynes Stephens collaborated in the conceptualization and design of the research with co-authors James Franke and Elisabeth Moyer. Stephens led the performance of the research, conducted the data analysis and project management, and led the writing of the manuscript.

In Chapter 3, Haynes Stephens conceptualized, designed and performed of the research. Stephens conducted the data analysis and project management, and led the writing of the manuscript.

In Chapter 4, Haynes Stephens conceptualized, designed and performed of the research. Stephens conducted the data analysis and project management, and led the writing of the manuscript.

In Chapter 5, Haynes Stephens conceptualized the research. Stephens led the design and performance of the research with co-author Sophia Horigan. Stephens conducted the data analysis and project management, and led the writing of the manuscript.

All figures contained within were produced by Haynes Stephens using data from the publicly available sources listed in each section.

ABSTRACT

Importance: Climate change may put our ability to feed future populations at risk. The prospects of those risks are limited by our understanding of how environmental factors impact crop yields. Present-day correlations of yields with individual factors may involve confounding variables whose relationships shift in future climates. Numerical models of crop yields are built on untested assumptions, and their projected impacts under climate change are not clearly attributed to underlying mechanisms. This dissertation aims to improve our understanding of climate impacts on agriculture through a series of studies that address (1) how yield responses are driven by factors other than temperature, (2) whether assumptions about crop maturities in models are consistent with observations, (3) how crop maturity rates factor into future yield responses, and (4) how changes to soil moisture in future climates affect not only crop yields but the ability of farmers to plant at all.

Approach: This work extracts insight into maize crop production using creative combinations of agricultural models and observational data. Process-based models simulate daily crop growth based on numerical representations of physiological mechanisms, offering a direct link between weather inputs and crop yields. This work both seeks to understand what factors drive yield losses in models and uses those models as sources of synthetic data in "perfect model" experiments to test statistical methods of crop yield prediction. This work makes novel use of observational datasets to investigate whether modeled maturity parameters and responses reflect real-world crop behaviors. Lastly, this work addresses agricultural impacts disregarded in crop yield models, using a machine-learning approach to understand how soil and weather conditions prevent farmers from planting their intended maize crops, and whether prevented planting outcomes might become worse under climate change. This work focuses on the U.S. Corn Belt, the most productive maize region in the world, but results may generalize to other mid-latitude maize regions such as China.

Key Findings: We find that (1) commonly used statistical methods using temperature

variables overproject yield losses under climate change by a factor of two because they omit the changing relationship of humidity and temperature under climate change. Methods using moisture variables produce consistent responses over time, suggesting moisture stress is more relevant than temperature stress in driving yield responses. Process-based models accurately reflect both (2) observed historical maize maturities and (3) the acceleration of maturity rates in warmer temperatures, but are inconsistent in how accelerated maturity impacts yields. Lastly, we find that (4) prevented maize planting is strongly influenced by winter and springtime soil moisture and drainage conditions, and is projected to become less frequent but more severe on average under climate change. Findings from this dissertation highlight the importance of agricultural models accurately reflecting the real-world drivers of crop production and suggest that U.S. maize production may fare better under climate change than previously suspected.

CHAPTER 1

INTRODUCTION

Climate change may put society's ability to feed future populations at risk. As the global population increases to as much as 10.8 billion by 2050 and individual diets become more meat-heavy, a substantial increase in crop production will be required to ensure food security [1]. However, our ability to project future food security suffers from a limited understanding of how future environmental conditions will influence crop production.

Researchers increasingly use agricultural models to better understand the environmental drivers of maize production and future projections. Process-based models predict crop yield outcomes from input weather and management conditions by simulating daily crop growth processes, often tuned using lab or field experiments [2]. These models originated to run crop growth and yield simulations for a single location [3, 4, 5], but advances over the past decade have established parallelized models able to run global gridded simulations. Models in the Agricultural Model Intercomparison and Improvement Project (AgMIP) [6] produced the first ensemble outputs of global gridded crop yield outcomes under controlled climate perturbations, through what is known as the Global Gridded Crop Model Intercomparison (GGCMI) initiative [7]. These outputs are well-suited for comparing behaviors between process-based models. Additionally, such harmonized outputs can be used as synthetic data to train and test statistical methods of crop yield prediction, employing what is referred to as the "perfect model" approach [8]. Statistical models primarily calibrate their yield responses to selected weather variables (typically temperature and precipitation) [9, 10, 11, 12]—if these selected variables do not reflect the underlying crop physiology, then the statistical model's historical responses may inaccurately project yield impacts under climate change scenarios. Evaluating the accuracy of statistical yield projections through the "perfect model" approach can reveal insight as to whether temperature and precipitation variables are directly related to yield responses, or whether other weather variables may be better suited for future

projections.

While process-based models are valuable for numerically representing crop growth responses to environmental factors, they still face challenges in reflecting real-world crop behaviors [13, 14]. Uncertainty in historical and future simulations may be due in part to errors in calibrated parameters related to cultivar maturity, which can significantly affect absolute yield values [15, 16]. Validating the use of these parameters by comparing them to observed crop maturities would help to assess whether model parameterizations reflect real-world conditions.

In contrast to the numerous studies that project how climate change will impact future crop yields, little is known about how it may impact the ability of farmers to plant crops altogether. Since we currently lack a process-based understanding of how extreme moisture conditions might prevent crop planting, two studies have attempted to model environmental impacts on prevented planting through statistical methods [17, 18]. However, studies to date disregard the effects of soil moisture conditions to prevent planting, which qualitative literature suggests could be a key factor. Machine-learning techniques provide an approach to understanding the likely complex and nonlinear effects of soil and weather on prevented planting, akin to their recent momentum in comprehending crop yield responses [19, 20, 21]. They can also project whether climate change conditions may increase the risk to planting practices compared to historical conditions.

The United States plays a key role in global agriculture, particularly for maize. The U.S. is the largest maize producer in the world, growing roughly a third of the global supply [22, 23]. Climate responses to increasing greenhouse gas emissions are projected to cause substantial warming over maize farming regions in the U.S. through the end of the century [24, 25, 26], likely affecting rain and soil conditions as well [27, 28, 29, 30, 31, 32]. Therefore, it is particularly important to understand how such climate change could impact U.S. maize production.

Studying the environmental drivers of U.S. maize production is inherently a geoscience research endeavor. U.S. maize farming spans nearly 40 million hectares [33], covering a range of soil types and hydrological zones including underlying aquifer systems [34]. Maize crops in these regions are directly influenced by environmental conditions, and changes in these conditions under increased carbon levels are determined by geophysical mechanisms [35]. Additionally, just as agriculture is affected by the environment, crop and management processes can also alter surrounding environmental conditions (e.g., soil makeup, temperature, humidity) [36]. Consequently, advances in the understanding of interactions between climate and large-scale agriculture require geoscientific expertise.

Pursuits to the aforementioned research opportunities would allow us to better understand and project food security outcomes under climate change. Here, I conduct four research projects aimed at better understanding how climate change may affect maize agriculture in the U.S. In the first project, I evaluate the projections of statistical crop models using the first ensemble-based "perfect model" approach. In the second project, I validate the use single-year crop calendar to parameterize maize cultivar maturities in process-based models, comparing them to newly available observations. In the third project, I use the newly available observations to evaluate the response of growing periods to temperature and process-based models, assessing the efficacy of simulated growing-period adaptation strategies under climate change. Finally, in the fourth project, I develop a novel machine-learning model to understand how weather soil-hydrology conditions can prohibit farmers from planting maize altogether, damaging food production beyond the metric of harvested yields. Altogether, this dissertation improves the understanding of historical and future climate impacts on U.S. maize production.

CHAPTER 2

STATISTICAL MODELS BASED ON HEAT STRESS OVERPROJECT FUTURE CLIMATE DAMAGES TO CROP YIELDS

Haynes Stephens[1,2], Jonathan Proctor[3], Christoph Müller[4], Katherine P. Dixon[5], María D. Hernández Limón[1], Harshil Sahai[6], James A. Franke[7], Jonas Jägermeyr[8,9], Alex C. Ruane[8], and Elisabeth Moyer[1,2]

[1]Department of Geophysical Sciences, University of Chicago, Chicago, IL, USA [2]Center for Robust Decision-making on Climate and Energy Policy (RDCEP), University of Chicago, Chicago, IL, USA [3]University of British Columbia Faculty of Land and Food Systems, Vancouver, BC, Canada [4]Potsdam Institute for Climate Impacts Research (PIK), Member of the Leibniz Association, Potsdam, Germany [5]Department of Ecology and Evolution, University of Chicago, Chicago, IL, USA [6]Department of Economics, University of Chicago, Chicago, IL, USA [7]Toyota Technical Institute at Chicago, Chicago, IL, USA [8]NASA Goddard Institute for Space Studies, New York, NY, USA [9]Columbia Climate School Center for Climate Systems Research, New York, NY, USA

2.1 Abstract

Training statistical models on historical yield and weather data and then applying them to future climates is a popular approach for projecting how climate change will influence agricultural productivity. However, future projections may inaccurate if the selected weather variables do not directly relate to underlying crop yield responses, and evaluating the accuracy of such projections is complicated by the fact that future yields are not observable. Here, we evaluate the ability of such statistical models to project the impacts of climate change on crop yields using a "perfect model" approach, whereby each model is trained on historical yields simulated by a process-based crop model and then evaluated on its ability to reproduce simulated future yields under climate change. Using an ensemble of process-based crop models, we find that statistical models based temperature and precipitation, commonly used in recent literature, overproject yield damages from climate change by roughly a factor of two. Statistical models including features of temperature exposure conflate heat- and

moisture-related damages due to a strong historical association between hot and dry conditions. However, this association weakens as the climate warms, leading the historically trained models to overstate damages from high-temperature under warmer climate states. Statistical models based on moisture stresses (atmospheric or soil) show more accurate projections under climate warming, despite having lower historical goodness-of-fits relative to temperature-precipitation models. Our results highlight the importance of understanding and modeling the direct drivers of yields rather than their proxies for making accurate projections under climate change.

2.2 Introduction

Climate change may lead to large negative socio-economic impacts [37], with food security a particular area of concern [38, 39, 40]. Statistical crop models have been increasingly used, along with process-based models, to project climate change impacts on agricultural productivity.

Statistical crop modeling originated in the early twentieth century with the development of linear regressions to predict hindcasts of yield records based on changes in temperature and precipitation [41, 42, 43, 44]. A hundred years later, linear models similar to their predecessors were used to project future climate impacts in high-impact studies [45, 9].

Recent advances have allowed statistical models to capture nonlinear relationships between environmental variables and crop yield, uncovering a particularly strong and nonlinear relationship for temperature that projects severe yield damages under climate change [10, 46, 47, 48, 49, 50, 51, 52, 53, 54]. Statistical model development has also focused on better capturing the physical drivers of crop yield by modeling soil moisture (SM) supply [55, 56] and 'vapor pressure deficit' (VPD), a measure of atmospheric moisture demand based on temperature and humidity [57, 20, 58]. Importantly, these moisture-based models tend to project less yield damages from climate change than models based on temperature and

precipitation, both in the U.S. [55] and globally [56]. However, it is unclear which model projections are more accurate.

The differences in projected yield damages under climate change across statistical models raise the question: how does one select which model to use for projecting future yield impacts? A common approach is to select models based on their ability to reproduce historical data, which is often implemented by evaluating predictions of yields in years or locations held out during training [58, 56, 59]. However, it is possible that a model's predictive performance within historical climates may not indicate its accuracy in predicting yield impacts from climatic changes [60, 61]. Some environmental variables may correlate well with historical yield anomalies, serving as proxies for the true set of complex environmental determinants of yield. However, if correlations between environmental variables shift under climate change [62, 63], historically effective proxies may become ill-suited for future projections.

Because future yields under climate change are not observed, evaluating the accuracy of a statistical crop model's projections poses a serious challenge. To address this challenge, Lobell & Burke (2010) proposed a "perfect model" approach [8] wherein a statistical model is trained on historical yields simulated by a process-based model, and then tested on its ability to reproduce future yields simulated by the same process-based model. Process-based models provide a useful reference target because they are based on processes of crop growth that have been developed and validated by field and laboratory experiments [2, 64, 12, 65]. Moreover, the "perfect model" approach does not depend on the process-based model being exactly perfect, so long as its underlying processes are reasonable and consistent between historical and future contexts [8]. Inability of a statistical model to reproduce future target yields would result in projection error, signifying the statistical model's failure to capture the relevant yield responses to climate change as represented in the process-based model. Importantly, the "perfect model" approach is useful for identifying key environmental variables the statistical models may be missing. More broadly, this approach is useful for analyzing the assumptions

and limitations of both statistical and process-based models.

The "perfect model" approach in this context differs from studies that compare general projections between process-based models and statistical models [12, 64, 66], as those statistical models are trained on observations and therefore lack known future yield targets to evaluate projection accuracy. This approach also differs contextually from studies that create statistical emulators of process-based models by training them on one ESM-based scenario and testing them on another [67, 68]—these studies include both historical and future simulated yields in their training sets.

Lobell & Burke (2010) used a "perfect model" approach to evaluate statistical models based on growing-season aggregates of mean temperature and total precipitation, finding little bias in model projections under a low uniform-warming (+2 °C) scenario [8]. In a follow-up study, Holzkämper et al. (2012) evaluated statistical models using features of temperature, precipitation, sunlight, and reference evapotranspiration, with different model variations aggregating features at different timescales (monthly to growing-season) [69]. Holzkämper et al. (2012) found that the statistical models were able to provide good predictions of impacts under a moderate uniform-warming (+4 °C) scenario based on Spearman's rank correlation metrics. However, limitations of these studies leave key gaps in the knowledge of statistical model projections under climate change. First, neither study evaluated more recent statistical model structures based on nonlinear responses to daily temperature and precipitation exposure (hereafter referred to as TP models), nor did they evaluate moisture-based models. Second, both studies drove their models using synthetic weather inputs and uniform warming scenarios, possibly missing the yield impacts of coupled heat-moisture exposure in observations and the potential shift in that coupling under emissions-driven climate change. Third, each study looked at a single process-based model, which may be unrepresentative of the emergent behavior across an ensemble of models. Advances in statistical and process-based modeling practices today allow us to address these knowledge gaps.

Here, use a "perfect model" approach to evaluate the abilities of TP and moisture-based statistical models to project yield impacts under climate change. The TP model uses a piecewise linear response to daily temperature accumulation and a quadratic response to daily precipitation, and the moisture-based models use various nonlinear and interacted responses to daily atmospheric moisture stress and growing-season soil moisture supply [similar to ref. 58, further information and equations are shown in Methods]. We focus on rainfed maize yields in the U.S. Corn Belt, a globally crucial agricultural region frequently studied through statistical models [10, 12, 51] but not yet investigated using a "perfect model" approach. We test each of the statistical models under uniform warming scenarios (up to +6 °C), as well as under a high-greenhouse-gas emissions scenario (RCP8.5) simulated by the HadGEM2-ES earth system model [ESM, 70]. Simulated yield datasets are taken from an ensemble of seven process-based maize models in the Global Gridded Crop Model Intercomparison (GGCMI) project [14], each with a unique and internally consistent representation of maize physiology (e.g. phenology, photosynthesis, carbon allocation). Historical yield simulations in each process-based model are driven by daily climate forcings from the AgMERRA ("agricultural"-modified Modern-Era Retrospective analysis for Research and Applications) dataset, which combines reanalysis data and weather observations.

The goal of this exercise is to address the following questions: 1) Do commonly used TP models accurately project the influence of climate change on U.S. crop yield? 2) If not, why? 3) Do moisture-based models produce more accurate projections? To answer these questions, we train statistical models on historical simulations and evaluate their projections under climate change scenarios. Collectively our findings inform projections of how climate change will impact agricultural productivity, with important implications for food security..

2.3 Data and Methods

2.3.1 Data

We use a dataset of gridded, process-based maize simulations from the GGCMI Phase 2 Experiment models [14]. Process-based models simulate daily and sub-daily growth processes from planting to maturity on a 0.5° x 0.5° global grid. Simulations are run using inputs of weather data, soil characteristics, and management parameters. We focus on rainfed maize yields within the boundaries of twelve states of the U.S. Corn Belt (North Dakota, South Dakota, Illinois, Indiana, Iowa, Kansas, Michigan, Minnesota, Missouri, Nebraska, Ohio, and Wisconsin). All simulations include a uniform Nitrogen application of 200 kg N/ha.

We exclude simulated yield outputs less than 0.1 ton/ha or that occur on grid cells with less than 10% reported harvesting area for rainfed maize; gridded harvest areas are taken from the MIRCA2000 (Monthly Irrigated and Rainfed Crop Areas around the year 2000) dataset [71]. We further exclude any outputs with a reported planting date or maturation length of 0, indicating an error in the simulated grid cell for a given year.

For the uniform warming scenarios, we select yield outputs from the seven process-based models (CARAIB, EPIC-TAMU, GEPIC, LPJ-GUESS, LPJmL, pDSSAT, PEPIC) whose historical simulations are driven by the same weather input, the AgMIP climate forcing data set based on the NASA Modern-Era Retrospective Analysis for Research and Applications [AgMERRA, 72]. Forcings include daily air temperature (maximum, minimum, average), precipitation, relative humidity, wind speed, and solar radiation; the set of input forcings considered varies by the specific data needs of each process-based crop model. Historical simulations cover the period 1981–2010. Additional historical simulations are run under fully irrigated conditions; we use these to determine water sensitivity in the process-based models. Uniform warming scenarios are created by increasing each daily temperature value by the indicated perturbation (+2, +4, or +6 °C) while holding all other weather conditions

fixed. Additional simulations are ran under the +6 °C perturbation where maize cultivars are adapted to counteract the shortening of growing periods under increased temperatures; we use these to determine yield sensitivity to growing period in the process-based models. We only include grid cells in the Corn Belt with 20+ years of valid yield outputs in the historical scenario, as well as 20+ years of valid outputs in each uniform warming scenario.

To determine water sensitivity in the process-based models, we compare simulated yields under historical conditions between rainfed and fully irrigated conditions. Fully irrigated conditions in this context fulfills all water requirements for the crop regardless of local water supply limitations [14], effectively eliminating water stress. For each process-based model, we calculate the mean yield change when switching all crops in the region from rainfed to fully irrigated conditions, serving as a measures of water sensitivity.

For the ESM-based climate scenario, simulated yields are only available by the LPJmL process-based model. Historical and future daily weather conditions are simulated by the HadGEM2-ES Earth System model [70], which is bias-adjusted to match observed mean annual temperatures and interpolated to a 0.5° x 0.5° resolution by ISIMIP [73]. Historical forcing exists for the period 1951–2014 and future conditions (2015–2099) are simulated under a high-emissions scenario following the Representative Concentration Pathway (RCP) 8.5 forcing. We use the period 1981–2010 to train statisical models, and test projections on the period 2011–2099, to be consistent with the approach under uniform warming scenarios. We only include grid cells in the Corn Belt with 20+ years of valid yield outputs in each thirty-year interval of the total period (i.e. 1981—2010, 2011–2040, 2041–2070, 2071–2099).

2.3.2 Statistical crop models

We use a statistical panel model based on temperature and precipitation, which we refer to as the TP model. The model has a piecewise linear yield response to daily temperature accumulation, based on the concept of growing-degree days (GDD) and high-degree days

(HDDs), two temperature ranges thought to have beneficial and harmful effects, respectively. We construct the GDD and HDD features according to the standard approach of previous literature [10, 12], with GDD defined as:

$$GDD = \int_{\text{Mar. } 1}^{\text{Aug. } 31} \min\{T - 10, 19\}\phi(T \mid T > 10)dT \tag{2.1}$$

where $\phi(T|T > 10)$ is the estimated hourly time series of temperatures, conditional on $T > 10$ (ultimately measured in days). Hourly temperature time series are constructed analogously to the literature [74, 10, 12, 51], where daily max and min temperatures are interpolated into hourly sinusoidal shapes, with each day's max temperature occurring at noon and min temperature occurring at midnight. These hourly time series are then aggregated across the defined growing seasons Mar. 1–Aug. 31 for each feature's temperature range. The HDD feature is defined as:

$$HDD = \int_{\text{Mar. } 1}^{\text{Aug. } 31} (T - 29)\phi(T \mid T > 29)dT. \tag{2.2}$$

The statistical model also has a quadratic response to daily precipitation values. In all, the TP model can be written as:

$$\log(Y_{i,t}) \ = \alpha_i + \beta_{GDD} \cdot GDD_{i,t} + \beta_{HDD} \cdot HDD_{i,t} + \beta_P \cdot P_{i,t} + \beta_{P^2} \cdot P_{i,t}^2 + \epsilon_{i,t}. \tag{2.3}$$

We also consider a cross-sectional TP model that trains on spatial variations in yield and weather conditions for the mean historical growing seasons.

We consider a cross-sectional version of the TP model, where independent and dependent variables are calculated using the historical mean in each location, and can be written as:

$$\log(\overline{Y}_i) \ = \beta_{GDD} \cdot \overline{GDD}_i + \beta_{HDD} \cdot \overline{HDD}_i + \beta_P \cdot \overline{P}_i + \beta_{P^2} \cdot \overline{P^2}_i + \epsilon_i. \tag{2.4}$$

To consider the robustness of results across functional forms, we use a similar TP model with a stepwise response to daily binned temperature exposure. We construct the binned temperature features (ϕ) across three-degree intervals according to the standard approach of previous literature [10, 51]. This model can be written as:

$$log(Y_{i,t}) = \alpha_i + \sum_{h=0,3,6,...}^{39} \beta_h[\phi_{i,t}(h+3) - \phi_{i,t}(h)] + \beta_P \cdot P_{i,t} + \beta_{P^2} \cdot P_{i,t}^2 + \epsilon_{i,t}, \quad (2.5)$$

where $\phi(h)$ is the cumulative distribution function of days during the growing season spent at temperature h.

We also use multiple models based on features of atmospheric moisture demand and soil moisture supply, which we refer to as moisture-based models. Daily vapor-pressure deficit (VPD) is calculated from temperature and relative humidity conditions in the repsective weather data according to the Clausius–Clapeyron relation,

$$VPD = e_0 * e^{((L_v/R_v)*((1/T_0)-(1/T)))} * (1 - (RH/100)), \quad (2.6)$$

where $e_0 = 0.611$ kPa, $T0 = 273.15$ K, $Lv = 2.5e6$ J/kg, and $Rv = 461$ J/(kg K), T is the daily average air temperature, and RH is the daily average relative humidity. Soil moisture supply (SM) is output by the LPJmL process-based model as growing-season totals, in units of either mm/yr or kg/m^3/yr. We use two separate statitical models with quadratic responses to VPD and SM, respectively. Additionally, we use an interacted VPD-SM response inspired by the literature [58], where VPD and SM values are binned by terciles of their respective historical ranges in the region. This model can be written as

$$log(Y_{i,t}) = \alpha_i + \sum_{j=1}^{3}\sum_{k=1}^{3} \beta_{j,k} VPD_{i,t}(j)\, SM_{i,t}(k) + \epsilon_{i,t}, \quad (2.7)$$

where $VPD_{i,t}(j)$ is the exposure in the j^{th} VPD tercile and $SM_{i,t}(k)$ is the supply in the

k^{th} SM tercile.

For each process-based simulation, a separate statistical model is trained on the historical scenario (1981-2010) of the corresponding uniform warming or ESM-based climate scenarios. We exclude linear or quadratic time trends in all statistical models, unlike previous model studies using real-world observations [10, 12, 75], because there are no apparent trends in the simulated historical yields or their input weather conditions. Model training and prediction is executed using the FIXEST R package [76].

2.4 Results

2.4.1 Statistical models based on temperature and precipitation overproject yield damages under climate change

We find that statistical TP models overestimate climate impacts on maize in the U.S. Corn Belt by roughly a factor of two (Figure 2.1). Under a uniform warming scenario of +6 °C, these statistical models project yield losses of -59% on average, consistent with prior analyses using models trained on county-level yield observations [10] The statistical models also show high proficiency in predicting historical yield anomalies (within R^2=0.49 for the ensemble mean). However, target yield losses in the simulations are only -31% under the +6 °C scenario. Over-projection of yield damages scales roughly proportionately with mean temperature increases.

Our main finding is robust across the ensemble of process-based yield models used for training and testing, with statistical TP models over-projecting yield losses by factors of 1.8–2.9 for five out of the seven simulated yield datasets (CARAIB, EPIC-TAMU, GEPIC, LPJmL, PEPIC, Figure S1). For the other two simulated yield datasets (LPJ-GUESS, pDSSAT), the statistical TP models project impacts accurately relative to the target losses; we examine these cases further in the Discussion. We find the same results using a statistical

model with a stepwise yield response to temperature (Figure S2). Our main finding also holds when using weather data from climate model simulations following RCP 8.5 rather than a uniform warming scenario (Figure 2.1b, simulated dataset only available for LPJmL), indicating that the causes of projection-error under emissions-driven climate change are similar to those in the uniform warming scenarios.

Going forward, we focus on results using a piecewise linear TP model trained and tested on simulated yields for LPJmL. This statistical model accurately captures the ensemble mean behavior in uniform warming scenarios (Figure 2.1a) and facilitates a consistent comparison between uniform warming and ESM-based climate scenarios.

The spatial pattern of mean projection error under the +6 °C scenario (Figure 2.1a, inset) resembles the corresponding increase in high-degree days (HDDs, Figure S4, $r = -0.93$, $p < 0.001$). This suggests that the statistical model's over-projected yield losses are related to its treatment of high-temperature impacts—a hypothesis we explore further below. The spatial similarity between projection error and HDD changes is less distinct in the ESM climate scenario (Figure 2.1b, inset map), likely due to colder areas warming relatively more and the inclusion of precipitation changes (Figure S3, bottom center).

2.4.2 The association between yield losses and high temperatures shifts under climate change

For a statistical model to produce accurate long-term projections, its estimated response to historical weather shocks must be consistent with how yields change under longer-term climate change. We find that yield responses to temperature do not meet this criterion. To illustrate how statistical yield responses to temperature change under different climate states, we train separate statistical models on the simulated yields in each uniform warming scenario (Figure 2.2).

The statistical TP model trained on simulated yield variation within the historical sce-

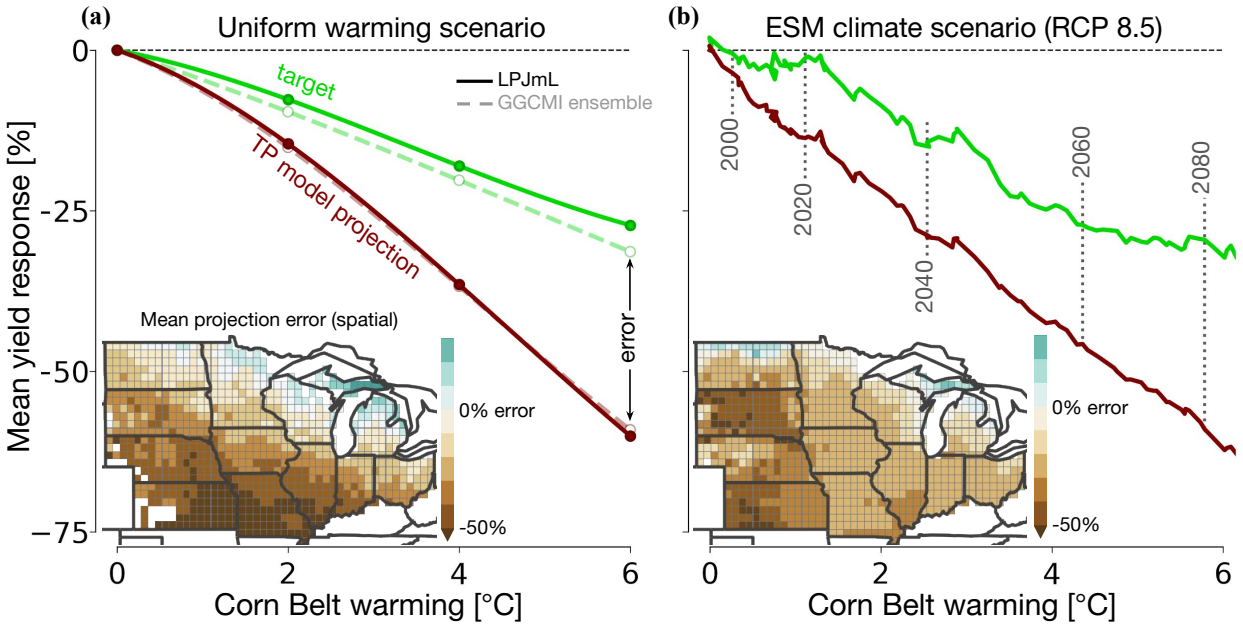

Figure 2.1: Target yield responses and statistical model yield projections under warming scenarios. **(a)** Line plots show mean yield change against increases in growing-season mean temperature under uniform warming scenarios. The solid green line represents the target response of simulated yields by the LPJmL process-based model. The solid blue line represents the projection of a TP statistical model trained on historical weather and simulated yields, intended to reproduce the target response. Dashed colored lines show the mean target response of simulated yields in the GGCMI ensemble (including LPJmL) and the mean projection of the corresponding TP statistical models. The inset map shows the spatial pattern of mean projection error (difference between projection and target responses) under the +6 °C uniform warming scenario; grid cells colored light green or brown indicate positive or negative error, respectively. **(b)** Mean yield changes in the same fashion as (a) under the ESM-based scenario, where historical and future weather inputs are taken from the HadGEM2-ES earth system model under a high-greenhouse-gas emissions scenario (RCP8.5). Simulated yields are only available by the LPJmL process-based model. Vertical dotted lines denote the warming at vicennial markers. The inset map, in the same fashion as the inset map of (a), shows the spatial pattern of mean projection error in the period 2067–2096, when mean growing-season temperatures increase by roughly +6 °C. TP statistical models trained on historical variations overproject yield losses under climate warming by roughly double.

nario shows a similar response to prior analyses of county-level yield observations [10, Figure 2.2a], indicating yield losses of -6.7% under 24-hour exposure to 39 °C relative to 29 °C. However, a statistical model trained on variation within the +6 °C scenario is notably less sensitive to high temperatures, indicating yield losses of -3.4% for the same exposure. Furthermore, a statistical model trained on variations across all warming scenarios (i.e., pooling data from the +0 °C, +2 °C, +4 °C, and +6 °C experiments) indicates yield losses of -

2.4% for the same exposure. We find similar results in the ensemble mean responses across process-based crop models (Figure S7). These results demonstrate a type of Simpson's Paradox, where the relationship between yields and HDDs across climate states is less sensitive than the respective relationships within individual states (Figure 2.3a). This behavior appears in most of the simulated yield datasets in our study (Figure S8). The statistical model trained pooling data across climate states can accurately project yield impacts under climate change (Figure S6); however, such a model cannot be estimated when limited to using historical data.

While yield responses estimated from historic interannual temperature and precipitation variations within locations lead to overprojected yield damages under climate warming, yield responses estimated from variations in mean conditions across space can more accurately project changes in yields under climate change (Figure 2.4a, cross-sectional model described in Methods). A similar result is found for a cross-sectional model under the ESM-climate scenario (Figure S12). However, cross-sectional models in both scenarios still show some error in projections relative to the realized simulated yield losses. Though diminished sensitivity to longer-run changes in temperature is often interpreted as evidence of farmer adaptation [77], that cannot be the case in this setting because management practices are held fixed across all scenarios. Rather, lesser yield sensitivity to temperature across changing climate states indicates that temperature may not be a direct determinant of yields, but rather a proxy thereof, whose effectiveness wanes as the climate warms.

2.4.3 Statistical models based on atmospheric and soil moisture stresses project yield losses more accurately under climate change

Following the suggested importance of atmospheric moisture demand (i.e. vapor pressure deficit, VPD) and soil moisture supply to crop yields in recent literature [57, 20, 58, 56], we explore the associations between yields, HDDs, and moisture stresses across the warming

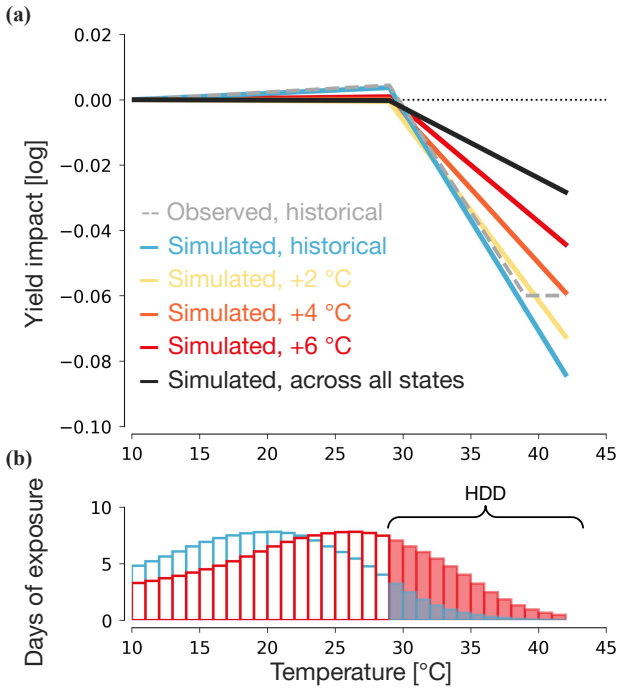

Figure 2.2: Statistical yield responses to temperature under warming climate conditions. **(a)** Line plots show the yield responses to 24-hour exposure at each one-degree temperature interval. The solid blue line corresponds to the piecewise response of a TP statistical model trained on simulated yield variations within the historical scenario (+0 °C). The dashed gray line corresponds to the response of a similar TP statistical model from the literature trained on observed U.S. maize yield variations within historical conditions [10], for comparison; note that this model is slightly different in its flattened response for temperatures above 39 °C. Solid lines of yellow, orange, and red correspond to the responses of TP statistical models trained on simulated yield variations within the +2 °C, +4 °C, and +6 °C climate states, respectively. The solid black line corresponds to the response of a TP statistical model trained on simulated yield variations *across* all climate states (+0, +2, +4, and +6 °C). **(b)** Histograms show hourly temperature exposure during the growing season, normalized to days, in the U.S. Corn Belt for historical (blue) and +6 °C uniform warming (red) scenarios. The distribution of solid bars corresponds to severe heat exposure above 29 °C, aligned with the hinge point of the piecewise linear response function. The historical yield responses are similar between a model trained on observed yields and a model trained on simulated yields. However, the yield response in the +6 °C scenario (for simulated yields) is notably less sensitive to severe heat. The climatological response, needed to reproduce target yield losses under warming (Figure S6), is less sensitive than the interannual response at any given warming level.

scenarios.

Similarly to crop yields, extreme VPD values are strongly associated with severe heat exposure in the historical climate (Figure 2.3b). Also, this historical VPD-HDD association is stronger than the association across climate states. As VPD is a function of temperature

and relative humidity [78], this discrepancy results from a changing temperature-humidity correlation, where HDDs in the warmer climate are associated with less VPD than historical relationships suggest. This changing correlation occurs by design in a uniform warming scenario (relative humidity is held fixed) but also occurs in the ESM climate scenario, where future changes in humidity are proportionally small relative to HDD (SI Figure S10).

Unlike the yield-HDD relationship, the yield-VPD relationship within the historical climate is similar to the relationship across climate states (Figure 2.3c, see SI Figure S9 for all ensemble members). These results suggest that VPD is a more mechanistically relevant factor than temperature exposure for yield loss under climate warming in process-based crop models. We find similar results for the yield relationship to soil moisture supply (Figure S11).

Motivated by the similarities in yield-moisture relationships between historical and climate states, we test the performance of moisture-based models through the "perfect model" approach. We find that moisture-based models consistently project yield impacts more accurately than TP models relative to the target yield losses (Figure 2.4, functional forms described in Methods and Section S1.1). A statistical model using an interactive yield response to atmospheric moisture demand and soil moisture supply projects yield losses most accurately under climate change (solid black line in Figure 2.4), consistent with recent empirical findings highlighting the importance of these interactions [58]. Notably, statistical models using a temperature response in tandem with features of VPD or soil moisture supply still overproject yield losses. This suggests that the inclusion of temperature features dominates the statistical models' historical yield responses and, consequently, their climate change projections.

We find that moisture-based statistical models (excluding temperature responses) project impacts under uniform warming scenarios more accurately than TP models despite having less explanatory power within the historical climate (Table 2.1). Temperature features may

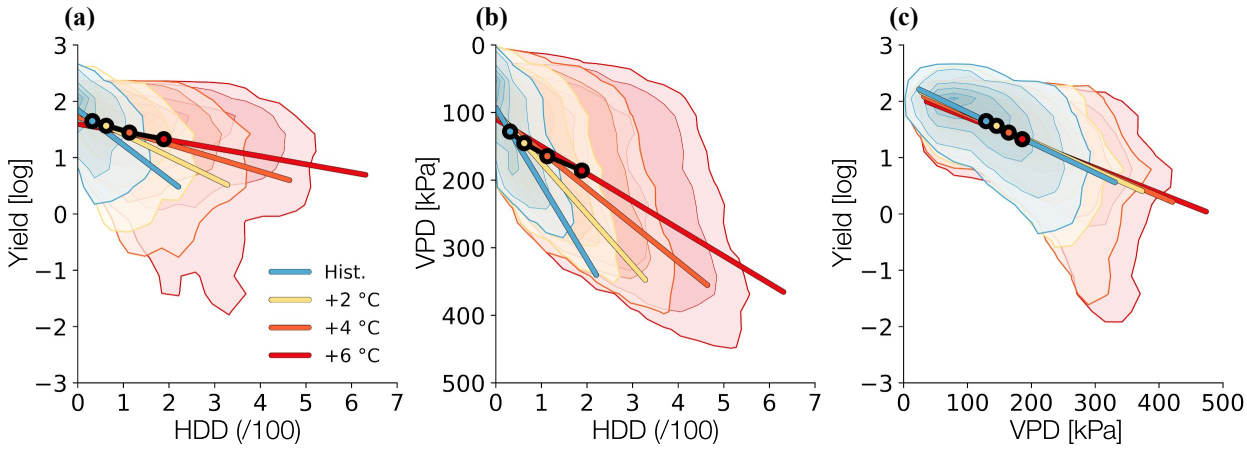

Figure 2.3: Associations between yield, severe heat, and atmospheric moisture demand under uniform warming scenarios. **(a)** Blue contours represent the historical distribution of annual simulated maize yields (by LPJmL) and growing-season HDDs in the U.S. Corn Belt; changing colors indicate distributions for the +2 °C (yellow), +4 °C (orange), and +6 °C (red) warming scenarios. Contour lines in each scenario indicate the 1%, 5%, 25%, 50%, 75%, 95%, and 99% probability values based on a normalized kernel density estimate. Colored straight lines show the linear relationship within each warming scenario. Colored dots with black outlines show the mean yield and HDD values in each scenario, with the solid black line connecting mean values as a representation of the association across climate states. **(b)** Contour plots in the same format as (a) shown for (b) distributions of annual HDD values and growing-season total VPD, a measure of atmospheric moisture demand, and. **(c)** distributions of annual simulated maize yields and growing-season total VPD. The extrapolation of a historical yield-HDD association incorrectly projects how yields change under warming, esimating that future hot years would have greater yield damages than they actually do. This changing association suggests that high temperatures are not a primary driver of yield losses under climate change, but a hisotrical proxy whose effectiveness wanes with warming. Yield-VPD associations are similar between historical and climate states, indicating that VPD may be a more direct driver, and subsequently more appropriate for future projections.

serve as a viable proxy for the complex interactions determining historical yield variations due to the strong association of hot and dry conditions during years of minimal yields. However, the viability of this proxy does not hold fixed into the future, suggesting that historical proficiency is not always indicative of accurate projections under climate change and emphasizing the importance of developing *causal*, rather than simply *predictive*, models in situations where distributional shifts occur.

Consistent with our result that moisture-based models project more accurate yield losses than TP models, we look across our ensemble and find that the overprojection of heat dam-

ages under climate change is associated with the underlying process-based model's water sensitivity (Figure 2.4b). We assess water sensitivity by calculating the yield benefits between irrigated and rainfed conditions, and determine the overestimation of heat-related yield damages by calculating the ratio of yield-HDD sensitivities (linear slopes) between historical and climate states. This finding suggests that it is confounding of temperature and moisture stress that is driving the overprojection by TP models.

Discussion

To project accurate climate change impacts, statistical crop models should use features representing the direct environmental drivers of yields. However, what the direct drivers of yield are remains an open question in the literature, making model selection a challenge. Some features may serve as effective proxies of these drivers due to a strong historical coupling. However, climate change may alter this coupling, rendering a historically strong proxy ill-suited for future projections.

The "perfect model" approach is a promising way to evaluate the ability of statistical crop models to project accurate climate change impacts. Models have been typically evalu-

Model	Within R^2 (historical)	Yield change [%] (+6 °C)
Simulation "ground truth"	**n/a**	**-27**
Temperature, precipitation (TP)	0.51 (± 0.00)	-61
Soil moisture (SM) supply	0.30 (± 0.00)	-35
VPD	0.28 (± 0.00)	-25
SM, VPD (interacted)	0.28 (± 0.00)	-28

Table 2.1: Comparison of model historical performances and climate change projections. Simulated yields are used in effect as "ground truth" to evaluate statistical model projections. TP corresponds to the statistical model with piecewise linear yield response to temperature. SM corresponds to the statistical model with quadratic yield response to growing-season total moisture supply. VPD corresponds to the statistical model with quadratic yield response to daily atmospheric moisture demand (VPD). SM, VPD corresponds to the statistical model with an interacted yield response to binned SM and VPD exposure (terciles).

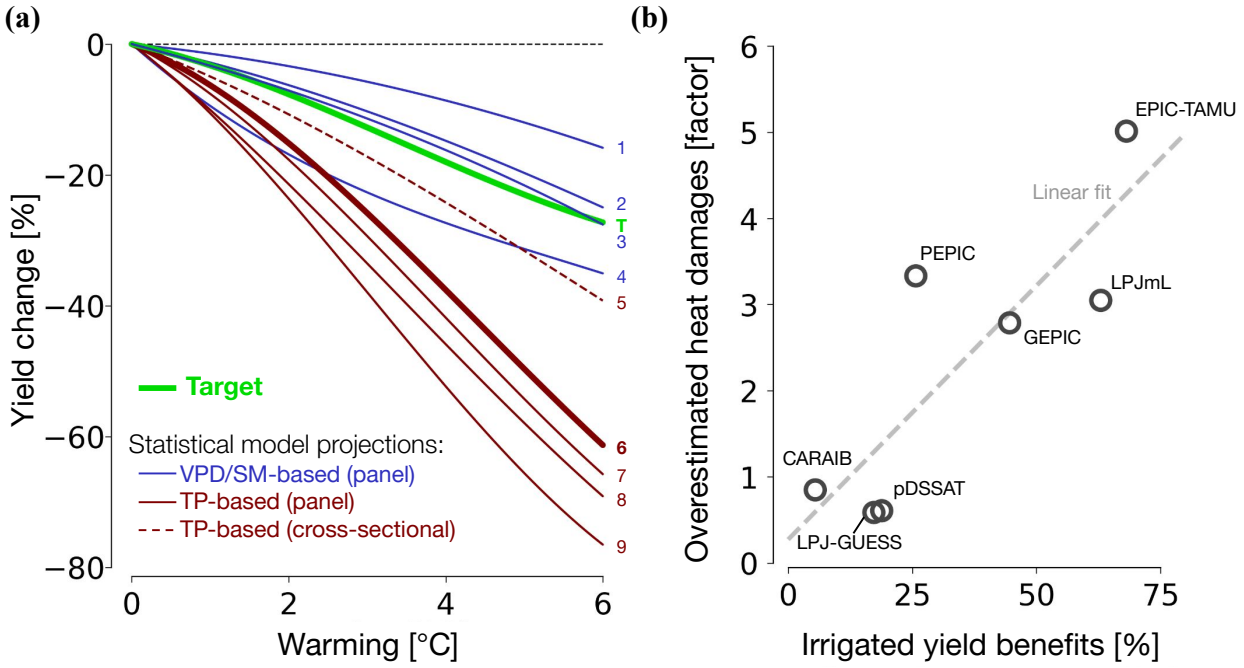

Figure 2.4: Investigating the influence of water sensitivity on statistical model projection error. **(a)** Line plots show the target yield projection for simulated yield by LPJmL under uniform warming (green), along with projections for various statistical models. Line number 6 represents projections from the historically trained TP statistical model, in the same fashion as Figure 2.1a. Line number 5 represents projections from a cross-sectional TP statistical model. Line number 3 represents projections from a panel statistical model using an interactive SM-VPD response. All other lines are described in the Supplement. **(b)** Scatter plot shows overstimated HDD damages, defined as the ratio of linear associations between the historical and climatological timescales (taken from Figure 2.3a), plotted against underlying water sensitivity in the simulated yields, defined as the yield increase (%) due to switching from rainfed to irrigated crop management under historical conditions. The dashed gray line shows a linear fit to the scatter points. Statistical models based on atmospheric moisture demand and/or soil moisture supply project yield losses under warming more accurately than TP-based models. However, this is dependent on the underlying water sensitivity of the simulated yields, where greater water sensitivity is associated with greater projection error by the TP statistical models.

ated and selected based on their historical goodness-of-fit [56, 58, 59]. The "perfect model" approach can add additional insight. From our use of the approach, we find that commonly used statistical models based on temperature and precipitation have high historical goodness-of-fits but substantially overproject yield damages under climate change. We also find that models based on atmospheric moisture demand and/or soil moisture supply project yield losses under climate change more accurately, despite having lower goodness-of-fits in

historical data.

For two out of seven of the simulated yield datasets in our study—pDSSAT and LPJ-GUESS—the corresponding statistical models project impacts accurately relative to the target losses. Upon further investigation, we find these two models to be particularly sensitive to yield losses caused by accelerated maturity under warming (Figure S13). The sensitivity of these two models to accelerated maturity dominates their yield changes under warming, leaving them relatively insensitive to water stresses. Because the temperature responses of TP models in our study are based on heat accumulation, they effectively serve as a proxy for accelerated maturity. This difference across process-based crop models highlights the importance—for both process-based and statistical crop modelling communities—of determining and modeling the true climatological drivers of yield. The efficacy of projecting future yields with a TP statistical model may therefore depend on the extent to which climatic yield losses in the real world are driven by accelerated maturity versus moisture stress.

Our finding that TP models overproject climate change damages to yields contrasts with that of Lobell & Burke (2010) who find that statistical TP models based on growing-season temperature and precipitation generally project accurate impacts under low-warming (+2 °C) scenarios. However, Lobell & Burke used simulated yields from only a single process-based model—CERES-Maize [3]—which is a predecessor to the pDSSAT maize model used in our ensemble [79]. For the case of pDSSAT in our study, the simulated yield impacts and corresponding statistical model projections under uniform warming of +2 °C are nearly identical to results in Lobell & Burke (Figure S1). However, the results from pDSSAT are an outlier in our ensemble of models, for the reasons discussed above. This difference in findings highlights the value of our ensemble approach.

The "perfect model" approach evaluates how well statistical crop models capture the physiological mechanisms in process-based models relevant to climate change [8]. Consequently, the degree to which our results reflect statistical model accuracy in real-world future pro-

jections depends on how well process-based models represent true crop physiology. While process-based models have been designed to accurately represent crop physiology, they have known issues, such as challenges reproducing historical yield records [13] and minimizing adverse yield effects from excess precipitation [80, 81], and are also subject to uncertainty in their climate change projections [81]. It is possible that a statistical crop could perform better or worse in capturing process-based yield responses to climate change than it does in capturing real-world yield responses.

Despite potential limitations, the "perfect model" approach still serves as a useful tool when analyzing statistical crop models. Process-based crop models include detailed representations of crop growth and management processes, with physiological mechanisms founded in agronomic experiments and management parameters (e.g. planting, harvesting, cultivar choice) often tuned to real-world observations [82, 83]. Furthermore, the importance of moisture stress to yield responses aligns with recent findings from the statistical modeling literature [84, 58, 78, 85, 57, 56] rooted in real-world data, supporting the findings of our study.

Further research to advance the "perfect model" approach could improve the evaluation of statistical crop model projections under climate change by expanding the analysis of this study to other key crops and agricultural regions [40, 86], shedding light on the consistency of findings in our study. Additionally, evaluating the ability of other models to project crop yields under climate change, such as a long-difference regression [77] or cutting-edge machine-learning algorithms [19, 87, 88, 89, 48, 90] could be key to guiding the field forward.

Our study highlights the importance of considering moisture effects in physiological responses under climate change, with application beyond crop yield impacts. For example, recent statistical modeling research highlights the effects of atmospheric moisture (i.e. humidity) on mortality [91, 92, 93, 94]. Whereas crop heat stress is relatively greater under dry conditions [50], human heat stress is greater under humid conditions, as the body be-

comes less efficient at shedding heat through evaporative cooling [63]. Evaluating statistical model projections of human mortality and other social outcomes through a "perfect model" approach, with the use of physiologically based models [95], may improve our understanding of societal concerns under future climate change.

2.5 Data Availability

All data used in this analysis are publicly available. Simulation outputs from GGCMI phase 2 are available at *https://zenodo.org/*. AgMERRA weather data is available at *https://data.giss.nasa.gov/impacts/agmipcf/agmerra/*. LPJmL RCP8.5 simulation outputs are available upon request.

CHAPTER 3

VALIDATING MAIZE MATURITIES USED IN MODELS USING MULTIPLE OBSERVATIONAL DATA SETS

Haynes Stephens[1,2], James Franke[1,2], Jonas Jägermeyr[3], Christoph Müller[4], Charles Gardner[1], Katherine Dixon[5], Eva Burgos[1], Lori J. Abendroth[6], and Elisabeth Moyer[1,2]

[1]Department of Geophysical Sciences, University of Chicago, Chicago, IL, USA [2]Center for Robust Decision-making on Climate and Energy Policy (RDCEP), University of Chicago, Chicago, IL, USA [3]NASA Goddard Institute for Space Studies, New York City, USA [4]Potsdam Institute for Climate Impacts Research (PIK), Member of the Leibniz Association, Potsdam, Germany [5]Department of Ecology and Evolution, University of Chicago, Chicago, IL, USA [6]USDA Agricultural Research Service, Cropping Systems and Water Quality Research Unit, Columbia, MO

3.1 Abstract

Understanding the impacts of climate change on food production requires accurately modeling crop yields in historical and future climates. Absolute yield levels in process-based crop models can be significantly affected by parameterizations of cultivar maturity (total heat accumulation needed to reach full crop development), indicating that the use of inaccurate maturity parameterizations can lead to unrealistic model behavior. For models in the Global Gridded Crop Model Intercomparison (GGCMI) Phase 2 Experiment, historical cultivar maturities for U.S. maize are parameterized using state-level growing periods (days from planting to maturity) derived from a single-year crop calendar (1996). However, it is not yet understood how this crop calendar compares to calendars of increased temporal or spatial resolution, nor is it understood how well calendar-derived maturities reflect the maturities of real-world maize cultivars. Here, we evaluate the single-year, state-level crop calendar against three observational data sources of increasing detail for maize cultivars in the U.S. Corn Belt: a multi-year state-level crop calendar, a multi-year district-level crop calendar, and county-level cultivar maturity estimates from maize sales data. At the state level, planting and harvest dates in the single-year crop calendar agree with mean dates in

the multi-year calendar, indicating that the hand-picked 1996 dates reasonably represent average historical farming schedules. However, observed durations between maturity and harvest dates frequently exceed the 21 days assumed in the GGCMI Phase 2 protocol. In the GGCMI models, the accuracy of tuning cultivar maturities based on input crop calendars varies in execution, but models that follow the protocol ultimately show accurate growing periods and cultivar maturities on average. District-level crop calendars reveal substantial in-state heterogeneity in planting and harvest dates, but district-level dates still align on average with their respective state-level dates, suggesting little bias from the use of state-level dates to tune maturity parameterizations. Comparing cultivar maturities derived from the district-level crop calendar with county-level maturity estimates based on maize sales data, we find that calendar-derived maturities agree with estimates in the northern districts but exceed estimates in southern districts, indicating that current maturity-tuning protocol may be not uniformly reflect observed maize cultivars throughout the Corn Belt. While GGCMI models reasonably represent historical maize growing periods and cultivar maturities in the Corn Belt, refining maturity parameterizations to higher spatiotemporal resolutions and closer agreement with sales-data estimates may reduce noise in absolute yield levels, clarifying the comparison of model responses to weather fluctuations and future climate change.

3.2 Introduction

Process-based crop models are vital tools in understanding the impacts of climate change on food production, simulating the effects of future weather conditions on daily crop development and yields [2, 96]. Gridded crop models in the Agricultural Model Intercomparison and Improvement Project (AgMIP) [97] project strong negative effects of climate change on global maize production, but reducing uncertainty among projections remains a challenge [6, 81].

Diagnosing differences between maize model response to climate factors remains a challenge [13, 98], in part due to limited information on underlying crop management conditions [15]. Information on cultivar maturities, defined as the heat accumulation needed for a crop to reach full development, is particularly important for crop modeling, as maturity parameterizations can significantly influence the resulting yield values [15, 16]. If maturity parameterizations do not reflect real-world cultivars, then models may not accurately reflect yield outcomes under historical and future climate conditions.

In the Global Gridded Crop Model Intercomparison (GGCMI) Initiative Phase 2 Experiment [14], maize maturities in the U.S. Corn Belt are parameterized using a single year of state-level crop calendars taken from Sacks et al. (2010) [99], which provide median planting and harvesting dates for the 1996 growing season [100]. These crop calendars are used to calculate growing periods (days from planting to maturity) by assuming that crops reached maturity 21 days prior to harvest [7]; the intervening period is assumed for in-field dry down. Cultivar maturities are finally derived at each grid location by calculating the growing-degree days (GDDs) within each growing period, then holding that maturity constant across all years in the historical period [101]. To date, it remains unclear whether single-year crop calendars accurately represent average planting and harvesting practices in the Corn Belt, or if their state-level values might obscure important information at finer spatial scales. Furthermore, it is uncertain whether maturities derived from crop calendars reflect the true physiological maturities of real-world cultivars.

Here, validate the single-year, state-level crop calendars used to parameterize maize maturities in the GGCMI Phase 2 Experiment, comparing them to three observational data sources: (1) multi-year state-level crop calendars, (2) multi-year district-level crop calendars, and (3) county-level maturity estimates from cultivar sales data. We compare the single-year and multi-year crop calendars at the state level to determine whether 1996 growing periods align with average values across the historical period. We compare the multi-year

state-level crop calendars against a newly compiled dataset of multi-year calendars at the agricultural district level, evaluating whether the disregard of in-state heterogeneity might introduce bias of growing periods. Finally, we compare average cultivar maturities derived from district-level crop calendars against county-level maturities estimates from sales data, assessing how closely the data sets agree across the region. We aim to answer the question: do current maturity parameterizations in the GGCMI models accurately represent real-world maize cultivars in the U.S. Corn Belt?

3.3 Data and Methods

3.3.1 Crop Calendar Observations

The subject of our study is the dataset of state-level planting and harvest dates in Kansas, Illinois, Indiana, Iowa, Missouri, and Wisconsin, as published in Sacks et al. (2010) [99]. Median planting and harvest dates are taken for the 1996 growing season [100]. These dates are use to tune maize growing periods in the GGCMI Phase 2 Experiment, assuming crops reached maturity 21 days prior to harvest.

We evaluate the single-year calendars used in Sacks et al. (2010) using two data sets of crop calendars at increased spatial and temporal resolution. Weekly reports of maize sowing and harvest progress (0 to 100%) were taken from the United States Department of Agriculture (USDA) at the state level for the same states for the period 1981—2010 [102]. Additionally, weekly progress reports at the district level were taken from USDA regional offices for the same states and period. Reports for two districts in Missouri—Western Central and Eastern Central—were unavailable. Annual reports of total planted acreage, harvested acreage, and harvested yields are also included for the available districts. Weekly progress reports for each granularity (district or state) do not always cover progress from 0–100%. Therefore we designate sowing, maturity, and harvest dates in each growing season as the

first respective report to exceed 50% progress. Maturity dates at the district level were not available, so we calculate district-level growing periods by applying maturity-harvest offsets from the state level S15 to all districts, for a given state and year. Finally, we calculate annual anomalies for sowing dates, maturity dates, harvest dates, growing periods, and detrended yields.

3.3.2 Climate Data

Daily temperature data were obtained from the AgMERRA ("agricultural"-modified Modern Era Retrospective analysis for Research and Applications) gridded reanalysis product [72] at a resolution of 0.5° x 0.5° for the years 1981–2010. We calculate daily growing-degree days (GDDs) for each gridcell using minimum and maximum temperatures, according to common practice in the literature [103]. We aggregate daily gridcell values to district-level means, weighted by maize harvest area (Figure S14 taken from the MIRCA2000 dataset [71] at the same resolution as AgMERRA. Cumulative GDDs across the growing period (sowing to maturity) are calculated in each district and year for both models and observations to derive cultivar maturities.

3.3.3 Crop Model Output

Annual output of yields, planting dates, and maturity dates are taken from six maize models (CARAIB, EPIC-TAMU, GEPIC, LPJ-GUESS, LPJmL, pDSSAT) in the GGCMI Phase 2 Experiment [14] at a resolution of 0.5° x 0.5° for the years 1981–2010. Each model is driven by daily AgMERRA climate inputs (temperature, precipitation, solar radiation, in some cases also relative humidity and wind speed). State-level sowing dates in the models are held fixed at each location across all years. Modeling teams tune their cultivar maturities independently, based on the respective maturity thermal time process in each model [101], such that the results growing periods match or closely align with 1996 growing periods

assuming the 21-day offset between maturity and harvest [7]. Cultivar maturities are then held fixed at each location across all years the period 1981–2010. Models consider only high-input systems with nitrogen fertilization levels of 200 kg N/ha and no other nutrient limitations (e.g., Phosphorus and Potassium). We aggregate annual outputs of sowing date, maturity date, growing period and yield to the district level using weighted means of harvest area, and calculate annual anomalies.

3.4 Results

3.4.1 Planting and harvest dates from Sacks et al. (2010) align with multi-year averages across the historical period

We find that single-year planting and harvest dates published by Sacks et al. (2010) align with average dates in multi-year calendars (Figure 3.1). Within each state, the single-year planting dates from Sacks et al. (2010) are within 5 days of their respective multi-year averages, and single-year harvest dates are within 8 days of their respective multi-year averages. Multi-year planting dates vary from year to year, with standard deviations ranging from 6 to 14 days (1 sigma) across states. Planting-date variation in Wisconsin is less than half the variation in Missouri, consistent with the understanding that northern planting windows can be constrained by colder springtime temperatures. Harvest-date variations do not show significant differences between states, ranging from 10–12 days across the region.

Inferred maturity dates used in the GGCMI Phase 2 Experiment protocol, on the other hand, occur consistently later than multi-year observations suggest, with delays ranging from 4–20 days across states. Observed intervals between maturity and harvest range from 23 to 36 days across states, indicating that the assumed 21-day interval does not reflect historical maize crops in the Corn Belt. Altogether, validation of the single-year planting and harvest dates from Sacks et al. (2010) suggest they are suitable to represent average historical crop

calendars in models, save for a slight bias in the assumed maturity-harvest intervals.

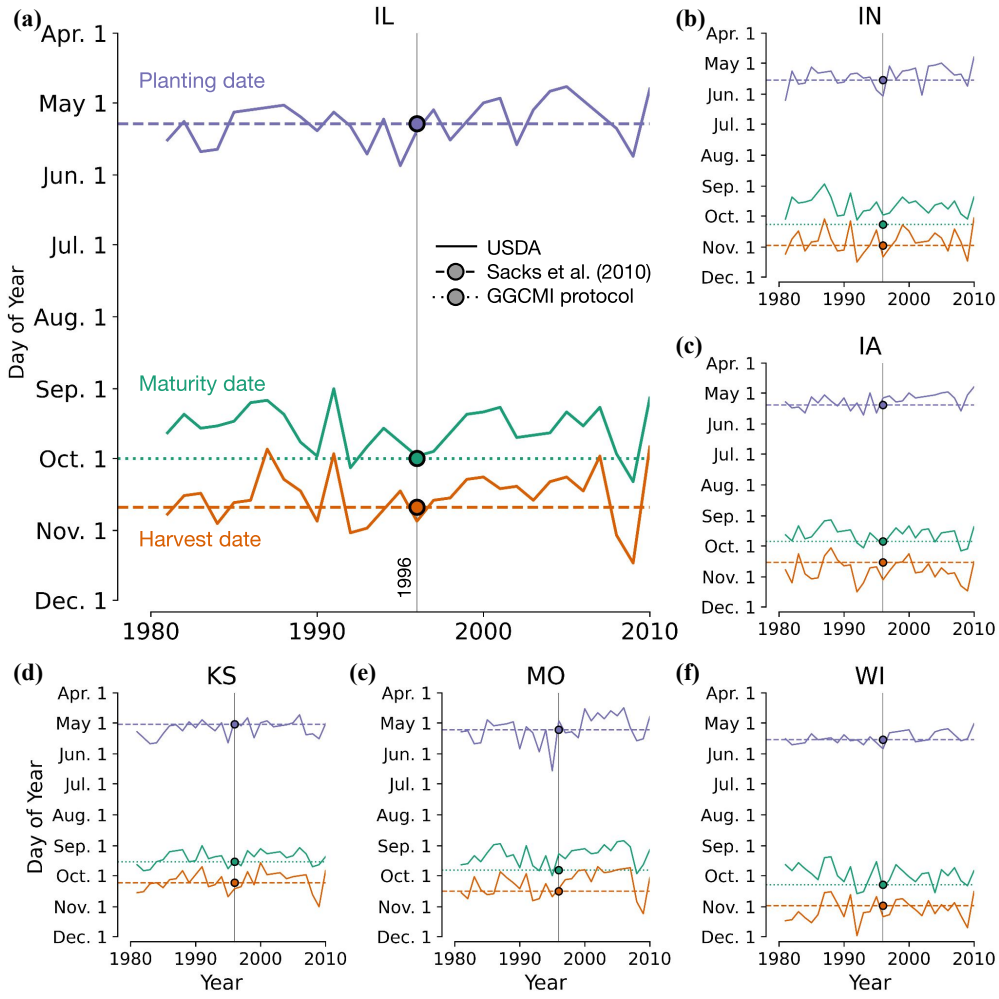

Figure 3.1: State-level planting and harvest dates between Sacks et al. (2010) and multi-year observations in the U.S. Corn Belt. **(a)** Line plots show annual state-level dates for planting (blue), maturity (green), and harvest (orange) in Illinois. Dates from multi-year observations are shown by solid lines. Single-year planting and harvest dates for the 1996 growing season, taken from Sacks et al. (2010), are shown by circular markers with extended dashed lines. The tuned maturity date used in the GGCMI protocol assumes a 21-day offset between maturity and harvest, and is shown by a circular marker with an extended dotted line. Identical layouts are shown for **(b)** Indiana, **(c)** Iowa, **(d)** Kansas, **(e)** Missouri, and **(f)** Wisconsin. Single-year planting and harvest dates from 1996 reasonably represent average respective dates across the historical period. However, tuned maturity dates occur later that most observed maturity dates, suggesting real-world intervals between maturity and harvest are longer than the 21-day assumption.

3.4.2 Maize models also show similar growing periods and maturities to state-level observations

Even though single-year crop calendars from Sacks et al. (2010) reflect average calendars, the efficacy of parameter tuning determines whether models show the same accuracy in their resulting growing periods. For the GGCMI Phase 2 Experiment, we find that the resulting model growing periods in the Corn Belt are similar to observed growing periods across the historical period (Figure 3.2). Average observed growing periods are 126–137 days across all districts, which is similar to the range for most of the ensemble. CARAIB stands as a notable outlier with growing periods ranging from 100–110 calendar days, shorter than the rest of the Phase 2 ensemble whose growing periods range from 127–148 calendar days. Since CARAIB was the only model in the ensemble not tuned to match the input crop calendar [7], its outlier behavior is expected. Excluding CARAIB, the rest of the ensemble growing periods differ from observed values by -1–9% on average, with the slight bias toward longer growing periods reflecting how assumed maturity-harvest intervals in the GGCMI protocol [7] are shorter than observations suggest.

As a result of similar growing periods, parameterized cultivar maturities in models are also similar to maturities inferred from state-level growing periods (Figure S16). Average observed maturities in the state-level observations are 1220–1640 GDDs, which typically lies within model ranges in the ensemble. Again, the CARAIB model has substantially earlier maturities than the rest of the ensemble, with a range of 940–1400 GDDs. The rest of the ensemble maturities range from 1160–1770 GDDs, ultimately differing from observed values by -1–5% on average. Percentage differences between modeled and observed maturities are slightly smaller than differences in growing periods due to low-GDD values for days at the tail ends of the growing season (Figure S26).

Importantly, we find that calendar-derived cultivar maturities in maize models vary in each district from year to year, despite the modeling protocol dictating that location-specific

cultivars be held fixed across the historical period. We consider potential causes of this finding in the Discussion section.

Our validation of modeled growing periods and maturities suggests that parameterized growing periods and maturities in the GGCMI models agree with observed values at the state level. In addition to maturity characteristics, we find that modeled yield values align with observed yields on average (Figure S17). Average yields in both observations and the ensemble (sans CARAIB) are 8.5 ton/ha. pDSSAT shows outlier behavior, however, with an average historical yield of 13 ton/ha, substantially above observations and other model values.

3.4.3 District-level crop calendars reveal in-state heterogeneity in growing periods and cultivar maturities

To assess whether models may be able to accurately represent observations at increase spatial resolution, we examine in-state heterogeneity in observed crop calendars. We find that district-level observations of cultivar maturities and growing periods reveal substantial in-state heterogeneity (Figure 3.3, individual states shown in Figures S18–S23)). Across the Corn Belt, district-level mean growing periods typically vary within each state by approximately two weeks (Figure S24). However, observed maturity characteristics vary by state (Figures S18–S23).

We find that district-level growing periods can be shorter or longer than the state-level records by as much as a month or more (Figure 3.3). 40% of district-level growing periods differ from their respective state-level values by a week or more, and 13% differ by two weeks or more. Most states have an average north-south difference ranging from 11–19 days, except for Iowa and Wisconsin, the two northernmost states in the region. On average, however, district-level growing periods are 1.5 days shorter than state-level values; this difference is notably smaller than the weekly resolution at which state- and district-level values are both

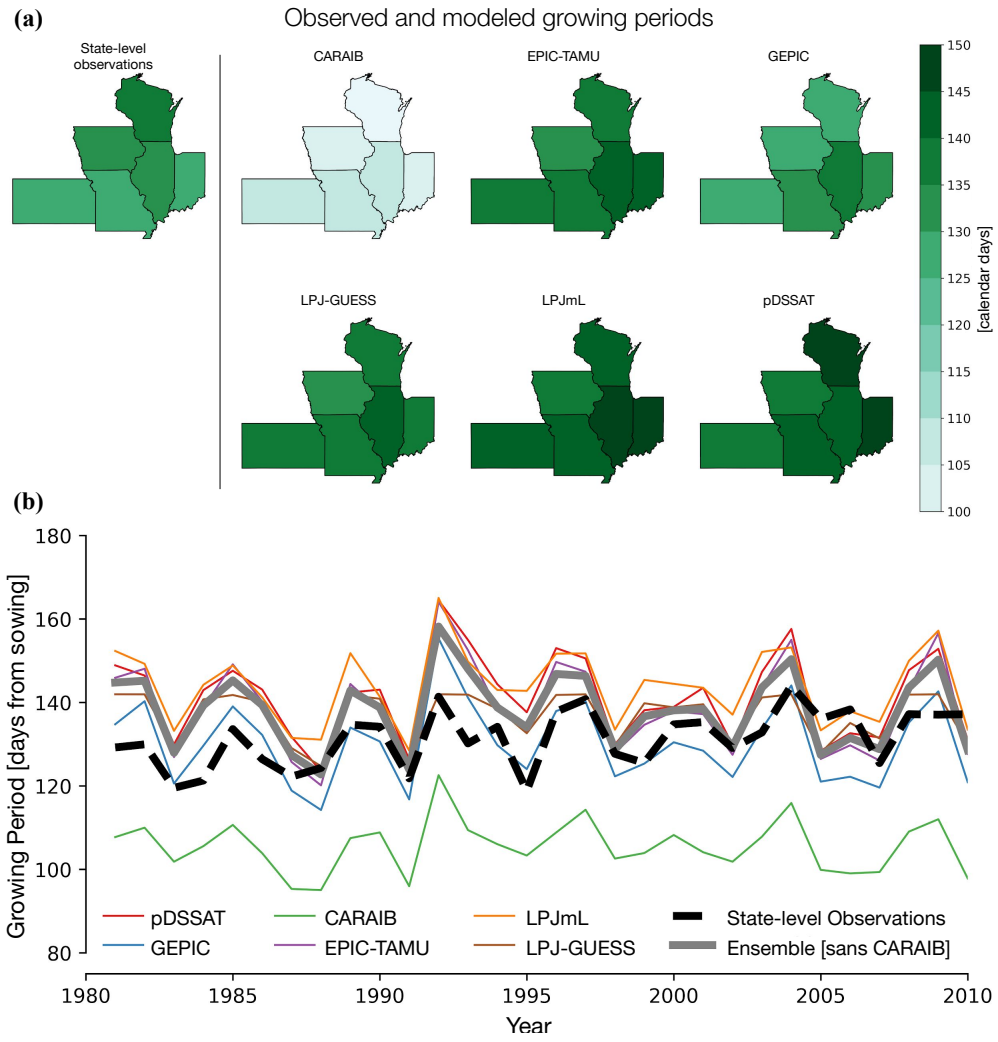

Figure 3.2: Comparisons of multi-year growing periods between models and observations. **(a)** Map subplots show average historical maize growing periods for observations, calculated from state-level crop calendars, and each process-based model considered in the ensemble. **(b)** Line plots show the historical timeseries of average growing periods for observations and models. Ensemble mean growing periods are calculated excluding values from CARAIB, which did not participate in the protocol to tune historical growing periods. Model growing periods align with state-level observations in the historical period, suggesting that the use of single-year crop calendars to tune model growing periods is generally reasonable.

reported.

District-level cultivar maturities can differ their respective state-level values by >10% (Figure 3.3). Cultivar maturities generally decrease with latitude, where northern districts typically have the earliest maturities and southern districts have the latest (Figure 3.3).

Cultivar maturities typically show greater agreement with the corresponding state-level values in northern districts relative to southern districts (see Figure S22 and Figure S23 for comparison). The largest difference in cultivar maturities exists between district and state levels in southern districts, where district values are roughly 270 °C days (14%) earlier.

Within each state, sowing and harvest dates in northern districts generally occur later than the state value, while dates for southern districts occur earlier (Figures S18–S23). However, this pattern is not apparent in Iowa, and perhaps inverted for Wisconsin, relative to the rest of the Corn Belt states (Figures S21 and S23). This is likely due to these two states having the least in-state heterogeneity for maturity durations (Figure S24) and may be due, in part, to them containing the most northern districts in the domain. District-state differences show similar patterns grouped by southwestern states and northeastern states, respectively; this orientation is similar to the spatial pattern of historical GDDs (Figure S25). Relative to other states in the region, Wisconsin has a combination of relatively lower daily GDD values and smaller discrepancies between district- and state-level dates (Figure S26). Thus, district-level maturities in Wisconsin are more similar to state values than in any other state in the domain. District-level data in some states, such as Illinois, suggest that sowing dates in northern districts sometimes precede those in southern districts (see Supplemental Figures), counterintuitive to the expected spring warming pattern across the state.

If future GGCMI experiments aim to reflect real-world maturity characteristics at finer-than-state resolutions, they will have to incorporate new crop calendars, such as the district-level calendars in this study, in future model parameterizations.

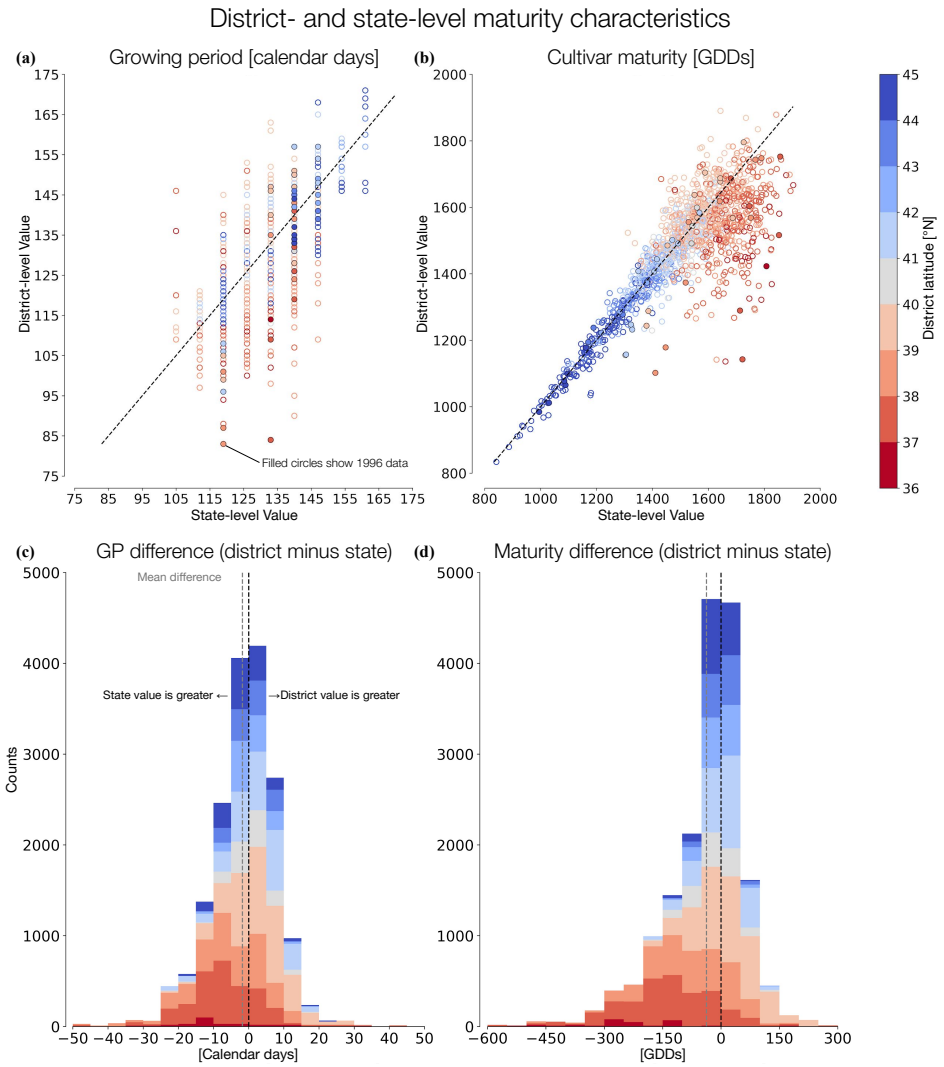

Figure 3.3: Differences in growing periods and calendar-derived maturities between district- and state-level observations in the Corn Belt. **(a)** Scatter plot shows growing periods based on district-level reports against values based on state-level reports (the standard USDA resolution) for districts in the Corn Belt. Data points are colored by the latitude of the corresponding district. Filled circles represent values from 1996, the year used to tune maturity parameterizations in the GGCMI models. The dashed one-to-one line denotes where state- and district-level values are equal. **(b)** Scatter plot shows the same format as (a), but for cultivar maturities. **(c)** Stacked histogram shows the difference in growing periods between district- and state-level observations. Bars are colored by the latitude ranges of the corresponding districts. The black vertical dashed line marks the zero point where state- and district-level values are equal. The gray vertical dashed line marks the mean difference. **(d)** Scatter plot shows the same format as (c) but for differences in cultivar maturities. State-level planting and harvest dates align with district-level dates on average. However, in-state heterogeneity can lead to district-level growing periods that differ from state-level values by up to a month or more, which is not captured in the GGCMI Phase 2 Experiment protocol.

3.4.4 Observed maturities from crop calendars show similar range and spatial pattern to maturity estimates from sales data

To assess whether crop calendars are reasonable for estimating cultivar maturity, we compare observed maturities with maturity estimates from sales data, originally presented in Abendroth et al. (2021) [104]. Since Abendroth et al. (2021) present average maturity estimates for the period 2000–2016, we compare their data to observations for overlapping years (2000–2010). Observed mean cultivar maturities (Figure 3.4) generally agree with maturity estimates (Figure 1b of Abendroth et al., 2021) in states where data is available from both sources. Observations and sales data show similar ranges of maturity values for districts in Iowa, northern Illinois, and northern Indiana. However, observed maturities are generally 50–100 GDDs later than maturity estimates for districts in Missouri and southern Illinois. Within the comparable agricultural districts, maturity estimates from sales data show in-district heterogeneity and some missing counties. No commercial sales data was available to compare with observations for districts in Kansas.

Observed mean maturities (Figure 3.4b) also show a similar relationship to latitude as that of estimates from sales data (Figure 2b of Abendroth et al., 2021, [104]). Unable to extract specific districts from the maturity estimates dataset, we compare the meridional relationship of maturity estimates in all sales data (including North Dakota, South Dakota, Minnesota, Michigan, and Ohio, excluding Kansas) to the relationship from mean maturities from observations (including Kansas). We perform a bilinear regression of the mean observed maturities in each district against the corresponding district latitude, with a hinge point at 41.5 °N, in the same fashion as Abendroth et al. (2021). Predictions from the bilinear regression show a high correlation to observations (R^2=0.84), although not as high as the respective predictions to sales data (R^2=0.92) [104].

Fitted slopes of cultivar maturity to latitude are consistently more negative in observations than in maturity estimates from sales data. The relationship between observed cultivar

maturities and latitude for districts below 41.5 °N is -12.0 GDDs/° latitude, similar to the relationship found from sales data (-13.7 GDDs/° latitude). However, the relationship between observed cultivar maturities and latitude for districts above 41.5 °N is -99.0 GDDs/° latitude, nearly twice as negative as the relationship found from sales data (-56.2 GDDs/° latitude). As expected, county-level sales data show substantially greater sampling for latitudinal locations across the region. County-level sales data is also represented for numerous latitudes up to 49 °N, whereas observations only contain six districts between 44–46 °N. The difference in regions considered for the comparison between observations and sales data likely influences the respective bilinear relationships to latitude. In all, spatial heterogeneity in agreement between calendar-derived maturity and sales data estimates suggests that southern crop calendars may require additional adjustments to reflect the true crop maturities.

3.5 Discussion

Providing sound representations of crop behavior under historical and future conditions requires process-based crop models to simulate accurate yield outputs for the right reasons. Model accuracy can be influenced by error in both the input parameters and the underlying crop growth processes [16, 98]. Validations of modeled growing periods and cultivar maturities in this study suggest that the input crop calendars of Sacks et al. (2010) are useful for tuning maize maturities in the Corn Belt.

Our comparison of cultivar maturities derived from crop calendars to maturity estimates from sales data suggest it is reasonable to drive cultivar maturities from observed crop calendars in the northern districts of our study region (Figure 3.4). Observed cultivar maturities in southern districts are slightly later than sales data estimates, suggesting that reported growing periods may be slightly delayed relative to the true phenological development. Discrepancies in cultivar maturities between the two sources might reveal errors in the use

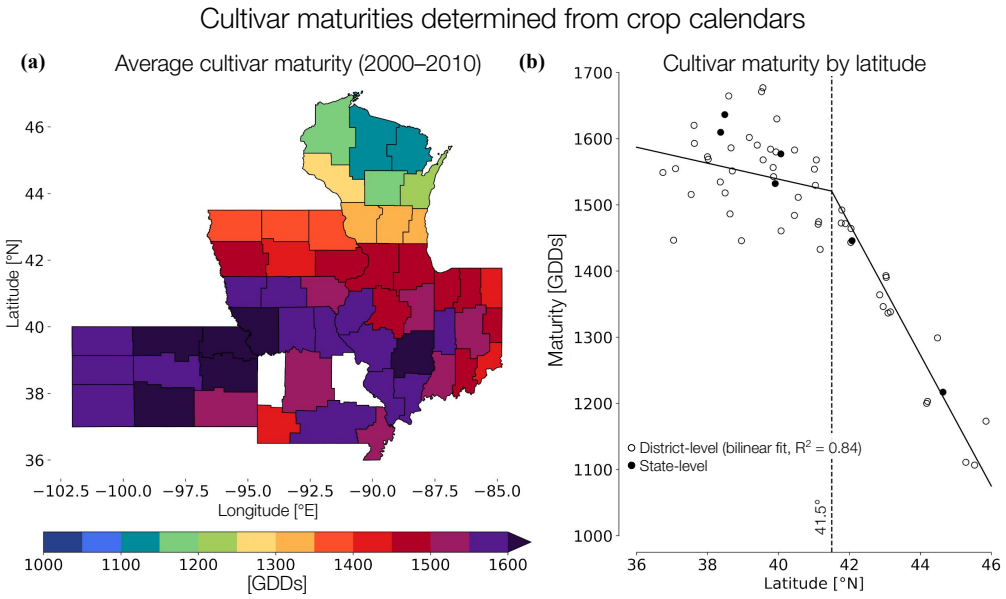

Figure 3.4: Average cultivar maturities derived from district-level crop calendars. **(a)** Map plot shows the average cultivar maturity calculated from district-level reports, in the same format as Figure 1b in Abendroth et al. (2021) [104], for comparison. **(b)** Scatter plot shows the same values plotted against the corresponding district latitude, in the same format as Figure 2b in Abendroth et al. (2021) for county-level sales data. The solid black line shows a bilinear fit with a hinge point at latitude 41.5 °N. Cultivar maturities derived from crop calendars align with estimates from sales data in northern districts, but typically exceed estimated values in southern districts. Meridional relationships, however, are similar between the two data sources in southern districts, while calendar-derived maturities show a more negative relationship to latitude in northern districts. Differing spatial resolutions and reference periods likely affect these findings, as does the imposed hinge-point of 41.5° N in meridional relationships.

of USDA observations, raising challenges for making accurate maturity parameterizations in crop models. However, maturity estimates from sales data may slightly differ from the realized physiological behavior of the farmed cultivars. Additionally, USDA observations consider all maize cultivars within each district, while sales data exclusively correspond to cultivars from Corteva Agriscience. Assuming the two sources are comparable, a possible explanation for observed later maturities in southern districts is that farmers and agronomists typically assign maturity in practice by the identification of a "black layer" at the base of the maize kernels [105]. Black layers can develop up to two weeks after reaching physiological maturity, which could lead to a difference between the phenological maturity date and USDA reports (surveyed weekly). The greatest differences between phenological maturities

and reported maturities would likely occur in southern districts, as they contain more GDDs per day relative to northern districts (Figure S26). Further research is required to compare data from USDA reports with sales data estimates over the same periods and spatial regions, as well as for individual years.

Increasing the spatiotemporal resolution of input crop calendars may ultimately help models to reproduce historical yield records with greater detail [101, 36, 106]. Particularly, introducing district-level crop calendars would provide the opportunity for models to represent in-state heterogeneity in maturity paremeterizations that is not currently considered. However, while this may be feasible at the state level in the U.S., annual crop calendars for major crops are not widely available for many regions of the world. Efforts to systematize annual crop calendars globally, similar to the practices of the Food and Agriculture Organization (FAO) for reporting country-level agricultural production, would greatly aid crop modelers in tuning models to observations with greater spatial and temporal detail.

Our use of district-level crop calendars reveals that northern districts in some states plant before the southern districts (Figure S19), counterintuitive to the expected spring warming pattern across the state [107]. For some regions, earlier sowing dates in northern districts can be associated with greater yield benefits relative to southern districts, as was found in a study of optimal Iowa sowing dates [108] (we also find early sowing dates in northern Iowa, Figure S21). Additionally, sowing dates in southern Illinois show a more positive historical trend relative to northern Illinois [107], potentially contributing to southern districts sowing later than northern districts in recent history. Additional research on in-state heterogeneity in farming practices may help to diagnose this finding.

The primary caveat of our study is highlighted by the finding that model maize maturities in each district vary across the historical time period (Figure S16), despite the fixed-maturity protocol of the Phase 2 experiment [7, 14]. We outline five possible reasons for this result. First, base temperatures, above which GDDs accumulate, vary across models in the ensemble

[101] and may vary across real-world maize cultivars. To consistently compare between models and observations, we use a base temperature of 10 °C that is commonly used in the literature [103], but discrepancies between our assumed base temperature and those in the models may lead to variation in the derived cultivar maturities. Second, derived cultivar maturities may be earlier than model specifications during cooler growing seasons, as some models impose hard limits on the number of days the plant can grow before it must be harvested, independent of the GDDs accumulated. Third, and conversely, derived cultivar maturities may be later than model specifications during hotter growing seasons, as some models cap the GDDs that can be accumulated within a single day, regardless of how much heat is available. Fourth, phenological development in some maize models is modified by water stress or sunlight exposure, which may cause derived cultivar maturities to be later than those realized in the models. Finally, some models separate their phenological development into multiple stages (e.g. vegative, reproductive), which can have their own respective base and maximum tempartures for accumulated GDDs, thus leading to discrepancies between the realized GDDs in the model and our calculated GDDs using the 10 °C base temperature.

Further research examining these reasons would clarify the robustness of our findings with respect to each model in the ensemble. Additionally, incorporating additional observations and models into future validation exercises would clarify the robustness of our findings across models, crops, and regions relevant to global agricultural production.

3.6 Data Availability

All data used in this analysis are publicly available. Simulation outputs from GGCMI phase 2 are available at *https://zenodo.org/*. AgMERRA weather data is available at *https://data.giss.nasa.gov/impacts/agmipcf/agmerra/*. State-level data from the USDA are available at *https://quickstats.nass.usda.gov/*. District-level data from the USDA are available upon request.

CHAPTER 4

GRIDDED MAIZE MODELS SHOW REALISTIC GROWING PERIOD RESPONSES TO TEMPERATURE BUT UNCERTAINTY IN SUBSEQUENT YIELD IMPACTS

Haynes Stephens[1,2], James Franke[1,2], Jonas Jägermeyr[3], Christoph Müller[4], Charles Gardner[1], Katherine Dixon[5], Eva Burgos[1], Lori J. Abendroth[6], and Elisabeth Moyer[1,2]

[1]Department of Geophysical Sciences, University of Chicago, Chicago, IL, USA [2]Center for Robust Decision-making on Climate and Energy Policy (RDCEP), University of Chicago, Chicago, IL, USA [3]NASA Goddard Institute for Space Studies, New York City, USA [4]Potsdam Institute for Climate Impacts Research (PIK), Member of the Leibniz Association, Potsdam, Germany [5]Department of Ecology and Evolution, University of Chicago, Chicago, IL, USA [6]USDA Agricultural Research Service, Cropping Systems and Water Quality Research Unit, Columbia, MO

4.1 Abstract

Climate change conditions are projected to substantially reduce maize yields in the U.S. if adaptation strategies are not implemented. Higher growing-season temperatures are thought to impact maize yields primarily by accelerating crop development to maturity, subsequently shortening the growing period (days from sowing to maturity). However, our understanding of how accelerated maturity factors into total yield responses under climate change is limited. Maize modeling studies project that adapting maize cultivars to counteract accelerated maturity could alleviate—even recover—yield losses under climate change, but these models do not isolate yield impacts driven by accelerated maturity from other temperature-induced damages. Moreover, studies examining the response of observed maize growing periods to temperature indicate that models may overestimate accelerated maturity under warming, yet these studies fail to consider confounding effects on growing periods from sowing date variability. Here, we improve the understanding of how growing periods respond to temperature, sowing date, and cultivar maturity, defined as the heat accumulation required for a

cultivar to reach full development. We also develop a framework for attributing yield impacts under warming to the mechanism of accelerated maturity, as well as to physiological responses to temperature stresses. Results suggest that modeled growing period responses to temperature are realistic after the effects of observed sowing date variability are accounted for, supporting the projected shortening of growing periods under climate change. However, models show a wide range of yield responses to accelerated maturity, with the mechanism accounting for 40–100% of total yield losses across the ensemble under a uniform warming of +6 °C. Nonetheless, accelerated maturity is consistently a major driver of warming-related yield losses and will likely play a key role in future adaptation strategies.

4.2 Introduction

Climate change could jeopardize future food security by negatively impacting crop production in key agricultural regions. One region of particular concern is the U.S. Corn Belt, where maize production has increased dramatically over the past century and currently accounts for a third of the world's supply [109]. Earth-system models project climate change to increase growing-season temperatures in the Corn Belt as much as 6 °C by the end of the century [24, 25, 26]. Crop modeling studies project increased temperatures to decrease maize yields in the Corn Belt as much as 80% by the same period [81, 10] [1] unless serious adaptation measures to crop management and breeding are implemented [110, 111, 112].

Higher temperatures impact maize yields primarily by increasing the rate of heat accumulation that drives crop development to maturity (i.e. accelerated maturity) [113, 114, 115, 116, 117, 118, 119], subsequently shortening the number of days allocated to the grain fill period [112, 104]. accelerated maturity is considered one of the main mechanisms to reduce yields under climate change [120, 121, 86]; other mechanisms of temperature-induced

1. Projected yield impacts vary across statistical and process-based modeling camps, as well as across models within each camp.

impacts include a reduction in carbon uptake under water deficits [122, 78] and a possible deterioration in the quality of growth processes (biochemical, physiological, and metabolic) under severe heat stress [123, 124].

In the face of accelerated maturity under warming, scientists propose using later maturity maize cultivars to exploit the increased heat availability and gain additional days in the grain fill period [125, 126, 127], referred to as cultivar adaptation. Cultivar adaptation has been identified as one of the most effective strategies under climate change [128], with the potential to alleviate or even reverse yield losses [129, 126]—later maturity cultivars in the Corn Belt today are also associated with higher yields [130], offering more promise for adaptation benefits. To quantify the benefits of cultivar adaptation under climate change, simulations of future maize yields often consider scenarios that adapt cultivars under warming to restore approximate historical growing periods (days from sowing to maturity) [119, 131, 101, 120, 132].

Simulated cultivar adaptation through process-based crop models suggest the strategy could substantially boost yields under climate change relative to no-adaptation practices [133, 132, 120]. Minoli et al. (2019) use crop models from the GGCMI Phase 2 ensemble and find that cultivar adaptation reduces or fully compensates for the negative impacts of warming on crop yields in most regions of the world [101]. Zabel et al. (2021) use emulators based on the GGCMI Phase 2 models to and project that future cultivar adaptation can outweigh climate-induced yield losses, increasing global crop production relatively by 17%, dependent on the availability of suitably adapted cultivars [132]. Liu & Basso (2020) use the SALUS model to simulate the impacts of adapting future crop maturities and sowing dates, finding that such adaptations can boost yields under climate change above historical levels in the U.S. Midwest [119]. Minoli et al. (2022) perform a similar analysis using the gridded LPJmL model (a member of the GGCMI ensemble) and find that adapting cultivar maturities and sowing dates increases maize yields in the Corn Belt by 10–30%

under an RCP6.0 projection relative to a no-adaptation scenario, with the vast majority of benefits attributed to cultivar adaptation [120]. Lv et al. (2020) find similar yield benefits of maize cultivar and sowing data adaptations in China [134]. Potential effects of water-supply limitations are implicitly considered under climate change projections from earth system models (e.g. RCP, SSP), as well as benefits from greater carbon fertilization under inceased CO2 concentrations.

While process-based model simulations suggest promise for adapting to counteract accelerated maturity, model representations of changing growing periods in response to temperature have been called into questions by recent studies. Zhu et al. (2019) compare growing period responses to temperature between gridded maize models and observations in the Corn Belt and suggest that models overestimate the sensitivity of growing periods to temperature [135]. Wu et al. (2019) suggest a similar finding for maize models in the North China Plain [136]. The findings together indicate that the degree of growing period shortening may be overstated in process-based models. Consequently, this may imply that the projected yield losses due to accelerated maturity under climate change, as well as the respective adaptation benefits, are also overstated, raising concern about the use of models in guiding adaptation strategies.

Since model projections do not currently attribute portions of yield losses to accelerated maturity versus other temperature-induced stresses, exact yield responses to the respective mechanisms are obscured. A standardized framework of comparing specific yield response functions, as has been called for by previous studies [98], would help clarify differences in model behaviors.

Here, we validate growing period responses to temperature for maize models in the U.S. Corn Belt. We also present a simple framework for attributing portions of yield changes under warming to their respective causes, incorporating crop yield simulations across different farming practices and environmental conditions. We focus again on the U.S. Corn Belt as

a case study example for our proposed framework. Specifically, we pursue the following questions for maize crops in the Corn Belt: (1) Do the modeled growing periods show similar sensitivities to historical temperature anomalies as observed data? (2) What portion of projected maize yield losses under warming can be attributed to accelerated maturity?

4.3 Data and Methods

4.3.1 Climate Data

Daily temperature data were obtained from the AgMERRA ("agricultural"-modified Modern Era Retrospective analysis for Research and Applications) gridded reanalysis product [72] at a resolution of 0.5° x 0.5° for the years 1981–2010. Uniform warming scenarios (+2 °C, +4 °C, +6 °C) are executed by increasing the minimum, mean, and maximum temperature of each day by the corresponding warming perturbation. We calculate daily growing-degree days (GDDs) for each gridcell using minimum and maximum temperatures, according to common practice in the literature [103]. We aggregate daily gridcell values to district-level means, weighted by maize harvest area (Figure S28 taken from the MIRCA2000 dataset [71] at the same resolution as AgMERRA. Cumulative GDDs across the growing period (sowing to maturity) are calculated in each district and year for both models and observations to derive cultivar maturities.

4.3.2 Crop Calendar Observations

Weekly reports of maize sowing and harvest progress were taken from the United States Department of Agriculture (USDA) regional offices at the district level for six states (Kansas, Illinois, Indiana, Iowa, Missouri, and Wisconsin) in the U.S. Corn Belt for the period 1981—2010 [102]. Reports for two districts in Missouri—Western Central and Eastern Central—were unavailable. Annual reports of total planted acreage, harvested acreage, and harvested

yields are also included for the available districts; yield values are detrended within each district. Weekly progress reports for each granularity (district or state) do not always cover progress from 0–100%. Therefore we designate sowing, maturity, and harvest dates in each year and district as the first respective report to exceed 50% progress. Maturity dates at the district level were not available. To calculate district-level growing periods, we apply maturity-harvest offsets from the state-level reports to all districts, for a given state and year S29. Finally, we calculate annual anomalies for sowing dates, maturity dates, harvest dates, growing periods, and detrended yields.

4.3.3 Crop Model Output

Annual output of yields, sowing dates, and maturity dates are taken from six maize models (CARAIB, EPIC-TAMU, GEPIC, LPJ-GUESS, LPJmL, pDSSAT) in the GGCMI Phase 2 Experiment [14] at a resolution of 0.5° x 0.5° for the years 1981–2010. We use maize yield outputs under rainfed and fully irrigate management scenarios. Each model is driven by daily AgMERRA climate inputs (temperature, precipitation, solar radiation, in some cases also relative humidity and wind speed). We include outputs for the same Corn Belt states as observations. In this region, model crop calendars are tuned based on state-level sowing and harvest dates from the year 1996 [100, 99, 7]; mean dates were taken for each state across the sowing and harvest windows. Sowing dates in the models held fixed at each location across all years. Maturity dates are determined assuming a 21-day offset between maturity and harvest. The resulting state-level, single-year growing periods (sowing to maturity) are used to tune cultivar maturity parameterizations based on the respective maturity thermal time process in each model [101]. Cultivar maturities are then held fixed at each location across all years in the historical scenario and in all non-adaptation scenarios under uniform temperature perturbations (+2, +4, +6 °C).

In adaptation scenarios under warming, the parameter of cultivar maturity (heat accu-

mulation requried to reach full development) are adjusted in each model so that average growing periods (in days) under all warming scenarios are the same as the respective historical averages. Modelers were asked to implement individual solutions to maintain the 1980—2010 mean growing period extent (e.g., precalculating changes in thermal time requirements based on fixed temperature shifts or adjusting by iteration) [101]. For models that separate crop development into multiple phenological stages (e.g., sowing-to-anthesis and anthesis-to-maturity), modelers were asked to scale parameters of each stage equally, so that the timing of intermediate stages such as anthesis stayed approximately the same.

Models consider only high-input systems with nitrogen fertilization levels of 200 kg N/ha and no other nutrient limitations (e.g., Phosphorus and Potassium). We aggregate annual outputs of sowing date, maturity date, growing period and yield to the district level using weighted means of harvest area, and calculate annual anomalies.

4.3.4 Partitioning Modeled Yield Impact Projections Under Warming

We attribute maize yield losses under uniform warming scenarios to the following drivers: accelerated maturity, temperature-induced physiological stress, and water-induced physiological stress. Yield losses under warming due to accelerated maturity are calculated under the +6 uniform warming scenario °C by taking the mean yield change (%) from adapted to non-adapated management conditions (i.e. fixed temperature, changing growing periods). Yield losses under warming due to temperature-induced physiological stress are calculated by taking the mean yield change (%) from the historical scenario to the +6 °C scenario with cultivar adaptation (i.e. changing temperature, fixed growing periods). For irrigated maize, we can additionally calculate yield losses under warming due to water-induced physiological stress by taking the mean yield change (%) when switching from fully irrigated to rainfed conditions in the historical scenario. For rainfed maize, it is Yield losses under warming due to water-induced physiological stress are unable to be calculated for initially rainfed maize,

as historical rainfed maize crops already experience an undetermined amount of water stress.

4.4 Results

4.4.1 Models show similar growing period response to temperature as observations after controlling for observed sowing date variation

We find that maize models show realistic growing period sensitivities to historical temperature variations after the effects of observed sowing date variability (Figure 4.1). We compare modeled growing periods with district-level observations across the same period (1981–2010), using a regression of district-level growing period anomalies against anomalies in temperature and cutlivar maturity (GDDs). This regression can be written as:

$$\Delta GP = \beta_T \Delta T + \beta_{GDD} \Delta GDD + \epsilon_{i,t}, \tag{4.1}$$

where ΔGP is the growing period anomaly, ΔT is the temperature anomaly, and ΔGDD is the anomaly in cultivar maturity. Based on this regression, the observed growing period response to temperature appears less sensitive than GGCMI models by roughly a factor of 3. However, the observed growing period response to temperature comes into agreement with the GGCMI ensemble when we account for variable sowing dates in observations through an additional covariate, with the regression written as:

$$\Delta GP = \beta_T \Delta T + \beta_{GDD} \Delta GDD + + \beta_{Pl} \Delta Pl + \epsilon_{i,t}, \tag{4.2}$$

where ΔPl is the anomaly in sowing date. Observed growing periods shorten by about 5% for every ten days that the sowing date is advanced relative to the local mean date. Sowing dates and cultivar maturities are held fixed at each location in the GGCMI models across all years and non-adaptation scenarios, per the Phase 2 Experiment protocol, and are therefore

not included in anomaly-based regressions of modeled growing periods to temperature. Robustness checks reveal that including covariates of ΔGDD and ΔPl in regressions on model output does not significantly alter the growing period response to temperature.

Under higher warming scenarios, models show that growing period responses become less sensitive to warming (Figure S31). For example, growing periods shorten by 12–16% under a +2 °C perturbation, while they only shorten by 24–32% under a +6 °C perturbation (warming triples while shortening doubles). The non-linear growing period response implies that the yield benefits due to cultivar adaptation would be more impactful during the 21st century relative to subsequent periods, where further warming under unmitigated climate change would cause proportionally less accelerated maturity.

4.4.2 Models attribute large portions of projected yield losses to accelerated maturity

Under +6 °C of warming in the Corn Belt, maize models in the Phase 2 ensemble project mean yields to decrease by 24–57% (Figure 4.2). Most models project yield losses of 24–30%, except for the pDSSAT model, which predicts losses twice as large as the rest of the ensemble (57%). Anomalously large yield losses in the pDSSAT model are likely related to the model having the highest baseline yield levels within the ensemble by over 5 ton/ha (Table S3), which are drastically reduced under the warming perturbation. Individual models project a range of spatial heterogeneity for yield losses in the region, with greater relative losses in Illinois, Indiana, and Missouri, for example, than losses in Iowa and Wisconsin (Figure S30). CARAIB projects the relatively largest losses of the ensemble for northern Wisconsin. However, this is likely due to issues with model output, as evidenced by missing data in northern Iowa.

Under +6 °C uniform warming, models consistently project growing periods to shorten on average by about 30% (Table S3). Similar magnitudes and spatial patterns of growing

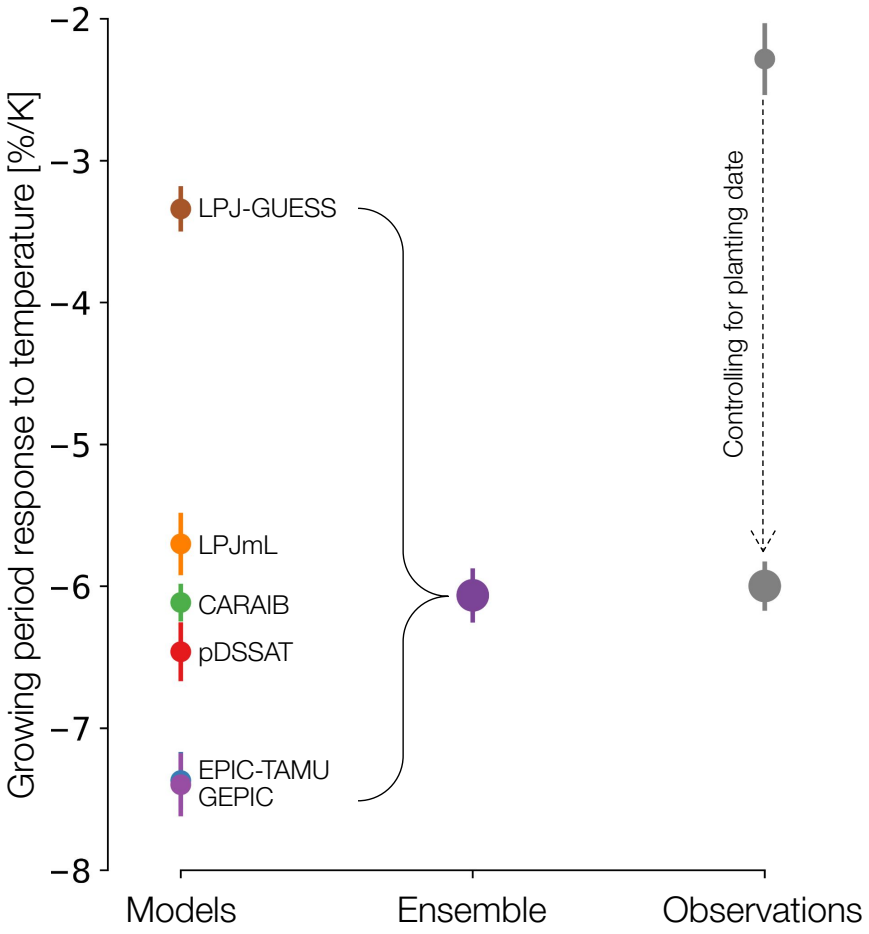

Figure 4.1: Comparison growing period responses to temperature in the Corn Belt between models and observations. Scatter plot shows regression coefficients for the historical response of growing period anomalies to temperature anomalies. Anomalies are calculated relative to each agricultural district. The small gray marker represents the coefficient for the observed growing period response when ignoring the effects of variable sowing dates in observations. The large gray marker represents the observed response when sowing dates are controlled for in the regression. Sowing dates are fixed in GGCMI simulations for a given location. Modeled growing period responses to temperature are in agreement with observations after controlling for the effects of variable sowing dates, suggesting that projected growing period shortening under climate change may be realistic.

period shortening (i.e. accelerated maturity) suggest that phenological maize processes across models in the ensemble are driven by similar processes of GDD accumulation (Figure S32).

For each model, we attribute portions of the total mean yield loss under +6 °C warming to growing period shortening and other temperature effects. We determine total mean yield losses under warming by calculating the percent yield change between the historical and

warming scenarios with no adaptations. We determine growing-period-related losses by calculating the percent yield change for the same warming scenario between fixed and adapted cultivar conditions (i.e. same temperatures, different growing periods). We determine losses from other temperature effects by calculating the percent yield change between historical scenario and the warming scenario under adapted cultivar conditions (i.e. same growing periods, different temperatures).

Across the ensemble, yield losses due to growing period shortening make up 28–100% of total mean yield losses under warming (solid bars in Figure 4.2), with an ensemble mean of 67%. These portions of growing-period-related yield losses are recovered through cultivar adaptation. The range of growing-period-related losses across the ensemble indicates a variety of yield responses to accelerated maturity within the models, despite similar phenological processes.

The LPJ-GUESS model stands out in the ensemble as the only model that projects positive yield responses to increased heat stress under +6 °C (Figure 4.2), thus accelerated maturity is the only contributor to yield losses (100% attribution). Combined with the heat stress benefits, cultivar adaptation in LPJ-GUESS subsequently leads to yields that exceed baseline levels.

Reconstructing total yield losses from growing-period and other-temperature attributions justify our proposed framework. Total yield losses under warming in the ensemble range from -57% to -24%. When we reconstruct yield losses under warming by adding our two attributed portions, which were calculated separately, we end up with losses ranging from -64% to -23%. Respective model differences range from -6.5% to 2.0%, showing that yield impacts under warming can be broken down reasonably through our framework. Discrepancies between total and reconstructed yield losses likely stem from minor weather effects during the portion of the growing period that is regained under adapted cultivar conditions.

Across GGCMI the ensemble, models with greater yield sensitivity to growing period

shortening are less sensitive to water stress (Figure S33). We determine sensitivity to water stress by comparing yield levels between rainfed and irrigated maize crops in the historical period. The roughly linear relationship between yield sensitivities to growing period shortening and yield sensitivities to increased water stress suggests that total yield responses to warming can be partitioned into these two drivers. This suggests that yield responses to the +6 °C perturbation may be broken down into changes caused by accelerated maturity and changes caused by increased water stress.

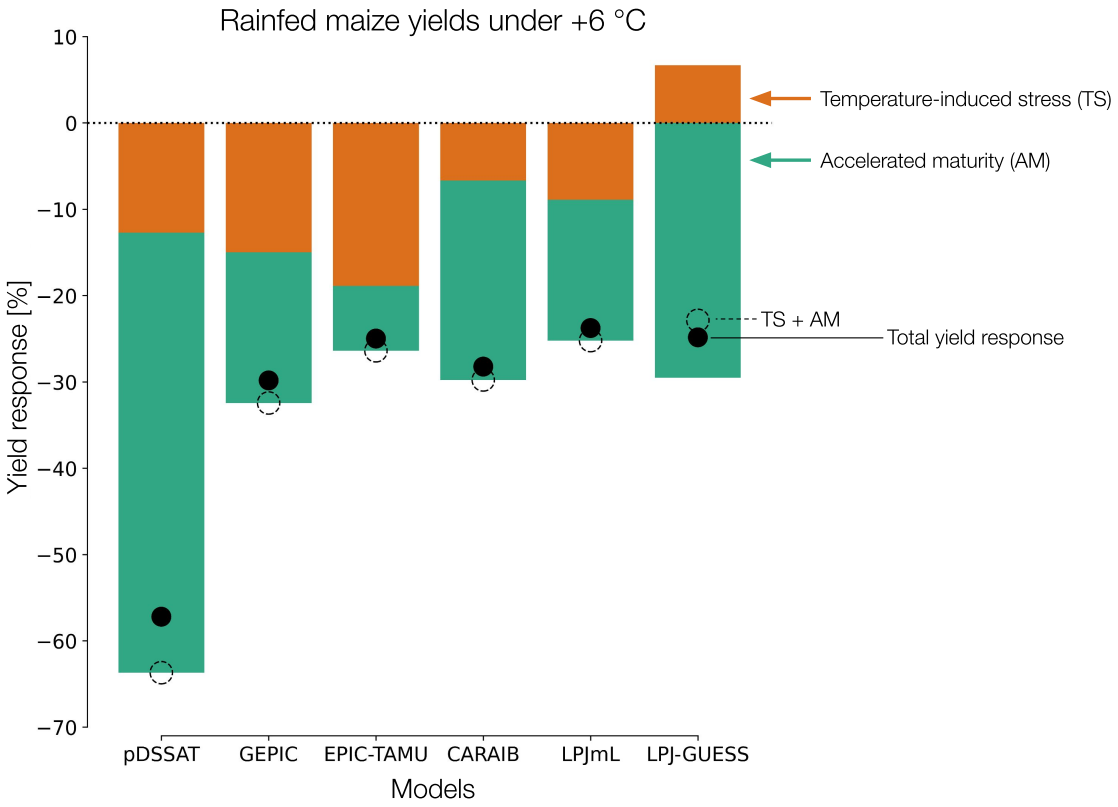

Figure 4.2: Projected yield impacts for rainfed maize under warming. The solid black dots show the average yield response under the +6 °C uniform warming scenario for each GGCMI model. Colored bar plots show the breakdown of yield losses into portions caused accelerated maturity (green) and portions caused by temperature-induced physiological stress (red), per the proposed attribution framework. The open dashed circles show the addition of the two attributed portions. Close agreement between the total yield response and the summed yield response, per our attribution framework, suggest that the framework is valid for separating rainfed yield losses under warming. The framework reveals large portions of yield losses under warming due to accelerated maturity, which can be theoretically alleviated through cultivar adaptation.

4.5 Discussion

In the absence of adaptation, increased temperatures under climate change are projected to accelerate the development of rainfed maize yields in the U.S. Corn Belt, shortening growing periods from sowing to maturity. Yield effects from accelerated maturity are considered to by the main driver of yield reductions under warming [121, 86]. Adapting maize cultivars to restore historical growing periods would effectively counteract this mechanism, with the potential to alleviate a large portion of yield losses under climate change

Our finding that models show realistic growing period responses to historical temperatures stands in contrast to previous studies that suggest models overestimate growing period shortening under warmer temperatures [135, 136]. We argue that this difference is primarily due to our control of variable sowing dates in observations through the multivariate regression; to our understanding, such technique was not performed in previous studies. Sowing date shows a significant negative influence on the growing period for a given maize cultivar maturity, with sowing dates in early spring associated with lower daily GDD values than sowing dates in later spring, resulting in a relatively longer duration of the growing period (in calendar days, Figure SX). Differences between our methodology and that of Zhu et al. (2019), such as the functional form of statistical regressions, may also factor into our different findings for Corn Belt maize [135]. A notable difference between our methods and those of Wu et al. (2019) is our use of historical observations that encompass changing cultivar maturities, while Wu et al. (2019) use field experiments where the same cultivars are used over 15 years [136]. Differences in maize cultivars and management between the Corn Belt and North China Plain may also play a role in this difference.

Our finding that yield responses induced by accelerated maturity drive two thirds of total losses under warming, on average, highlights the potential benefits of adaptation suggested by previous literature [101, 120, 132, 119, 134]. It is important to note, however, that many of these studies use the same process-based models, motivating the use of additional models

for simulated adaptation scenarios. Moreover, the substantial heterogeneity across model yield responses to accelerated maturity merits further research.

A caveat of theoretical cultivar adaptation under severe warming is that will likely require the breeding of cultivars with exceptionally late maturities. Zabel et al. (2021) find that maize farmlands in the Corn Belt are under moderate–serious risk of requiring new cultivars by 2100 to adapt successfully [132]. Analysis of our data corroborates their finding, where average maize maturities in our region range from 944–1770 GDDs in the historical baseline, but increase to 1440–2320 GDDs under the +6 °C adaptation scenario. Initial adaptation measures could shift cultivars in the Corn Belt northward as warming progresses [26], or potentially import cultivars currently bred for warmer pantropical climates. Developing new cultivars for adoption, however, can take up to 30 years [137], and may cause adaptation efforts to lag behind the related increases in Corn Belt warming.

An additional caveat to cultivar-adaptation studies, in general, is the assumption that farmers prioritize their chosen maize cultivar based on the growing period. Evidence shows that U.S. farmers have not historically chosen cultivars to maximize their maturities relative to local heat availability [104]. In some regions, farmers may prioritize other traits over maturity, such as drought tolerance. Under future conditions, Under concerns of extreme weather impacts, which may become more frequent, farmers may choose earlier-maturity cultivars to avoid the risk of potential negative impacts from delayed sowing or late-summer heatwaves. Alternatively, increasing Corn Belt temperatures under climate change are expected to lengthen the annual period of growth-promoting temperatures (i.e. growing seasons) [138], which may provide opportunities for new double cropping systems [139], perhaps similar to soybean-maize systems seen in Brazil [140].

Further research attributing yield response to specific mechanisms in greater depth and scope will help to better evaluate models through functionality-based techniques [98]. Examining modeled adaptation impacts and maturity behaviors in other key agricultural regions,

such as maize in the North China Plain [127, 136], could reveal whether findings in our study generalize across global maize agriculture. Research should also consider additional crops and breadbasket zones (e.g. soybean, wheat, rice) to better understand implications for global food production. Additionally, going beyond fixed-period adaptation to consider rule-based cultivars and shifting sowing dates may reveal greater opportunities for yield benefits under climate change [120].

4.6 Data Availability

All data used in this analysis are publicly available. Simulation outputs from GGCMI phase 2 are available at *https://zenodo.org/*. AgMERRA weather data is available at *https://data.giss.nasa.gov/impacts/agmipcf/agmerra/*. State-level data from the USDA are available at *https://quickstats.nass.usda.gov/*. District-level data from the USDA are available upon request.

CHAPTER 5

PHYSICAL DRIVERS OF U.S. PREVENTED PLANTING EVENTS DIAGNOSED WITH INTERPRETABLE MACHINE LEARNING

Haynes Stephens[1,2], Sophia Horigan[3], Samantha Lapp[4], Raphael Rossellini[5], Eva Burgos[1], Charles Gardner[1], James A. Franke[1,2], Christopher N. Boyer[6], and Elisabeth J. Moyer[1,2]

[1]Department of Geophysical Sciences, University of Chicago, Chicago, IL, USA [2]Center for Robust Decision-making on Climate and Energy Policy (RDCEP), University of Chicago, Chicago, IL, USA [3]Department of Ecology and Evolution, University of Chicago, Chicago, IL, USA [4]Department of Physics, University of Chicago, Chicago, IL, USA [5]Department of Statistics, University of Chicago, Chicago, IL, USA [6]Department of Agricultural & Resource Economics, University of Tennessee, Knoxville, TN, USA

5.1 Abstract

Numerous studies project how climate change will impact future crop yields, but little is known about how it may impact the ability of farmers to plant crops altogether. Extreme weather in 2019 prevented U.S. farmers from planting crops on 19.4 million acres, more than double the previous record. Insurance claims report that most prevented planting events are caused by "excess moisture/precipitation," but the environmental mechanisms underlying these events are not well understood and likely complex. Recent research efforts used statistical regressions to model the environmental drivers of prevented planting, but omitted the effects of soil moisture and soil-weather interactions. Machine learning provides a promising approach to capture potential nonlinear and interactive effects on prevented planting, and leading-edge model interpretation techniques may shed light on key mechanisms at play. Here, we develop a novel machine learning model to predict the occurrence and intensity of prevented planting events based on monthly soil moisture, precipitation, and air temperature, and geospatial information on soil hydrology characteristics. Interpreting the model's historical predictions, we identify spring soil moisture, spring precipitation, and soil drainage

class as primary environmental factors for prevented planting. Additionally, we highlight a interactive effect of heavy spring precipitation following below-freezing January temperatures, suggesting that thawing soils are at greater risk of experiencing prevented planting than unfrozen soils. Insights from model interpretation could enhance the mechanistic understanding of prevented planting and even aid the development of rule-based planting protocols in agricultural models. Under projected climate change, the model predicts prevented planting to become less frequent but more intense relative to the historical period, with high-damage years ($>$ 1m prevented hectares) occurring nearly twice as often. Complementary analysis reveals that prevented planting events often occur on lands above or near unconfined aquifers, and that the unprecedented prevented planting damages in 2019 correspond with the peak of a seven-year rise in groundwater levels; these conditions likely rendered such lands vulnerable to flooding under the year's extreme precipitation. Comprehensively, our findings suggest farmers and insurance providers should be mindful of planting windows that follow cold winters and have heavy spring rainfall forecasts, particularly if groundwater levels are high.

5.2 Introduction

Agricultural production must substantially increase into the future to ensure global food security [141, 142]. However, future soil moisture and precipitation conditions may jeopardize these increases by keeping crops out of the ground altogether.

Extreme weather events in 2019 prevented U.S. farmers from planting crops on over 19.4 million insured acres [143], more than double any year preceding, and resulted in record prevent-planting insurance payouts totaling over $4.5 billion [144]. The majority of prevented acres were planned for planting maize and prevented due to excess moisture or precipitation [144]. Prevented maize planting is a major factor of agricultural production loss for spring-planted crops in the U.S., with over $10 billion dollars in damages from 1996–2022 [144]—of

the 98 million planned maize acres in 2019, nearly 12% (11.4m acres) were prevented from planting, equivalent to a production loss of 129 million tonnes[1]

Saturated and flooded soil conditions can prevent planting by restricting the mobility of farming machinery, where the use of heavy equipment would risk getting stuck or damaging soil health through compaction zones [99]. If such conditions prolong up to the final planting deadlines set by insurance company policies (typically in May–June)[2] , farmers may be forced to claim prevented planting damages.

Weather events and soil characteristics interact in complex ways to determine soil hydrology conditions [145], and the underlying environmental mechanisms that lead to prevented planting are not well understood. A deeper understanding of these mechanisms would enhance our ability to address risk factors for prevented planting and project whether high-damage years (e.g. 2019) could become more common under climate change.

Miao et al. (2016) is, to the author's knowledge, the first study to indirectly model weather impacts on prevented maize planting, finding that heavy spring precipitation reduces planted maize area (a proxy for increased prevented planting) [146]. Boyer et al. (2023) is the first study to focus directly on modeling prevented planting, using a linear model to predict U.S. prevented planting based on monthly temperature and precipitation, and select soil characteristics [147]. Similar to Miao et al. (2016), Boyer et al. find late-spring rainfall values to be positively related to prevented planting intensity; they find soil characteristics to be insignificant. However, Boyer et al (2023) do not isolate areas prevented due to excess moisture and precipitation, instead choosing to include prevented planting by all possible causes. Lee et al. (2023) explore the impacts of monthly water surplus (precipitation minus evaporative demand) on prevented planting due to excess moisture/precipitaiton [18], using

1. Production loss is calculated given the prevented acres would have yielded the average yield of 2019.

2. The final planting date is the last day a producer can plant the insured crop and be eligible for their full crop insurance coverage. The late planting period begins the day after the final planting date for the insured crop and ends 25 days after the final planting date. Final planting date and late planting periods vary by crop and region.

a Poisson pseudo-maximum likelihood estimator to predict prevented planting outcomes in the U.S. Corn Belt—a collection of Midwestern and northern states that produce the vast majority of U.S. maize [148]. They find that greater water surplus in the late spring is associated with more intense prevented planting, and their model predicts prevented maize planting to decrease by 12% under moderate-emissions climate change. These studies form the basis for understanding the physical drivers of prevented planting. However, they do not consider the impacts of soil hydrology conditions or soil-weather interactions, both of which may have important and nonlinear effects.

Machine learning (ML) provides a promising approach to examine the environmental mechanisms that lead to prevented planting. ML models are well-suited to capture nonlinear and interactive effects, and have been previously used to model the complex responses of crop yields [19, 89, 149]. Binary classification models, in particular, are well-suited to identify conditions that lead to extreme weather occurrences [150], such as the infrequent conditions where severe prevented planting occurs. Additionally, leading-edge ML interpretation techniques can help extract physical intuitions from underlying model responses.

Here, we employ an originally developed machine-learning model to predict annual county-level prevented maize area due to excess moisture or precipitation, using monthly weather data and soil hydrology conditions. Due to the high portion of events with no prevented planting (68% of observations), we create a zero-inflated regression (ZIR) model by combining two random forest algorithms—a binary classifier and a regressor—in sequence. The binary classifier predicts the occurrence of prevented planting for a given county, and the regressor predicts the potential intensity of prevented planting as a fraction of the county's total planned maize area. We interpret the model's historical predictions using Shapley values [151], examining what features show the greatest effects on the predicted occurrences and intensities of prevented planting. We project changes in prevented planting under a high-emissions climate change scenario out to the end of the century, using simulations from

an ensemble of earth-system models. Finally, we conduct a supplemental analysis of aquifer distributions and historical groundwater levels in the region, assessing their role in making agricultural lands more or less vulnerable to prevented planting.

5.3 Data and Methods

5.3.1 Planted and Prevented Acreage Data

We use annual reports of county-level planned maize acreage from the U.S. Department of Agriculture (USDA) Farm Service Agency [143] for the years 1996–2022. We filter this data for county-years with over 100 acres of planned maize area. We use annual reports of county-level prevented maize acreage from the USDA Risk Management Agency [144] for the same time period. We filter the reports to include acres designated as prevented due to "excess moisture/precipitation" (see Table S4 for a list of insurance codes). We calculate the fraction of maize area prevented in each county-year by dividing the prevented maize area by the total planned maize area. We include counties within states that lie on or east of the 100th meridian—an arid–humid divide in the physical climate of the U.S. [152]—where the majority of national maize production occurs. This region contains the U.S. Corn Belt, the main area of maize production in the U.S., as well as the Mississippi River Valley, where the majority of prevented maize planting occurse outside of the Upper Midwest [153]. In all, our resulting dataset provides annual prevented planting values for 2305 counties across 37 states. Over 68% of entries in the results dataset have no occurrence of prevented planting (prevented fraction = 0), resulting in a zero-inflated historical sample.

5.3.2 Soil and Weather Data

We use data on natural soil drainage classes from the U.S. Geological Survey Gridded Soil Survey Geographic [154], aggregated from the native 30m resolution to county-level aver-

age values. Soil drainage classes, ranging from excessively drained soils (class=0) to very poorly drained (class=6), are distinguished partly based on the color and presence of iron compounds, which correspond to the frequency and duration of wet periods under natural conditions. We use additional soil hydrology characteristics for maize cropland in each county from Li et al. (2019) [80], including saturated water content, hydraulic conductivity, clay percentage, and organic matter percentage. Additionally, we consider the fraction of cropland in each county that has tile drainage, using cropland and tile drainage acres from the 2017 USDA Census Survey [33] and use them to calculate the county tile-drainage fractions. We assume soil hydrology and drainage characteristics to be fixed in time.

We use monthly historical weather conditions from the Famine Early Warning Systems Network Land Data Assimilation System (FLDAS) [155, 156], produced at a resolution of 0.1° x 0.1°. FLDAS, a product of the National Aeronautics and Space Administration (NASA), is driven by monthly measurements of air temperature and precipitation from the CHIRPS-final and MERRA-2 observations [157, 158], using modeling and data assimilation methods to generate fields of land surface states and fluxes. We use features of monthly air temperature, precipitation, and soil moisture aggregated to the county level for the months January–June (final planting dates across the domain occur by June at the latest).

To project climate change impacts, we use simulated future monthly weather conditions under the Shared Socioeconomic Pathway 8.5 W/m^2 forcing (SSP-585) pathway from five earth-system models in the Coupled Model Intercomparison Project Phase 6 (CMIP6) ensemble (BCC-CSM2-MR, CNRM-CM6-1, CNRM-ESM2-1, IPSL-CM6A-LR, MRI-ESM2-0) [159, 160, 161, 162, 163]. Monthly anomalies from the historical baseline (1996–2022) were taken for years 2023–2100 and aggregated to county levels (in some cases, earth-system model resolution was coarser than county level, and thus grid-cell outputs were dispersed to multiple counties). Projected future conditions were calculated by applying anomalies to historical average FLDAS conditions. We use absolute anomalies for air temperature and

fractional anomalies for precipitation and soil moisture.

5.3.3 Machine Learning Model: Zero-inflated Regression

We design a ZIR model structure to exploit the zero-inflated distribution of historical prevented planting values. Whereas ZIR models are commonly used with discrete count data [164, 165], we create a novel model to deal with our continuous prevented fraction values (0.0–1.0). The ZIR modeling concept is inspired by the framework of the `sci-kit lego` library [166]. Our ZIR model consists of two layers, both using random forest (RF) algorithms. A random forest is a supervised machine-learning algorithm consisting of many decision trees, whose respective predictions are aggregated together into a single prediction [167]. The first layer is an RF classifier that predicts whether prevented planting occurs (no=0, yes=1) for a given county and year. The second layer is an RF regressor that predicts the fraction of county cropland prevented (up to 1.0), given that prevented planting is predicted to occur. Using the two layers in sequence allows the model to predict whether prevented planting will occur, and if so, what the intensity will be. Each RF layer is trained using inputs of weather and soil data. The classifier layer is trained on historical occurrences of prevented planting in binary format (no=0, yes=1). The regressor layer is trained on the fraction of cropland prevented (up to 1.0) for counties with non-zero prevented planting damages. Each layer's hyperparameters (number of estimators, minimum samples per leaf, maximum tree depth, and maximum samples to train each tree) are tuned based on leave-one-out cross-validation for each year in the historical sample. In other words, each fold of the cross-validation is an individual year of the historical sample. For each layer and fold, 25 iterative random searches of the hyperparameter space are performed. We select the best parameter set (out of the 25 iterations) based on average performance across the held-out years.

For exercises related to predicting prevented planting events, we train the layers of the ZIR model on 80% of their respective historical sample, with the remaining 20% held out for

testing. We refer to this model as the predictive ZIR model and use it to predict historical prevented planting events as well as to project future prevented planting events under the SSP-585 emissions pathway.

For exercises related to interpreting model responses, we train the layers of a separate ZIR model on their entire respective historical samples to maximize interpretive power across predictions. We refer to this model as the interpretive ZIR model and use it to examine the marginal effects of weather and soil features on historical predictions. We determine marginal feature effects through Shapley values, a concept rooted in game theory, using the `SHAP` Python package [151, 168]. The Shapley value for a given feature is defined as the marginal effect of that feature on the final prediction, relative to the mean historical prediction. The RF classifier mean prediction is the mean likelihood of a prevented planting occurrence (approximately 30%). The RF regressor mean prediction is the mean fraction of county cropland prevented for non-zero events (5%).

5.3.4 U.S. Aquifer Maps and Groundwater Measurements

We use a map of unconsolidated and semiconsolidated sand and gravel aquifers from the United States Geological Survey to explore their spatial distributions within our region. We also use satellite measurements of groundwater storage from the Gravity Recovery and Climate Experiment (GRACE), a joint mission of the NASA and the German Aerospace Center [169, 170, 171, 172]. Using GRACE satellite data to estimate groundwater storage changes is a widely used practice [173]. We crop the gridded product to our study region and calculate groundwater storage anomalies relative to the mission's 2004–2009 baseline value in units of liquid water equivalent thickness (cm) for a given surface area.

5.4 Results

5.4.1 The zero-inflated regression model accurately predicts historical prevented planting, 2019 data is key for capturing extreme values

The predictive ZIR model demonstrates skill in predicting historical prevented planting events, achieving an overall historical RMSE of 0.042 in units of prevented fraction (Figure 5.1, Table 5.1). Training on data from 2019 is vital to capturing extreme damages, as a model trained without 2019 data predicts the year's total prevented area to be 2.02 million hectares, only about half of the observed 3.80 million hectares (dashed orange line in Figure 5.1). However, by training on some 2019 data (∼80% of the year), the model predicts the total prevented area for the year at 3.54 million hectares, just 7% below the observed value. The model also captures geographical hotspots around the Dakotas and along the Mississippi River Valley (Figure 5.1 inset map). The slight low bias of the model likely stems from its regressor layer, which predicts a maximum historical prevented fraction of 0.64 (relative to the observed maximum of 1.0); this not surprising given the rarity of observations above a 0.64 prevented fraction (n=97, less than 0.2% of the historical sample). Nonetheless, the ZIR model achieves more accurate projections than OLS models of comparable feature sets (Figure S34). Given the ZIR model's accuracy, interpreting its historical predictions may yield insight into the environmental mechanisms that underlie prevented planting events.

Table 5.1: Model score metrics for the RF classifier regressor, and overall model[3]

	RF classifier Accuracy (%)	**RF regressor** RMSE (frac.)	**Overall model** RMSE (frac.)	**Overall model** R^2
Training set (80%, incl. 2019)	95.4	0.062		
Test set	84.2	0.075		
Total historical sample	93.2	0.042	0.044	0.54

3. For the RF classifier and overall model, respective samples include both prevented and non-prevented occurrences. For the RF regressor, respective samples only include prevented occurrences.

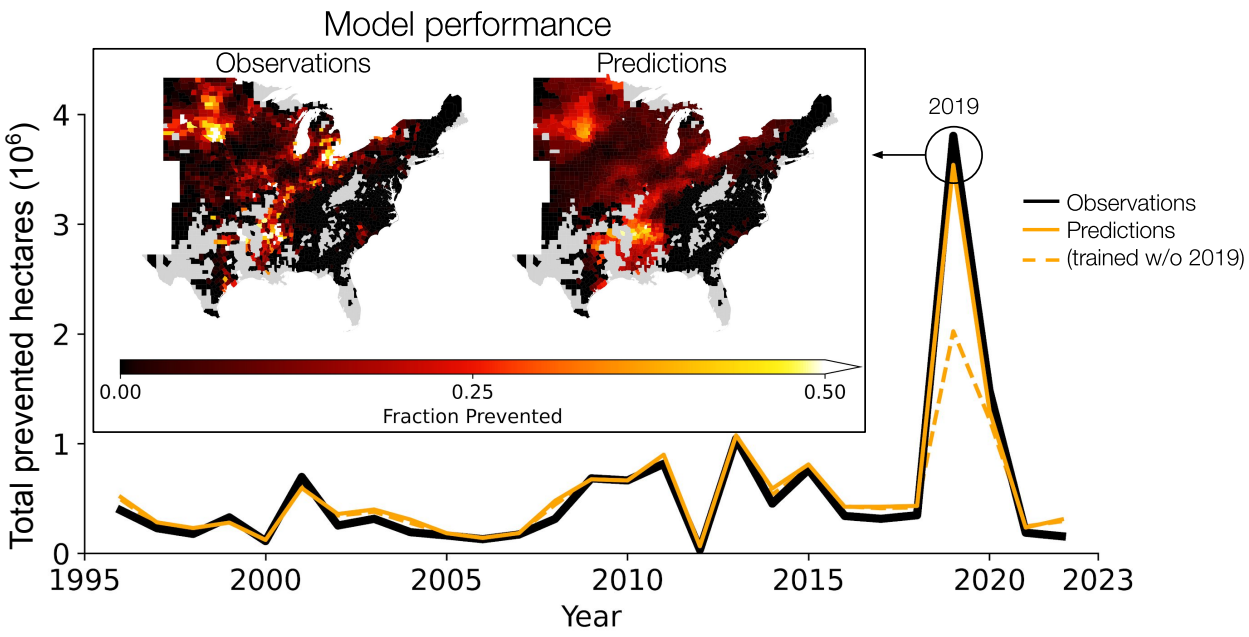

Figure 5.1: Historical performance of the zero-inflated regression model across time and space. The line plot shows historical prevented acres for corn due to excess moisture/precipitation. The black line corresponds to observational data. The solid orange line shows predictions for the model trained on data in all historical years. Inset maps show a comparison between observations and predictions in 2019, with fraction-prevented values corresponding to the color bar below. The dashed orange line shows predictions for a separate model trained without data from 2019. Despite not having training data from 2019, the model still predicts prevented planting in that year to be a record high. However, the predicted value is less than half its observed value, highlighting the importance of 2019 data for the model to reproduce extreme values.

5.4.2 Model interpretation highlights the effects of soil conditions and soil-weather interactions

To maximize the interpretation of non-zero events in a zero-inflated dataset, we train a separate ZIR model on the entire historical sample, referring to this model as the interpretive model.

We identify spring rain and soil moisture as the most important weather features to predicting prevented maize planting events (Figure 5.2). May precipitation ranks as the most important feature for predicting the occurrence of prevented planting, supporting the intuition that precipitation immediately preceding final planting deadlines (typically late

May to early June) is a key factor in prevented planting outcomes. May precipitation shows a nonlinear effect on the likelihood of prevented planting, where the effect is increasingly positive beyond 100 mm but saturates at 250 mm and above (Figure 5.3a).

While precipitation in May, and April to an extent, is important to predicting prevented planting occurrences, soil moisture conditions in April–June are the most important weather features for predicting prevented planting intensities (Figure 5.2). This is also consistent with the intuition that conditions close to the final planting deadlines are important to prevented planting outcomes. Soil moisture values show strong nonlinear effects on the intensity of prevented planting. For example, April soil moisture has little effect until it reaches 0.40 m^3/m^3, at which point the effect steeply increases (Figure 5.3b). Extreme April soil moisture coincides with observations of high-damage prevented planting, supporting the validity of this response in model predictions.

We highlight an interactive effect between between wintertime temperatures and spring precipitation on the predicted likelihood of prevented planting (Figure 5.4a). April precipitation increases the likelihood of prevented planting particularly when following January temperatures below approximately -4°C. The turning point of the January air temperature response around -4°C suggests the model may have derived some understanding of air-soil temperature differences, as -4°C air temperature corresponds to when soils freeze in FLDAS (Figure S35); the model has no explicit inputs of soil temperature[4]. This interactive effect's distinct change from negative to positive suggests that frozen soils may be more prone to prevented planting damages from excess moisture. Cold temperatures may also indicate a shorter upcoming planting window—farmers typically wait until soils reach a given temperature before planting their seed [174, 175, 176, 108]—which could be associated with a higher probability of prevented planting claims. Nonetheless, the ZIR model may be capturing the effects of soil properties implicitly through weather data.

4. We choose to use air temperature as it is more directly tied to observations, and the inclusion of soil temperature does not improve model performance

Soil hydrology characteristics are also important for model predictions, with soil drainage class being the most important characteristic for predicting both the occurrence and intensity of prevented planting (Figure 5.2). The importance of a fixed soil characteristic suggests that the spatial clustering of prevented planting events aligns with areas of poor drainage ability, making them more susceptible to being flooded or saturated under water accumulation. We highlight an interactive effect between soil drainage class and May soil moisture on predicted prevented-planting intensity (Figure 5.4b): whereas well-drained soils (drainage class = 2) require May soil moisture above 0.40 m^3/m^3 to increase prevented planting intensity by $\geq$0.05, poorly drained soils (drainage class = 5) can yield the same effect at a lower moisture threshold (0.35 m^3/m^3). The characteristic of saturated water content (Sat. H2O %) is also important to the predicted likelihood of prevented planting, possibly an indication of its similar spatial pattern with drainage class.

Understanding historically important weather features provides valuable insights into the underlying mechanisms of prevented planting, as well as a framework for understanding future projections under climate change.

5.4.3 High-damage prevented planting becomes more common under climate change

We return to the predictive ZIR model to project the changes in prevented planting occurrence and intensity under climate change. The model projects prevented planting to become less frequent, with occurrences decreasing 37% by the end of the century (Figure 5.5). This decrease in occurrences is likely due to rising temperatures, which consistently reduce the likelihood of occurrence. On the other hand, projected prevented planting intensities become intense under climate change relative to the historical period, increasing on average 28% by the end of the century. The projected increase in average intensity is primarily due to the reduction of low-intensity events, such that the overall average increases. Rare high-intensity

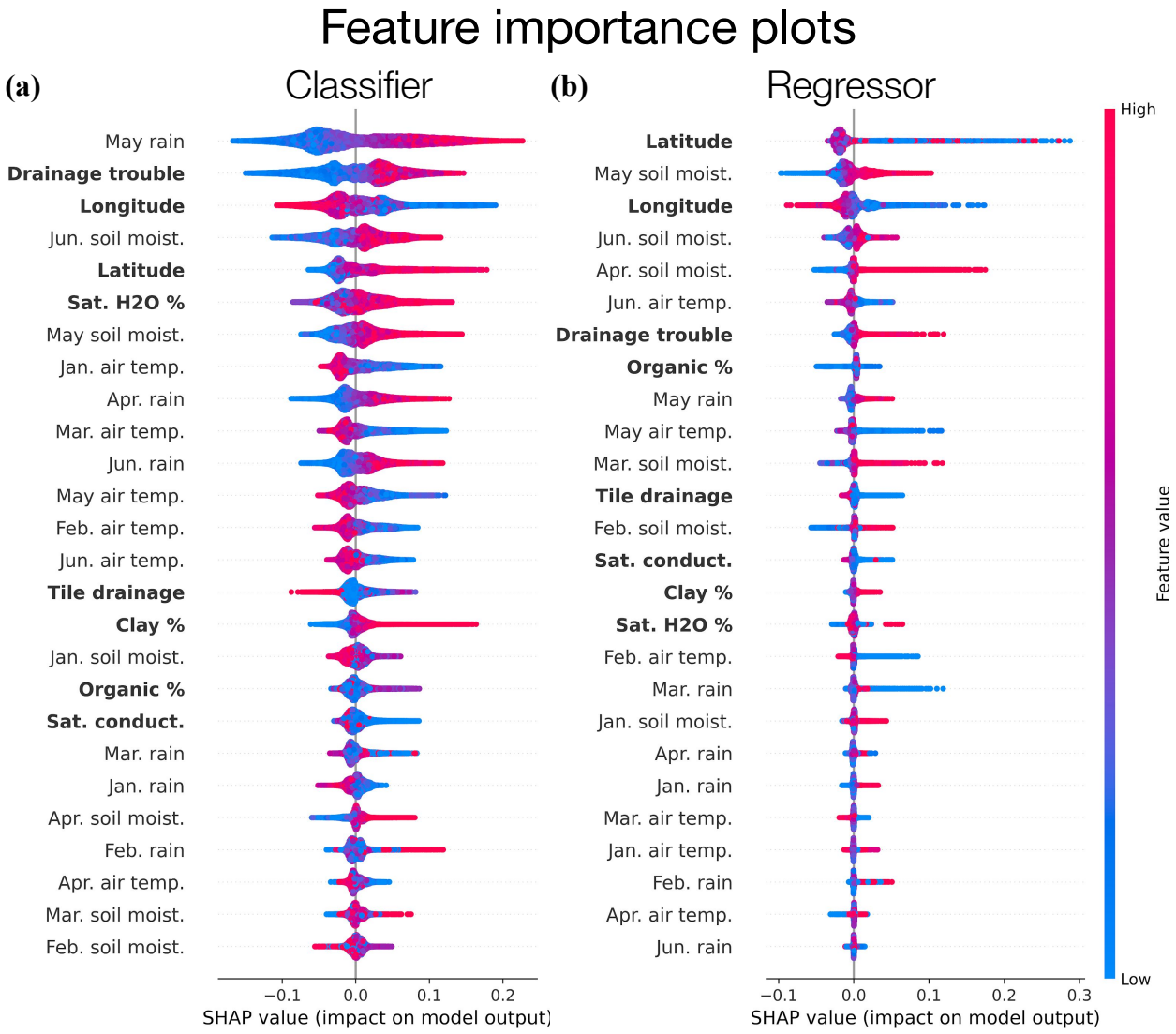

Figure 5.2: Feature importance plots for the **(a)** random forest classifier and **(b)** random forest regressor submodels of the zero-inflated regression model. Each feature of the respective submodel is shown along the y-axis. F or a given feature, each point corresponds to a single instance in the model. A point's color corresponds to the relative feature value, from low (blue) to high (red). The point's position on the x-axis corresponds to its `SHAP` value, i.e. the feature's marginal effect on the ultimate model prediction. The vertical range of points for a given feature shows the distribution of marginal effects across the historical sample. Features are ranked based on their mean absolute effect, from most important (top) to least important (bottom). Soil or spatial characteristics are marked in boldface. Late-spring rainfall and soil moisture features are important to both submodels, backing up physical intuition about prevented planting responses. Spatial features are also important to both submodels. For the classifier, the most important air temperature feature is for the January preceding the given year's planting window.

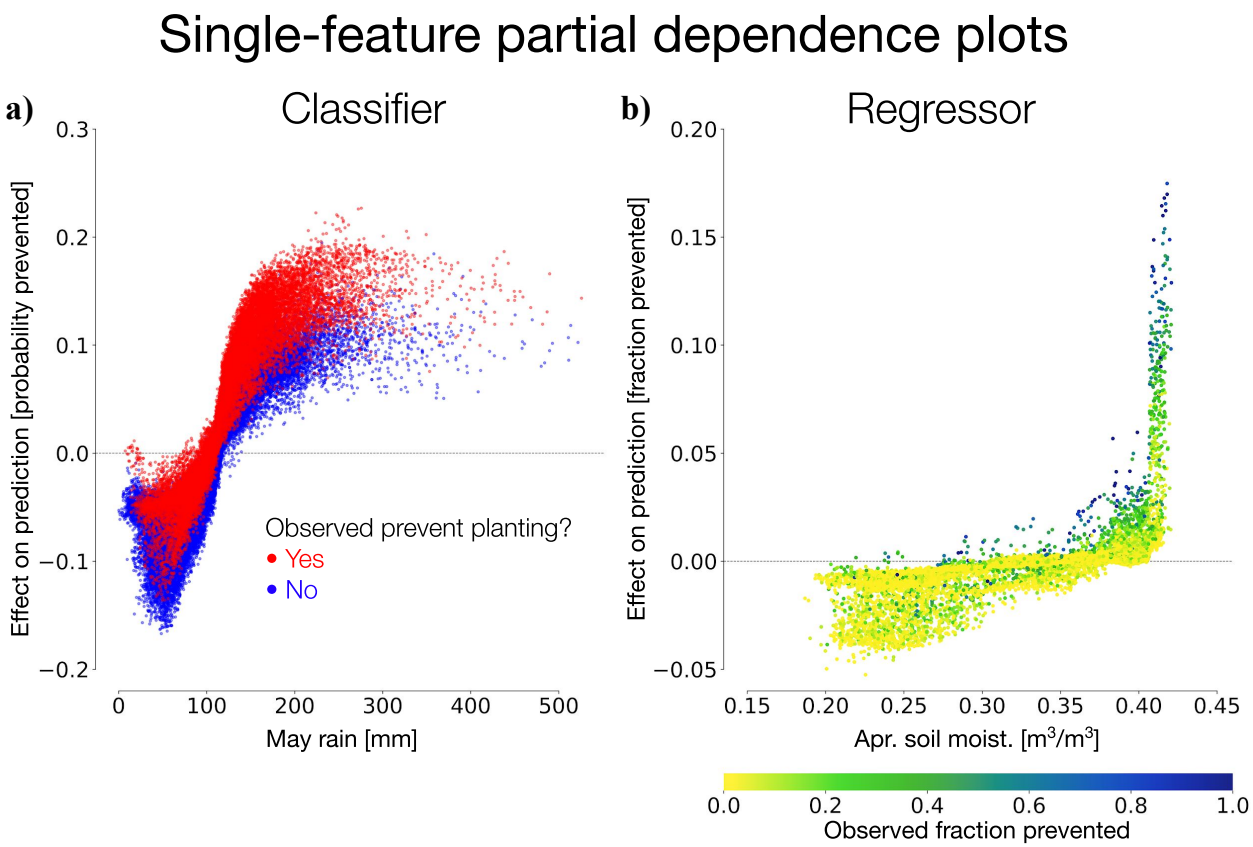

Figure 5.3: Partial dependence plots for some of the most important features in the random forest classifier and regressor submodels of the zero-inflated regression model. Scatter plot **(a)** shows May rainfall values on the x-axis and their marginal effect on classifier predictions on the y-axis. Marginal effects are relative to the mean historical classifier prediction, i.e. the mean probability of prevented planting in the training set ($\simeq$30%). Dot colors correspond to historical instances where prevented planting did occur (red) and did not occur (blue). Scatter plot **(b)** shows April soil moisture values on the x-axis and their marginal effect on regressor predictions on the y-axis. Marginal effects are relative to the mean historical regressor prediction, i.e. the mean intensity of prevented planting cases in the training set ($\simeq$5%) of planned corn acreage in a county). Points are colored based on the observed prevented fraction for a given county year. Model responses to important environmental features show nonlinear behaviors, with extreme rain and soil moisture values increasing predictions in the occurrence and intensity of prevented planting.

events, however, remain in future projections, likely due to extreme precipitation and soil moisture distributions being maintained under future climate scenarios.

While the model does not project single-year damages under climate change to exceed the 2019 record, it does project high-damage years (>1m hectares prevented) to happen more frequently relative to the historical period (Figure S36). In the historical record, total

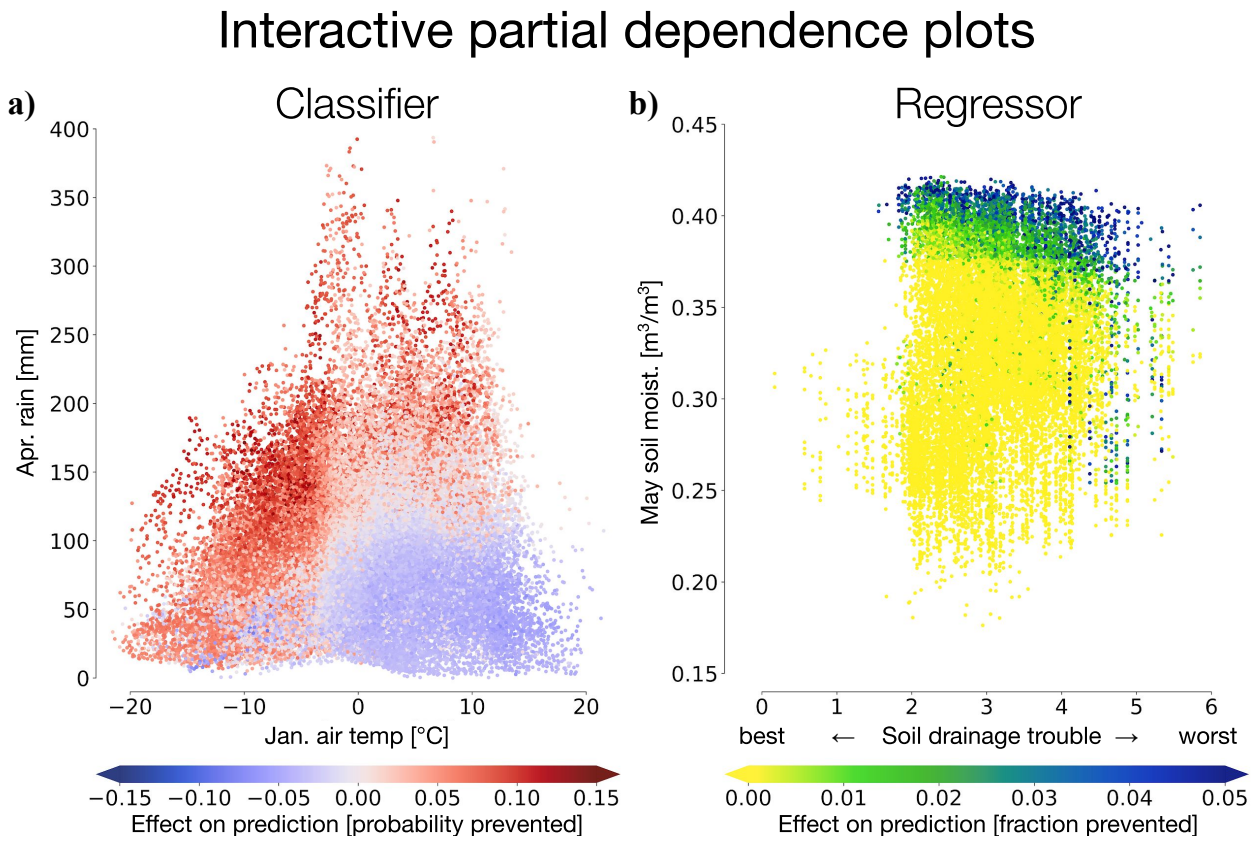

Figure 5.4: Two-dimensional partial dependence plots for some of the most important features in the random forest classifier and regressor submodels of the zero-inflated regression model. Scatter plot **(a)** shows historical instances of January air temperature on the x-axis and subsequent April rain values on the y-axis. Point colors correspond to their combined effect on classifier predictions, either decreasing (blue) or increasing (red) the predicted likelihood of prevented planting occurrences. Scatter plot **(b)** shows values of soil drainage class and May soil moisture, with point colors corresponding to their combined effect on the regressor's predicted intensity of prevented planting. Note: color schemes correspond to classifier or regressor subplots. Model responses to environmental features show interactive effects in the sequencing of weather conditions, as well as the combination of weather and soil characteristics.

U.S. prevented planting exceeds 1 million hectares approximately once every nine years. Under climate change, the model projects prevented planting to exceed 1 million hectares approximately once every five years on average.

We consider a possible adaptation strategy to mitigate prevented planting by increasing the tile drainage of counties in the region. Tile drainage within a given county shows some large negative effects on the predicted likelihood of prevented planting (Figure 5.2), suggest-

ing that areas with high tile drainage may be rendered less vulnerable to prevented planting. Since this is the only feature that deals with farm management, increasing tile drainage could be a potentially effective adaptation strategy to reduce future prevented planting. However, we find limited benefits to this strategy, with a maximum increase in tile drainage (to 100% in each county) leading to just a 10% decrease in total prevented planting area. Low sampling of counties with high tile drainage likely influences these projections, as well as spatial similarities between counties of no tile drainage and low prevented planting, which may cause the model to underestimate the beneficial effects of increased drainage.

5.4.4 Groundwater conditions also likely influence extreme prevented planting events

Areas of prevented planting have high spatial clustering (Figure 5.1 inset map). We see hotspots of prevented planting in the Upper Midwest and along the Mississippi River Valley, with relatively little prevented planting in the Eastern parts of the region. This clustering is reflected by the importance of latitude and longitude in predicting the likelihood and intensity of prevented planting (Figure 5.2), which may indicate that key spatial aspects are omitted from the feature set. To examine this, we investigate the subterranean conditions relevant to prevented planting by analyzing groundwater patterns in the historical period.

Prevented planting damages in 2019 show a spatial pattern similar to the distribution of semiconsolidated, unconsolidated, and glacial deposit aquifers (Figure 5.6). Such aquifers are unconfined, meaning they are open to the atmosphere and typically recharged by rainfall, streamflow, and snowmelt. Unconfined conditions make these aquifers prone to groundwater flooding under extreme rainfall [177] when the water table rises above the land surface. The distribution of semiconsolidated, unconsolidated, and glacial deposit aquifers in the region shares a similar spatial pattern to the total planned maize area, particularly with regards to irrigated maize (Figure 5.6), as aquifers provide groundwater resources for irrigation [178,

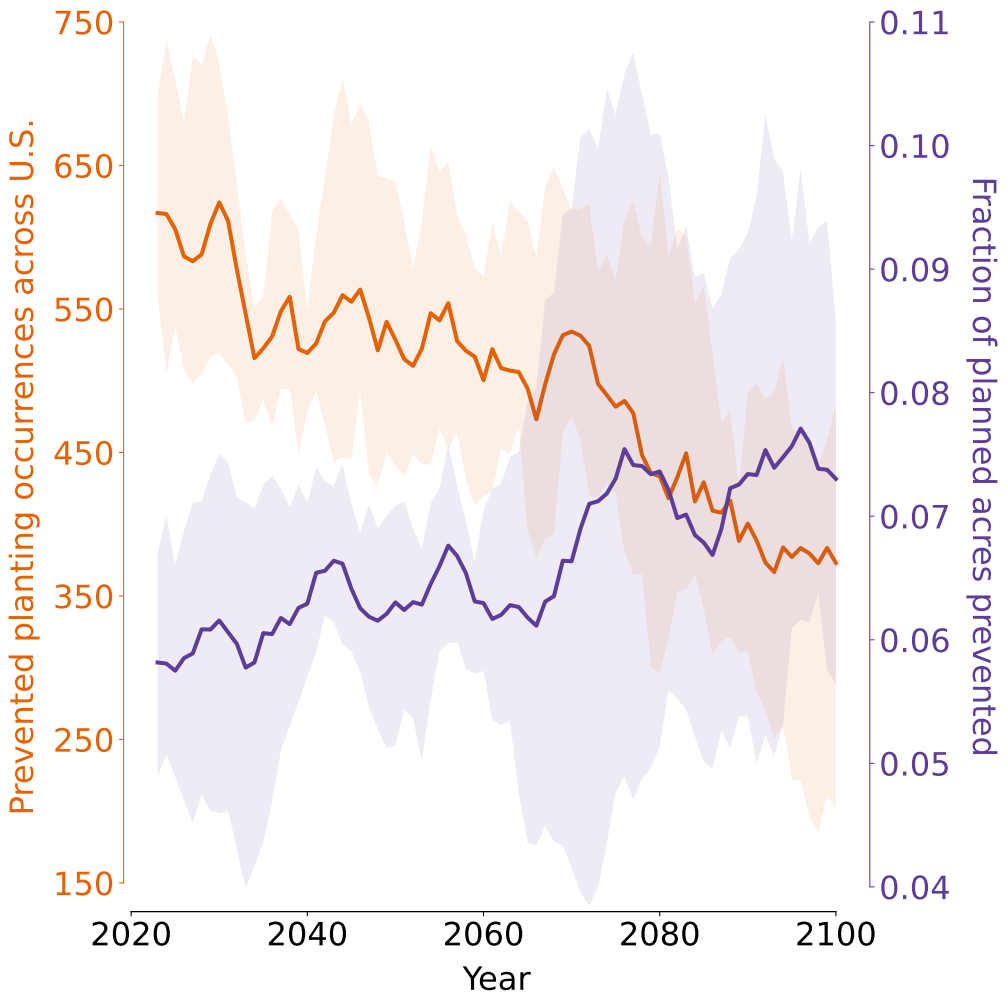

Figure 5.5: Future projections from the random forest classifier and regressor submodels of the zero-inflated regression model. The orange line corresponds to the left y-axis and shows the annual number of prevented planting events, as projected by the classifier, out to the end of the century. The purple line corresponds to the right y-axis and shows the average intensity of prevented planting that occurs, as predicted by the regressor. Colored lines and shaded windows show rolling ten-year averages. Altogether, the zero-inflated regression model projects prevented planting events to be less frequent, but more intense under high-emissions climate change.

179]. Altogether, unconfined aquifers may play a large role in making overlying farmlands prime for agriculture, but they may also put those farmlands at risk of prevented planting.

We also find an temporal association between groundwater levels and years with extreme prevented planting damages. We examine groundwater levels over the region using measurements from the NASA GRACE mission for the period 2004–2023 (Figure 5.7). Groundwater levels in the domain shows an annual cycle, reaching maxima in the spring and minima in the

fall (around November). Following the year 2012 (a major drought year in the region), there is an increasing trend in groundwater storage through the end of 2018, with groundwater levels in November 2018 being the highest of any previous November on record. June levels are likewise higher in 2019 than any previous year. The combination of high groundwater levels and heavy spring rainfall in 2019 may have played a large role in the year's record prevented planting damages. The association between groundwater levels and prevented planting is also present for the year 2020, which has the the second-highest total prevented area on record.

5.5 Discussion

Prevented planting can cause substantial shocks to U.S. maize production. Because the outcomes of prevented planting are determined through insurance claims, there is prime opportunity for developing practical scientific knowledge by deriving a physical understanding of the phenomena. Understanding how soil and weather conditions affect the occurrence and intensity of prevented planting is key to identify warning signs for future years and plan accordingly.

Our results suggest that farmers and insurance providers should be mindful of planting windows that follow cold winters and have heavy spring rainfall forecasts, particularly if groundwater levels are high. A major benefit of our analysis is the identification of risk factors that can be observed before planting windows begin. Testing for frozen soils in the winter months can help actors asses the risk of flooding under heavy spring precipitation. Additionally, timely monitoring of groundwater levels through in-situ techniques or remote observations such as GRACE can provide an idea of how vulnerable agricultural lands may be to prevented planting.

Literature on soil temperatures support the intuition that below-freezing winters increase the likelihood of prevented planting occurrence. Frozen winter soils take longer into the

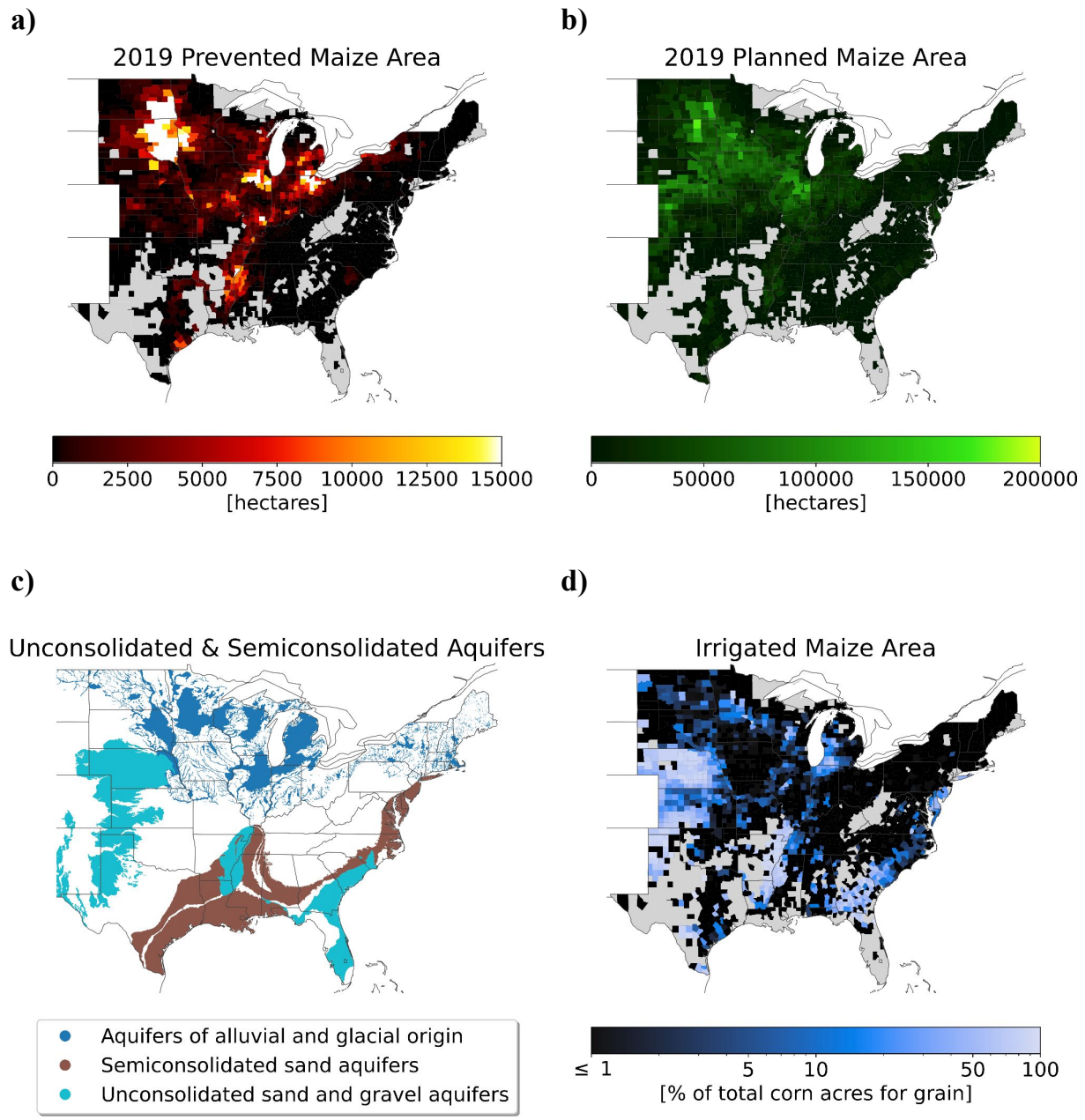

Figure 5.6: **Top left** shows a map of the total prevented maize acres due to excess moisture in 2019. Map plots show **(a)** 2019 determined prevented maize planting area, **(b)** 2019 total planned maize area, **(c)** maize irrigation area, and **(d)** unconsolidated and semiconsolidated aquifers in the domain. Spatial similarities between prevented maize planting and aquifers suggest that aquifers' groundwater storage may play a key role in making regions preferable for farming, particularly for irrigation practices. However, these aquifers may also put the same regions at risk for prevented planting under extreme precipitation.

spring to thaw and can be more prone to spring floods [180, 181]. Additionally, numerous field trials across the U.S. have resulted in robust recommendations for crop planting windows, indicating that soil temperature needs to be above 50 °F for the seeds to germinate [174, 175, 176, 108, 182]. Thus, a late freeze in January could delay planting by keeping soils colder into the planting window.

Incorporating aquifer and groundwater information effectively could aid future prevented planting forecasts. Increasing trends in aquifer groundwater storage in our study region have been identified before, and aquifer groundwater storage in the domain is shown to have a strong association with extreme precipitation [183]. Monitoring future increases in ground-

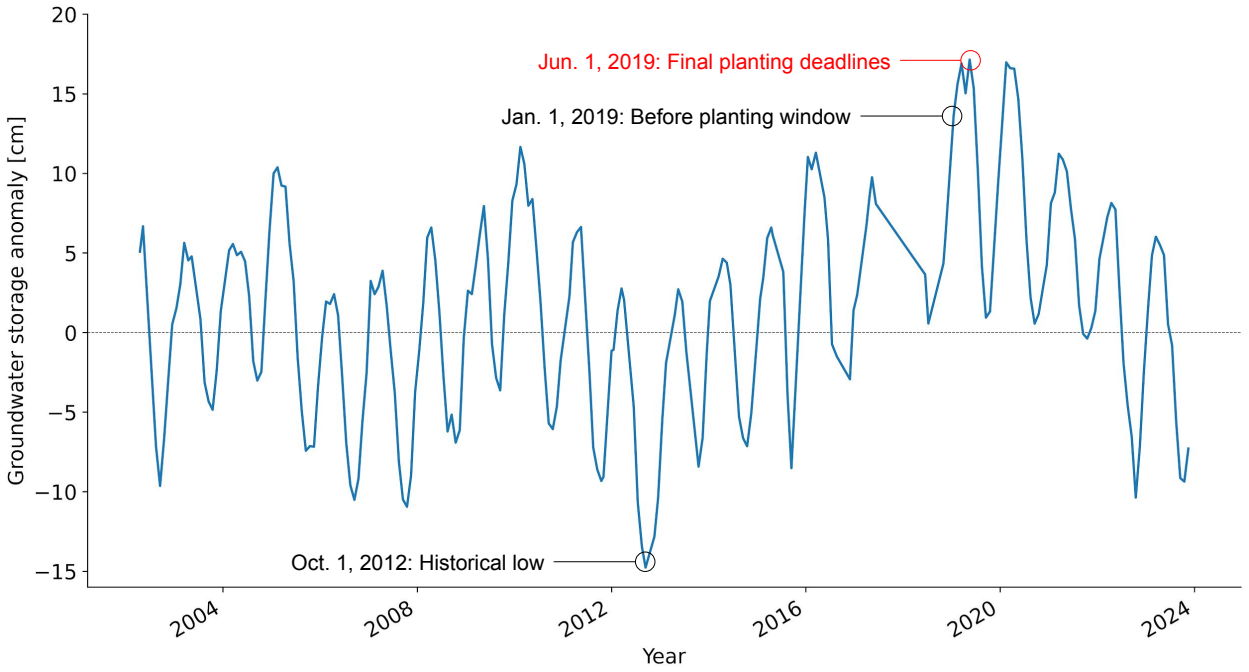

Figure 5.7: Historical records of groundwater storage in the domain. The line plot shows the average groundwater storage anomaly from the NASA GRACE mission (2002–present) in units of liquid water equivalent thickness (cm). Anomalies are relative to a 2004–2009 baseline value; seasonal averages are not removed (typically spring highs and fall lows). Circles mark dates of interest: record low storage in October 2012, as well as storage values in January and June 2019, occurring before and after the maize planting windows, respectively. Groundwater storage in the domain experienced an increasing trend before the 2019 extreme prevented planting outcomes, reaching a record high around the 2019 final planting deadlines. High groundwater levels may indicate years in the domain prone to extreme prevented planting, which could guide future warning forecasts.

water storage and improving seasonal precipitation forecasts may aid in identifying years with potentially high prevented planting damages. Further research examining groundwater levels and local flooding events related to prevented planting in greater detail, possibly using monitoring data from the National Ground-Water Monitoring Network [184], would be useful in guiding model advances. Additionally, the importance of latitude and longitude in both the RF classifier and regressor suggests that the feature set would benefit from additional geospatial information particular to each county, perhaps of higher-than-county resolution.

The importance of spring rainfall in our study aligns with the findings from Boyer et al. (2023) [147] and Lee et al. (2023) [18], who identify April and May precipitation as important features in their respective models. We also find that May air temperatures show an inverse relationship to prevented planting, also in agreement with Boyer et al. (2023) [147].

The importance of soil characteristics in our study is in contrast to the findings of Boyer et al. (2023) [147], which found similar characteristics to be insignificant. Two key differences may play roles in the discrepancy between the two studies. Boyer et al. (2023) model prevented planting due to all possible causes, which may obscure the importance of soil characteristics to acres prevented specifically by excess moisture/precipitation. Additionally, Boyer et al. (2023) consider prevented planting across the continental U.S., including data from the arid western half of the country [152]. Differing model architectures between the studies (OLS model in Boyer et al., 2023) may also play a role. Lee et al. (2023) do not consider soil characteristics in their study [18]. Our results suggest that information about soil hydrology is key to understanding prevented planting.

Lee et al. (2023) project prevented planting to decrease slightly under climate change [18]. Our projection of future prevented planting roughly agrees with this finding, with the decadal average in total prevented area decreasing by roughly 10% and 20% by the middle and end of the century, respectively. However, we project outcomes under a high-emissions

climate scenario, whereas Lee et al. (2023) use a moderate-emissions scenario (RCP4.5). Differences in the ensembles of earth-system models used for future projections may also play a role in the differences between the respective studies.

Our study highlights the finding that high-damage years are projected to become more frequent under climate change. Recurring high-acre damages might impact insurance policies regarding the allowed frequency of farmers to submit prevented-planting claims, similar to the 2021 revision requiring successful planting and harvest within the four most recent crop years [185].

There are notable limitations to our modeling approach. The RF classifier and regressor are both affected by an inability to extrapolate predictions when feature values go beyond their historical sample. Specifically, the RF regressor cannot predict future prevented fractions above its maximum historical prediction (0.67). Another limitation comes from our use of soil moisture outputs by FLDAS, which are subject to the same assumptions and limitations as the land surface model (Noah 3.6.1) that produced them [156]. Additionally, future changes in the possible couplings between temperature, precipitation, and soil moisture, as simulated by the CMIP6 models, may affect the ability of the ZIR model to project prevented planting outcomes beyond the historical sample. Finally, our model does not account for factors of farmer behavior, such as explicit final planting dates or economic considerations in reporting prevented planting versus alternative measures (e.g. moral hazard) [17], which may add noise or biases into the prevented planting observations and resulting model responses.

Future work explicitly incorporating earliest and final planting dates into a machine-learning model could allow for the exploration of adaptation toward prevented planting through advanced planting windows under warming conditions. Additionally, future impact projections could be improved with increased quality of soil moisture changes in the CMIP ensemble, as well as the incorporation of aquifer and groundwater-storage information and

the related changes under warming. We report our historical reproduction and highlight the importance of 2019 data to the ability of our model in capturing extreme prevented planting outcomes. Reports of these two analyses in future studies of prevented planting could aid in model selection and in the interpretation of model predictions.

Our study demonstrates the promise of ML approaches to understanding and predicting the societal impacts of extreme weather events. With the expected intensification of the hydrological cycle under climate change [186], it is pivotal to improve our understanding of these impacts as well as our confidence in accurate future predictions. Leading-edge ML interpretation packages, such as `SHAP`, offer the opportunity to extract detailed insights into historical outcome responses to environmental conditions. These insights, along with future predictions, would be valuable to stakeholders and decision-makers in their strategies to mitigate and adapt to ongoing climate change.

5.6 Data Availability

All data used in this analysis are publicly available. Planned and prevented acreage data can be found at *https://www.fsa.usda.gov/news-room/efoia/electronic-reading-room/frequently-requested-information/crop-acreage-data/index* and *https://www.rma.usda.gov/en/Information-Tools/Summary-of-Business/Cause-of-Loss*. Tile drainage data can be found at *https://quickstats.nass.usda.gov/*. FLDAS data can be found at *https://ldas.gsfc.nasa.gov/fldas*. Data for soil conditions on maize cropland can be found at Li et al. (2019) [80]. Data for soil drainage classifications can be found at *https://www.nrcs.usda.gov/resources/data-and-reports/gridded-soil-survey-geographic-gssurgo-database*. Shapefile maps of unconsolidated and semi-consolidated aquifers are available at *https://www.usgs.gov/mission-areas/water-resources/science/unconsolidated-and-semiconsolidated-sand-and-gravel-aquifers*. GRACE/GRACE-FO Mascon data are available at *http://grace.jpl.nasa.gov*.

CHAPTER 6

CONCLUSION

In this work, I present: a "perfect model" experiment evaluating the ability of degree-day-based statistical models to project yield impacts under climate warming; an evaluation of maturity acceleration responses in process-based models using a new observational dataset, and; an original machine learning model that predicts prevented planting due to excess moisture and precipitation, as well as impacts under projected climate change.

We conclude that statistical models that include features of heat stress or omit features of moisture stress are prone to overproject yield losses under warming. In addition, we determine that process-based models well represent the responses of changes in maturity length to temperature based on evaluations from observations, suggesting that projected yield losses due to accelerated maturity (and likewise gains from maturity adaptation) may be reasonable. Finally, we find that the prevalence of prevented maize acres is impacted by soil drainage, and springtime rain and soil moisture conditions, and frozen winter temperatures. Under future climate change, prevented planting instances are predicted to decrease but become more severe, with high-prevented years occurring more frequently relative to the historical period.

There are limitations to the models and data I use in this research. Process-based model outputs have known issues reproducing historical yield records [13, 14], which may limit the efficacy of applying findings from "perfect model" experiments into practice. Additionally, while we validate the growing period responses to warming in GGCMI models, the subsequential yield response to growing period changes varies widely among the models, a matter that has not yet been explained. Finally, using machine learning models to predict agricultural outcomes from environmental drivers is a recent and ongoing research topic [19, 187, 90]. Challenges to machine-learning models remain in extracting physical understanding from model predictions and reducing uncertainties in future projections [57, 149, 89, 188].

Nevertheless, these research chapters contribute valuable findings toward better understanding how environmental factors affect U.S. maize production and projections under future climate change. Future research would benefit from advancing "perfect model" experiments, using newer simulations and evaluating newer statistical models, such as machine learning yield models. Additionally, higher-resolution maturity observations should be incorporated into the tuning of process-based model for historical simulations, rooting the models further in ground truth data. Both process-based and statistical yield models could benefit from incorporating effects of extreme precipitation and moisture, based on the findings of our prevented planting model. Lastly, the expansion of the analyses used in these chapters onto other crops and agricultural regions would result in wider advances in understanding the impacts of climate change on global food security.

REFERENCES

[1] Ronald D. Sands, Birgit Meade, James L. Seale, Jr., Sherman Robinson, and Riley Seeger. Scenarios of Global Food Consumption: Implications for Agriculture. Technical Report ERR-323, U.S. Department of Agriculture, Economic Research Service, 2023.

[2] James W. Jones, John M. Antle, Bruno Basso, Kenneth J. Boote, Richard T. Conant, Ian Foster, H. Charles J. Godfray, Mario Herrero, Richard E. Howitt, Sander Janssen, Brian A. Keating, Rafael Munoz-Carpena, Cheryl H. Porter, Cynthia Rosenzweig, and Tim R. Wheeler. Brief history of agricultural systems modeling. *Agricultural Systems*, 155:240–254, 2017.

[3] J. W. Jones, G. Hoogenboom, C. H. Porter, K. J. Boote, W. D. Batchelor, L. A. Hunt, P. W. Wilkens, U. Singh, A. J. Gijsman, and J. T. Ritchie. The DSSAT cropping system model. *European Journal of Agronomy*, 18(3-4), 2003.

[4] C. A. Jones and J. R. Kiniry. *CERES-Maize: A Simulation Model of Maize Growth and Development*. Texas A\&M Univ. Press, College Station., 1986.

[5] Senthold Asseng, Ian Foster, and Neil C. Turner. The impact of temperature variability on wheat yields. *Global Change Biology*, 17(2):997–1012, 2011.

[6] Cynthia Rosenzweig, Joshua Elliott, Delphine Deryng, Alex C. Ruane, Christoph Müller, Almut Arneth, Kenneth J. Boote, Christian Folberth, Michael Glotter, Nikolay Khabarov, Kathleen Neumann, Franziska Piontek, Thomas A.M. Pugh, Erwin Schmid, Elke Stehfest, Hong Yang, and James W. Jones. Assessing agricultural risks of climate change in the 21st century in a global gridded crop model intercomparison. *Proceedings of the National Academy of Sciences of the United States of America*, 111(9):3268–3273, 2014.

[7] J. Elliott, C. Müller, D. Deryng, J. Chryssanthacopoulos, K. J. Boote, M. Büchner, I. Foster, M. Glotter, J. Heinke, T. Iizumi, R. C. Izaurralde, N. D. Mueller, D. K. Ray, C. Rosenzweig, A. C. Ruane, and J. Sheffield. The Global Gridded Crop Model Intercomparison: Data and modeling protocols for Phase 1 (v1.0). *Geoscientific Model Development*, 8(2):261–277, 2015.

[8] David B. Lobell and Marshall B. Burke. On the use of statistical models to predict crop yield responses to climate change. *Agricultural and Forest Meteorology*, 150(11):1443–1452, 2010.

[9] David B. Lobell and Christopher B. Field. Global scale climate-crop yield relationships and the impacts of recent warming. *Environmental Research Letters*, 2(1), 2007.

[10] Wolfram Schlenker and Michael J. Roberts. Nonlinear temperature effects indicate severe damages to U.S. crop yields under climate change. *Proceedings of the National Academy of Sciences of the United States of America*, 106(43):15594–15598, 2009.

[11] D. B. Lobell, Wolfram Schlenker, and Justin Costa-Robers. Climate Trends and Global Crop Production Since 1980. *Science*, 2011.

[12] Michael J. Roberts, Noah O. Braun, Thomas R. Sinclair, David B. Lobell, and Wolfram Schlenker. Comparing and combining process-based crop models and statistical models with some implications for climate change. *Environmental Research Letters*, 12(9), 2017.

[13] Christoph Müller, Joshua Elliott, James Chryssanthacopoulos, Almut Arneth, Juraj Balkovic, Philippe Ciais, Delphine Deryng, Christian Folberth, Michael Glotter, Steven Hoek, Toshichika Iizumi, Roberto C. Izaurralde, Curtis Jones, Nikolay Khabarov, Peter Lawrence, Wenfeng Liu, Stefan Olin, Thomas A.M. Pugh, Deepak K. Ray, Ashwan Reddy, Cynthia Rosenzweig, Alex C. Ruane, Gen Sakurai, Erwin Schmid, Rastislav Skalsky, Carol X. Song, Xuhui Wang, Allard De Wit, and Hong Yang. Global gridded crop model evaluation: Benchmarking, skills, deficiencies and implications. *Geoscientific Model Development*, 10(4):1403–1422, 2017.

[14] James A. Franke, Christoph Müller, Joshua Elliott, Alex C. Ruane, Jonas Jägermeyr, Juraj Balkovic, Philippe Ciais, Marie Dury, Pete D. Falloon, Christian Folberth, Louis François, Tobias Hank, Munir Hoffmann, R. Cesar Izaurralde, Ingrid Jacquemin, Curtis Jones, Nikolay Khabarov, Marian Koch, Michelle Li, Wenfeng Liu, Stefan Olin, Meridel Phillips, Thomas A.M. Pugh, Ashwan Reddy, Xuhui Wang, Karina Williams, Florian Zabel, and Elisabeth J. Moyer. The GGCMI Phase 2 experiment: Global gridded crop model simulations under uniform changes in CO2, temperature, water, and nitrogen levels (protocol version 1.0). *Geoscientific Model Development Discussions*, 13:2315–2336, 2020.

[15] Jonas Jägermeyr and Katja Frieler. Spatial variations in crop growing seasons pivotal to reproduce global fluctuations in maize and wheat yields. *Science Advances*, 4(11):eaat4517, November 2018.

[16] Christian Folberth, Joshua Elliott, Christoph Müller, Juraj Balkovic, James Chryssanthacopoulos, Roberto C. Izaurralde, Curtis D. Jones, Nikolay Khabarov, Wenfeng Liu, Ashwan Reddy, Erwin Schmid, Rastislav Skalský, Hong Yang, Almut Arneth, Philippe Ciais, Delphine Deryng, Peter J. Lawrence, Stefan Olin, Thomas A. M. Pugh, Alex C. Ruane, and Xuhui Wang. Uncertainties in global crop model frameworks: Effects of cultivar distribution, crop management and soil handling on crop yield estimates. *Biogeosciences Discussions*, December 2016.

[17] Christopher N. Boyer and S. Aaron Smith. Evaluating Changes to Prevented Planting Provision on Moral Hazard. *Journal of Agricultural and Applied Economics*, 51(02):315–327, May 2019.

[18] Seunghyun Lee and John T Abatzoglou. Effects of water surplus on prevented planting in the US Corn Belt for corn and soybeans. *Environmental Research Communications*, 5(9):095014, September 2023.

[19] Andrew Crane-Droesch. Machine learning methods for crop yield prediction and climate change impact assessment in agriculture. *Environmental Research Letters*, 13(11), 2018.

[20] Yanghui Kang, Mutlu Ozdogan, Xiaojin Zhu, Zhiwei Ye, Christopher Hain, and Martha Anderson. Comparative assessment of environmental variables and machine learning algorithms for maize yield prediction in the US Midwest. *Environmental Research Letters*, 15(6):064005, June 2020.

[21] Tianfang Xu, Kaiyu Guan, Bin Peng, Shiqi Wei, and Lei Zhao. Machine Learning-Based Modeling of Spatio-Temporally Varying Responses of Rainfed Corn Yield to Climate, Soil, and Management in the U.S. Corn Belt. *Frontiers in Artificial Intelligence*, 4:647999, May 2021.

[22] Food and Agriculture Organization of the United Nations (FAO). FAO Statistical Database, 2021.

[23] Peter Ranum, Juan Pablo Peña-Rosas, and Maria Nieves Garcia-Casal. Global maize production, utilization, and consumption. *Annals of the New York Academy of Sciences*, 1312(1):105–112, April 2014.

[24] Mansour Almazroui, M. Nazrul Islam, Fahad Saeed, Sajjad Saeed, Muhammad Ismail, Muhammad Azhar Ehsan, Ismaila Diallo, Enda O'Brien, Moetasim Ashfaq, Daniel Martínez-Castro, Tereza Cavazos, Ruth Cerezo-Mota, Michael K. Tippett, William J. Gutowski, Eric J. Alfaro, Hugo G. Hidalgo, Alejandro Vichot-Llano, Jayaka D. Campbell, Shahzad Kamil, Irfan Ur Rashid, Mouhamadou Bamba Sylla, Tannecia Stephenson, Michael Taylor, and Mathew Barlow. Projected Changes in Temperature and Precipitation Over the United States, Central America, and the Caribbean in CMIP6 GCMs. *Earth Systems and Environment*, 5(1):1–24, January 2021.

[25] R.S. Vose, D.R. Easterling, K.E. Kunkel, A.N. LeGrande, and M.F. Wehner. Ch. 6: Temperature Changes in the United States. Climate Science Special Report: Fourth National Climate Assessment, Volume I. Technical report, U.S. Global Change Research Program, 2017.

[26] James A. Franke, Christoph Müller, Sara Minoli, Joshua Elliott, Christian Folberth, Charles Gardner, Tobias Hank, Roberto Cesar Izaurralde, Jonas Jägermeyr, Curtis D. Jones, Wenfeng Liu, Stefan Olin, Thomas A.M. Pugh, Alex C. Ruane, Haynes Stephens, Florian Zabel, and Elisabeth J. Moyer. Agricultural breadbaskets shift poleward given adaptive farmer behavior under climate change. *Global Change Biology*, 28(1):167–181, 2021.

[27] Saman Armal, Naresh Devineni, and Reza Khanbilvardi. Trends in Extreme Rainfall Frequency in the Contiguous United States: Attribution to Climate Change and Climate Variability Modes. *Journal of Climate*, 31(1):369–385, January 2018.

[28] Jianting Zhu. Impact of Climate Change on Extreme Rainfall across the United States. *Journal of Hydrologic Engineering*, 18(10):1301–1309, October 2013.

[29] D.R. Easterling, J.R. Arnold, T. Knutson, K.E. Kunkel, A.N. LeGrande, L.R. Leung, R.S. Vose, D.E. Waliser, and M.F. Wehner. Ch. 7: Precipitation Change in the United States. Climate Science Special Report: Fourth National Climate Assessment, Volume I. Technical report, U.S. Global Change Research Program, 2017.

[30] Miroslav Trnka, Kurt Christian Kersebaum, Josef Eitzinger, Michael Hayes, Petr Hlavinka, Mark Svoboda, Martin Dubrovský, Daniela Semerádová, Brian Wardlow, Eduard Pokorný, Martin Možný, Don Wilhite, and Zdeněk Žalud. Consequences of climate change for the soil climate in Central Europe and the central plains of the United States. *Climatic Change*, 120(1-2):405–418, September 2013.

[31] C. Segura, G. Sun, S. McNulty, and Y. Zhang. Potential impacts of climate change on soil erosion vulnerability across the conterminous United States. *Journal of Soil and Water Conservation*, 69(2):171–181, March 2014.

[32] Tushar Sinha and Keith A. Cherkauer. Impacts of future climate change on soil frost in the midwestern United States. *Journal of Geophysical Research: Atmospheres*, 115(D8):2009JD012188, April 2010.

[33] USDA/NASS QuickStats Ad-hoc Query Tool. https://quickstats.nass.usda.gov/, 2023.

[34] Antoine Couëdel, Juan Ignacio Rattalino Edreira, Romulo Pisa Lollato, Sotirios Archontoulis, Victor Sadras, and Patricio Grassini. Assessing environment types for maize, soybean, and wheat in the United States as determined by spatio-temporal variation in drought and heat stress. *Agricultural and Forest Meteorology*, 307:108513, September 2021.

[35] J. Hansen, D. Johnson, A. Lacis, S. Lebedeff, P. Lee, D. Rind, and G. Russell. Climate Impact of Increasing Atmospheric Carbon Dioxide. *Science*, 213(4511):957–966, 1981.

[36] Ethan E. Butler, Nathaniel D. Mueller, and Peter Huybers. Peculiarly pleasant weather for US maize. *Proceedings of the National Academy of Sciences*, 115(47):11935–11940, 2018.

[37] Tamma A. Carleton and Solomon M. Hsiang. Social and economic impacts of climate. *Science*, 353(6304), 2016.

[38] John R. Porter, Liyong Xie, Andrew J. Challinor, Kevern Cochrane, S. Mark Howden, Muhammad Mohsin Iqbal, David B. Lobell, Maria Isabel Travasso, Pramod Aggarwal, Kaija Hakala, and Joanne Jordan. Food security and food production systems. *Climate Change 2014 Impacts, Adaptation and Vulnerability: Part A: Global and Sectoral Aspects*, 1:485–534, 2014.

[39] C. Mbow, C. Rosenzweig, L.G. Barioni, T.G. Benton, M. Herrero, M. Krishnapillai, E. Liwenga, P. Pradhan, M.G. Rivera-Ferre, T. Sapkota, F.N. Tubiello, and Y. Xu. Climate Change and Land: An IPCC special report on climate change, desertification, land degradation, sustainable land management, food security, and greenhouse gas fluxes in terrestrial ecosystems. In *IPCC*, pages 437–550. 2019.

[40] T. Wheeler and J. von Braun. Climate Change Impacts on Global Food Security. *Science*, 341(6145):508–513, 2013.

[41] R. H. Hooker. Correlation of the Weather and Crops. *Journal of the Royal Statistical Society*, 70(1):1–51, 1907.

[42] J. Warren Smith. The effect of weather upon the yield of corn. *Monthly Weather Review*, 42(2):78–92, 1914.

[43] H. A. Wallace. Mathematical Inquiry Into the Effect of Weather on Corn Yield in the Eight Corn Belt States. *Monthly Weather Review*, 48(8):439–446, 1920.

[44] J A Hodges. The Effect of Rainfall and Temperature on Corn Yields in Kansas. *Journal of Farm Economics*, 13(2):305–318, 1932.

[45] David B. Lobell and Gregory P. Asner. Climate and management contributions to recent trends in U.S. agricultural yields. *Science*, 299(5609):1032, 2003.

[46] Deepak K. Ray, Paul C. West, Michael Clark, James S. Gerber, V. Prishchepov, and Snigdhansu Chatterjee. Climate change has likely already affected global food production. *PLoS ONE*, pages 1–18, 2019.

[47] Xiao Zhu, Tara J Troy, and Naresh Devineni. Stochastically modeling the projected impacts of climate change on rainfed and irrigated US crop yields. *Environmental Research Letters*, 14(7):074021, July 2019.

[48] James Rising and Naresh Devineni. Crop switching reduces agricultural losses from climate change in the United States by half under RCP 8.5. *Nature Communications*, 11(1):4991, October 2020.

[49] Jesse Tack, Andrew Barkley, and Lawton Lanier Nalley. Effect of warming temperatures on US wheat yields. *Proceedings of the National Academy of Sciences*, 112(22):6931–6936, June 2015.

[50] Mingfang Ting, Corey Lesk, Chunyu Liu, Cuihua Li, Radley M. Horton, Ethan D. Coffel, Cassandra D. W. Rogers, and Deepti Singh. Contrasting impacts of dry versus humid heat on US corn and soybean yields. *Scientific Reports*, 13(1):710, January 2023.

[51] Bernhard Schauberger, Sotirios Archontoulis, Almut Arneth, Juraj Balkovic, Philippe Ciais, Delphine Deryng, Joshua Elliott, Christian Folberth, Nikolay Khabarov,

Christoph Müller, Thomas A.M. Pugh, Susanne Rolinski, Sibyll Schaphoff, Erwin Schmid, Xuhui Wang, Wolfram Schlenker, and Katja Frieler. Consistent negative response of US crops to high temperatures in observations and crop models. *Nature Communications*, 8, 2017.

[52] Daljeet S. Dhaliwal and Martin M. Williams. Evidence of sweet corn yield losses from rising temperatures. *Scientific Reports*, 12(1):18218, October 2022.

[53] Jianghao Wang, Junjie Zhang, and Peng Zhang. Rising temperature threatens China's cropland. *Environmental Research Letters*, 17(8):084042, August 2022.

[54] Xiaoguang Chen, Xiaomeng Cui, and Jing Gao. Differentiated agricultural sensitivity and adaptability to rising temperatures across regions and sectors in China. *Journal of Environmental Economics and Management*, 119:102801, May 2023.

[55] Ariel Ortiz-Bobea, Haoying Wang, Carlos M. Carrillo, and Toby R. Ault. Unpacking the climatic drivers of US agricultural yields. *Environmental Research Letters*, 14(6), 2019.

[56] Jonathan Proctor, Angela Rigden, Duo Chan, and Peter Huybers. More accurate specification of water supply shows its importance for global crop production. *Nature Food*, 3(9):753–763, September 2022.

[57] Yan Li, Kaiyu Guan, Albert Yu, Bin Peng, Lei Zhao, Bo Li, and Jian Peng. Toward building a transparent statistical model for improving crop yield prediction: Modeling rainfed corn in the U.S. *Field Crops Research*, 234, 2019.

[58] A. J. Rigden, N. D. Mueller, N. M. Holbrook, N. Pillai, and P. Huybers. Combined influence of soil moisture and atmospheric evaporative demand is important for accurately predicting US maize yields. *Nature Food*, 1(2):127–133, 2020.

[59] Andrew Hultgren, Tamma Carleton, Michael Delgado, Diana R. Gergel, Michael Greenstone, Trevor Houser, Solomon Hsiang, Amir Jina, Robert E. Kopp, Steven B. Malevich, Kelly McCusker, Terin Mayer, Ishan Nath, James Rising, Ashwin Rode, and Jiacan Yuan. Estimating Global Impacts to Agriculture from Climate Change Accounting for Adaptation. *SSRN Electronic Journal*, 2022.

[60] Alex C. Ruane, Nicholas I. Hudson, Senthold Asseng, Davide Camarrano, Frank Ewert, Pierre Martre, Kenneth J. Boote, Peter J. Thorburn, Pramod K. Aggarwal, Carlos Angulo, Bruno Basso, Patrick Bertuzzi, Christian Biernath, Nadine Brisson, Andrew J. Challinor, Jordi Doltra, Sebastian Gayler, Richard Goldberg, Robert F. Grant, Lee Heng, Josh Hooker, Leslie A. Hunt, Joachim Ingwersen, Roberto C. Izaurralde, Kurt Christian Kersebaum, Soora Naresh Kumar, Christoph Müller, Claas Nendel, Garry O'Leary, Jørgen E. Olesen, Tom M. Osborne, Taru Palosuo, Eckart Priesack, Dominique Ripoche, Reimund P. Rötter, Mikhail A. Semenov, Iurii Shcherbak, Pasquale Steduto, Claudio O. Stöckle, Pierre Stratonovitch, Thilo Streck, Iwan Supit, Fulu Tao,

Maria Travasso, Katharina Waha, Daniel Wallach, Jeffrey W. White, and Joost Wolf. Multi-wheat-model ensemble responses to interannual climate variability. *Environmental Modelling and Software*, 81:86–101, 2016.

[61] James A. Franke, Christoph Müller, Joshua Elliott, Alex C. Ruane, Jonas Jägermeyr, Juraj Balkovic, Philippe Ciais, Marie Dury, Pete D. Falloon, Christian Folberth, Louis François, Tobias Hank, Munir Hoffmann, R. Cesar Izaurralde, Ingrid Jacquemin, Curtis Jones, Nikolay Khabarov, Marian Koch, Michelle Li, Wenfeng Liu, Stefan Olin, Meridel Phillips, Thomas A.M. Pugh, Ashwan Reddy, Xuhui Wang, Karina Williams, Florian Zabel, and Elisabeth J. Moyer. The GGCMI Phase 2 emulators: Global gridded crop model responses to changes in CO2, temperature, water, and nitrogen (version 1.0). *Geoscientific Model Development*, 13:3995–4018, 2020.

[62] Corey Lesk, Weston Anderson, Angela Rigden, Onoriode Coast, Jonas Jägermeyr, Sonali McDermid, Kyle F. Davis, and Megan Konar. Compound heat and moisture extreme impacts on global crop yields under climate change. *Nature Reviews Earth & Environment*, 3(12):872–889, December 2022.

[63] Ethan D Coffel, Radley M Horton, and Alex De Sherbinin. Temperature and humidity based projections of a rapid rise in global heat stress exposure during the 21st century. *Environmental Research Letters*, 13(1):014001, January 2018.

[64] Frances C. Moore, Uris Lantz C. Baldos, and Thomas Hertel. Economic impacts of climate change on agriculture: A comparison of process-based and statistical yield models. *Environmental Research Letters*, 12(6), 2017.

[65] Dean P. Holzworth, Neil I. Huth, Peter G. deVoil, Eric J. Zurcher, Neville I. Herrmann, Greg McLean, Karine Chenu, Erik J. van Oosterom, Val Snow, Chris Murphy, Andrew D. Moore, Hamish Brown, Jeremy P.M. Whish, Shaun Verrall, Justin Fainges, Lindsay W. Bell, Allan S. Peake, Perry L. Poulton, Zvi Hochman, Peter J. Thorburn, Donald S. Gaydon, Neal P. Dalgliesh, Daniel Rodriguez, Howard Cox, Scott Chapman, Alastair Doherty, Edmar Teixeira, Joanna Sharp, Rogerio Cichota, Iris Vogeler, Frank Y. Li, Enli Wang, Graeme L. Hammer, Michael J. Robertson, John P. Dimes, Anthony M. Whitbread, James Hunt, Harm van Rees, Tim McClelland, Peter S. Carberry, John N.G. Hargreaves, Neil MacLeod, Cam McDonald, Justin Harsdorf, Sara Wedgwood, and Brian A. Keating. APSIM - Evolution towards a new generation of agricultural systems simulation. *Environmental Modelling and Software*, 62:327–350, 2014.

[66] David B Lobell and Senthold Asseng. Comparing estimates of climate change impacts from process-based and statistical crop models. *Environmental Research Letters*, 12:1–12, 2017.

[67] Elodie Blanc and Benjamin Sultan. Emulating maize yields from global gridded crop models using statistical estimates. *Agricultural and Forest Meteorology*, 214–215:134–147, 2015.

[68] Élodie Blanc. Statistical emulators of maize, rice, soybean and wheat yields from global gridded crop models. *Agricultural and Forest Meteorology*, 236:145–161, 2017.

[69] A Holzkämper, P Calanca, and J Fuhrer. Statistical crop models : Predicting the effects of temperature and precipitation changes. *Climate Research*, 51:11–21, 2012.

[70] C. D. Jones, J. K. Hughes, N. Bellouin, S. C. Hardiman, G. S. Jones, J. Knight, S. Liddicoat, F. M. O'Connor, R. J. Andres, C. Bell, K.-O. Boo, A. Bozzo, N. Butchart, P. Cadule, K. D. Corbin, M. Doutriaux-Boucher, P. Friedlingstein, J. Gornall, L. Gray, P. R. Halloran, G. Hurtt, W. J. Ingram, J.-F. Lamarque, R. M. Law, M. Meinshausen, S. Osprey, E. J. Palin, L. Parsons Chini, T. Raddatz, M. G. Sanderson, A. A. Sellar, A. Schurer, P. Valdes, N. Wood, S. Woodward, M. Yoshioka, and M. Zerroukat. The HadGEM2-ES implementation of CMIP5 centennial simulations. *Geoscientific Model Development*, 4(3):543–570, July 2011.

[71] Felix T. Portmann, Stefan Siebert, and Petra Döll. MIRCA2000-Global monthly irrigated and rainfed crop areas around the year 2000: A new high-resolution data set for agricultural and hydrological modeling. *Global Biogeochemical Cycles*, 24(1):n/a–n/a, 2010.

[72] Alex C. Ruane, Richard Goldberg, and James Chryssanthacopoulos. Climate forcing datasets for agricultural modeling: Merged products for gap-filling and historical climate series estimation. *Agricultural and Forest Meteorology*, 200:233–248, 2015.

[73] S. Hempel, K. Frieler, L. Warszawski, J. Schewe, and F. Piontek. A trend-preserving bias correction – the ISI-MIP approach. *Earth System Dynamics*, 4(2):219–236, July 2013.

[74] R. L. Snyder. Hand calculating degree days. *Agricultural and Forest Meteorology*, 35(1-4):353–358, 1985.

[75] Jonathan Proctor. Atmospheric opacity has a nonlinear effect on global crop yields. *Nature Food*, 2(March):166–173, 2021.

[76] Laurent Berge, Sebastian Krantz, and Grant McDermott. Package "fixest", 2021.

[77] Marshall Burke and Kyle Emerick. Adaptation to Climate Change: Evidence from US Agriculture. *American Economic Journal: Economic Policy*, 8(3):106–140, August 2016.

[78] Jennifer Hsiao, Abigail L.S. Swann, and Soo Hyung Kim. Maize yield under a changing climate: The hidden role of vapor pressure deficit. *Agricultural and Forest Meteorology*, 279(December 2018):107692, 2019.

[79] Joshua Elliott, David Kelly, James Chryssanthacopoulos, Michael Glotter, Kanika Jhunjhnuwala, Neil Best, Michael Wilde, and Ian Foster. The parallel system for integrating impact models and sectors (pSIMS). *Environmental Modelling and Software*, 62:509–516, 2014.

[80] Yan Li, Kaiyu Guan, Gary D. Schnitkey, Evan DeLucia, and Bin Peng. Excessive rainfall leads to maize yield loss of a comparable magnitude to extreme drought in the United States. *Global Change Biology*, 25(7):2325–2337, 2019.

[81] Jonas Jägermeyr, Christoph Müller, Alex C Ruane, Joshua Elliott, Juraj Balkovic, Oscar Castillo, Babacar Faye, Ian Foster, Christian Folberth, James A Franke, Kathrin Fuchs, Jose R Guarin, Jens Heinke, Gerrit Hoogenboom, Toshichika Iizumi, Atul K Jain, David Kelly, Nikolay Khabarov, Stefan Lange, Tzu-shun Lin, Wenfeng Liu, Oleksandr Mialyk, Sara Minoli, Elisabeth J Moyer, Masashi Okada, Meridel Phillips, Cheryl Porter, Sam S Rabin, Clemens Scheer, Julia M Schneider, Joep F Schyns, Rastislav Skalsky, Andrew Smerald, Tommaso Stella, Haynes Stephens, Heidi Webber, Florian Zabel, and Cynthia Rosenzweig. Climate impacts on global agriculture emerge earlier in new generation of climate and crop models. *Nature Food*, 2021.

[82] Bernhard Schauberger, Susanne Rolinski, and Christoph Müller. A network-based approach for semi-quantitative knowledge mining and its application to yield variability. *Environmental Research Letters*, 11(12):123001, December 2016.

[83] Kenneth J. Boote, James W. Jones, Jeffrey W. White, Senthold Asseng, and Jon I. Lizaso. Putting mechanisms into crop production models. *Plant, Cell and Environment*, 36(9):1658–1672, 2013.

[84] David B. Lobell, Graeme L. Hammer, Greg McLean, Carlos Messina, Michael J. Roberts, and Wolfram Schlenker. The critical role of extreme heat for maize production in the United States. *Nature Climate Change*, 3(5):497–501, May 2013.

[85] Wenping Yuan, Yi Zheng, Shilong Piao, Philippe Ciais, Danica Lombardozzi, Yingping Wang, Youngryel Ryu, Guixing Chen, Wenjie Dong, Zhongming Hu, Atul K. Jain, Chongya Jiang, Etsushi Kato, Shihua Li, Sebastian Lienert, Shuguang Liu, Julia E.M.S. Nabel, Zhangcai Qin, Timothy Quine, Stephen Sitch, William K. Smith, Fan Wang, Chaoyang Wu, Zhiqiang Xiao, and Song Yang. Increased atmospheric vapor pressure deficit reduces global vegetation growth. *Science Advances*, 5(8):1–13, 2019.

[86] Chuang Zhao, Bing Liu, Shilong Piao, Xuhui Wang, David B. Lobell, Yao Huang, Mengtian Huang, Yitong Yao, Simona Bassu, Philippe Ciais, Jean Louis Durand, Joshua Elliott, Frank Ewert, Ivan A. Janssens, Tao Li, Erda Lin, Qiang Liu, Pierre Martre, Christoph Müller, Shushi Peng, Josep Peñuelas, Alex C. Ruane, Daniel Wallach, Tao Wang, Donghai Wu, Zhuo Liu, Yan Zhu, Zaichun Zhu, and Senthold Asseng. Temperature increase reduces global yields of major crops in four independent estimates. *Proceedings of the National Academy of Sciences of the United States of America*, 114(35):9326–9331, 2017.

[87] Saeed Khaki and Lizhi Wang. Crop Yield Prediction Using Deep Neural Networks. *Frontiers in Plant Science*, 10:621, May 2019.

[88] Saeed Khaki, Lizhi Wang, and Sotirios V. Archontoulis. A CNN-RNN Framework for Crop Yield Prediction. *Frontiers in Plant Science*, 10(January):1–14, 2020.

[89] Guoyong Leng and Jim W. Hall. Predicting spatial and temporal variability in crop yields: An inter-comparison of machine learning, regression and process-based models. *Environmental Research Letters*, 15(4), 2020.

[90] Yanbin Chang, Jeremy Latham, Mark Licht, and Lizhi Wang. A data-driven crop model for maize yield prediction. *Communications Biology*, 6(1):439, April 2023.

[91] Tamma Carleton, Amir Jina, Michael Delgado, Michael Greenstone, Trevor Houser, Solomon Hsiang, Andrew Hultgren, Robert E Kopp, Kelly E Mccusker, Ishan Nath, James Rising, Ashwin Rode, Hee Kwon Seo, Arvid Viaene, Jiacan Yuan, and Alice Tianbo Zhang. Valuing the Global Mortality Consequences of Climate Change Accounting for Adaptation Costs and Benefits. *The Quarterly Journal of Economics*, 2022.

[92] Jie Zeng, Xuehai Zhang, Jun Yang, Junzhe Bao, Hao Xiang, Keith Dear, Qiyong Liu, Shao Lin, Wayne Lawrence, Aihua Lin, and Cunrui Huang. Humidity May Modify the Relationship between Temperature and Cardiovascular Mortality in Zhejiang Province, China. *International Journal of Environmental Research and Public Health*, 14(11):1383, November 2017.

[93] Alan I. Barreca. Climate change, humidity, and mortality in the United States. *Journal of Environmental Economics and Management*, 63(1):19–34, January 2012.

[94] Colin Raymond, Tom Matthews, and Radley M. Horton. The emergence of heat and humidity too severe for human tolerance. *Science Advances*, 6(19):eaaw1838, May 2020.

[95] Jennifer Vanos, Gisel Guzman-Echavarria, Jane W. Baldwin, Coen Bongers, Kristie L. Ebi, and Ollie Jay. A physiological approach for assessing human survivability and liveability to heat in a changing climate. *Nature Communications*, 14(1):7653, November 2023.

[96] James W. Jones, John M. Antle, Bruno Basso, Kenneth J. Boote, Richard T. Conant, Ian Foster, H. Charles J. Godfray, Mario Herrero, Richard E. Howitt, Sander Janssen, Brian A. Keating, Rafael Munoz-Carpena, Cheryl H. Porter, Cynthia Rosenzweig, and Tim R. Wheeler. Toward a new generation of agricultural system data, models, and knowledge products: State of agricultural systems science. *Agricultural Systems*, 155:269–288, 2017.

[97] C. Rosenzweig, J. W. Jones, J. L. Hatfield, A. C. Ruane, K. J. Boote, P. Thorburn, J. M. Antle, G. C. Nelson, C. Porter, S. Janssen, S. Asseng, B. Basso, F. Ewert, D. Wallach, G. Baigorria, and J. M. Winter. The Agricultural Model Intercomparison and Improvement Project (AgMIP): Protocols and pilot studies. *Agricultural and Forest Meteorology*, 170:166–182, 2013.

[98] Christoph Müller, Jonas Jägermeyr, James A. Franke, Alex C. Ruane, Juraj Balkovic, Philippe Ciais, Marie Dury, Pete Falloon, Christian Folberth, Tobias Hank, Munir

Hoffmann, R. Cesar Izaurralde, Ingrid Jacquemin, Nikolay Khabarov, Wenfeng Liu, Stefan Olin, Thomas A. M. Pugh, Xuhui Wang, Karina Williams, Florian Zabel, and Joshua W. Elliott. Substantial Differences in Crop Yield Sensitivities Between Models Call for Functionality-Based Model Evaluation. *Earth's Future*, 12(3):e2023EF003773, March 2024.

[99] William J. Sacks, Delphine Deryng, Jonathan A. Foley, and Navin Ramankutty. Crop planting dates: An analysis of global patterns. *Global Ecology and Biogeography*, 19(5):607–620, 2010.

[100] U.S. Department of Agriculture. Usual Planting and Harvesting Dates for U.S. Field Crops. *Agricultural Handbook*, (628):51, 1997.

[101] Sara Minoli, Christoph Müller, Joshua Elliott, Alex C. Ruane, Jonas Jägermeyr, Florian Zabel, Marie Dury, Christian Folberth, Louis François, Tobias Hank, Ingrid Jacquemin, Wenfeng Liu, Stefan Olin, and Thomas A. M. Pugh. Global Response Patterns of Major Rainfed Crops to Adaptation by Maintaining Current Growing Periods and Irrigation. *Earth's Future*, 7(12):1464–1480, December 2019.

[102] USDA National Agricultural Statistics Service. (dataset) USDA National Agricultural Statistics Service. https://quickstats.nass.usda.gov/.

[103] Lori J. Abendroth, Fernando E. Miguez, Michael J. Castellano, and Jerry L. Hatfield. Climate Warming Trends in the U.S. Midwest Using Four Thermal Models. *Agronomy Journal*, 111(6):3230–3243, November 2019.

[104] Lori J. Abendroth, Fernando E. Miguez, Michael J. Castellano, Paul R. Carter, Carlos D. Messina, Philip M. Dixon, and Jerry L. Hatfield. Lengthening of maize maturity time is not a widespread climate change adaptation strategy in the US Midwest. *Global Change Biology*, 27(11):2426–2440, 2021.

[105] Lori J Abendroth, Roger W Elmore, Matthew J Boyer, and Stephanie K Marlay. *Corn Growth and Development*. Ames: Iowa State University, 2011.

[106] M. E. Baum, S. V. Archontoulis, and M. A. Licht. Planting Date, Hybrid Maturity, and Weather Effects on Maize Yield and Crop Stage. *Agronomy Journal*, 111(1):303–313, January 2019.

[107] Jillian M. Deines, Anu Swatantran, Dening Ye, Brent Myers, Sotirios Archontoulis, and David B. Lobell. Field-scale dynamics of planting dates in the US Corn Belt from 2000 to 2020. *Remote Sensing of Environment*, 291:113551, June 2023.

[108] Lori J. Abendroth, Krishna P. Woli, Anthony J.W. Myers, and Roger W. Elmore. Yield-Based Corn Planting Date Recommendation Windows for Iowa. *Crop, Forage & Turfgrass Management*, 3(1):cftm2017.02.0015, December 2017.

[109] U.S. Department of Agriculture. World Agricultural Production, November 2023.

[110] Ethan E. Butler and Peter Huybers. Adaptation of US maize to temperature variations. *Nature Climate Change*, 3(1):68–72, 2013.

[111] Daniel Urban, Michael J. Roberts, Wolfram Schlenker, and David B. Lobell. Projected temperature changes indicate significant increase in interannual variability of U.S. maize yields: A Letter. *Climatic Change*, 112(2):525–533, May 2012.

[112] Zhenong Jin, Qianlai Zhuang, Jiali Wang, Sotirios V. Archontoulis, Zachary Zobel, and Veerabhadra R. Kotamarthi. The combined and separate impacts of climate extremes on the current and future US rainfed maize and soybean production under elevated CO2. *Global Change Biology*, 23(7):2687–2704, July 2017.

[113] Simona Bassu, Nadine Brisson, Jean-Louis Durand, Kenneth Boote, Jon Lizaso, James W. Jones, Cynthia Rosenzweig, Alex C. Ruane, Myriam Adam, Christian Baron, Bruno Basso, Christian Biernath, Hendrik Boogaard, Sjaak Conijn, Marc Corbeels, Delphine Deryng, Giacomo De Sanctis, Sebastian Gayler, Patricio Grassini, Jerry Hatfield, Steven Hoek, Cesar Izaurralde, Raymond Jongschaap, Armen R. Kemanian, K. Christian Kersebaum, Soo-Hyung Kim, Naresh S. Kumar, David Makowski, Christoph Müller, Claas Nendel, Eckart Priesack, Maria Virginia Pravia, Federico Sau, Iurii Shcherbak, Fulu Tao, Edmar Teixeira, Dennis Timlin, and Katharina Waha. How do various maize crop models vary in their responses to climate change factors? *Global Change Biology*, 20(7):2301–2320, July 2014.

[114] Jerry L. Hatfield and John H. Prueger. Temperature extremes : Effect on plant growth and development. *Weather and Climate Extremes*, 10:4–10, 2015.

[115] Nicole Estrella, Tim H. Sparks, and Annette Menzel. Effects of temperature, phase type and timing, location, and human density on plant phenological responses in Europe. *Climate Research*, 39(3):235–248, 2009.

[116] Ehsan Eyshi Rezaei, Stefan Siebert, Hubert Hüging, and Frank Ewert. Climate change effect on wheat phenology depends on cultivar change. *Scientific Reports*, 8(1):1–10, 2018.

[117] Fulu Tao, Shuai Zhang, Zhao Zhang, and Reimund P. Rötter. Maize growing duration was prolonged across China in the past three decades under the combined effects of temperature, agronomic management, and cultivar shift. *Global Change Biology*, 20(12):3686–3699, 2014.

[118] R. Žydelis, L. Weihermüller, and M. Herbst. Future climate change will accelerate maize phenological development and increase yield in the Nemoral climate. *Science of The Total Environment*, 784:147175, August 2021.

[119] Lin Liu and Bruno Basso. Impacts of climate variability and adaptation strategies on crop yields and soil organic carbon in the US Midwest. *PLOS ONE*, 15(1):e0225433, January 2020.

[120] Sara Minoli, Jonas Jägermeyr, Senthold Asseng, Anton Urfels, and Christoph Müller. Global crop yields can be lifted by timely adaptation of growing periods to climate change. *Nature Communications*, 13(1):7079, November 2022.

[121] S. Asseng, F. Ewert, P. Martre, R. P. Rötter, D. B. Lobell, D. Cammarano, B. A. Kimball, M. J. Ottman, G. W. Wall, J. W. White, M. P. Reynolds, P. D. Alderman, P. V.V. Prasad, P. K. Aggarwal, J. Anothai, B. Basso, C. Biernath, A. J. Challinor, G. De Sanctis, J. Doltra, E. Fereres, M. Garcia-Vila, S. Gayler, G. Hoogenboom, L. A. Hunt, R. C. Izaurralde, M. Jabloun, C. D. Jones, K. C. Kersebaum, A. K. Koehler, C. Müller, S. Naresh Kumar, C. Nendel, G. O'leary, J. E. Olesen, T. Palosuo, E. Priesack, E. Eyshi Rezaei, A. C. Ruane, M. A. Semenov, I. Shcherbak, C. Stöckle, P. Stratonovitch, T. Streck, I. Supit, F. Tao, P. J. Thorburn, K. Waha, E. Wang, D. Wallach, J. Wolf, Z. Zhao, and Y. Zhu. Rising temperatures reduce global wheat production. *Nature Climate Change*, 5(2):143–147, 2015.

[122] M. M. Chaves. Effects of Water Deficits on Carbon Assimilation. *Journal of Experimental Botany*, 42(1):1–16, 1991.

[123] Ivica Djalovic, Sayanta Kundu, Rajeev Nayan Bahuguna, Ashwani Pareek, Ali Raza, Sneh L. Singla-Pareek, P. V. Vara Prasad, and Rajeev K. Varshney. Maize and heat stress: Physiological, genetic, and molecular insights. *The Plant Genome*, page e20378, August 2023.

[124] Hafiz Athar Hussain, Shengnan Men, Saddam Hussain, Yinglong Chen, Shafaqat Ali, Sai Zhang, Kangping Zhang, Yan Li, Qiwen Xu, Changqing Liao, and Longchang Wang. Interactive effects of drought and heat stresses on morpho-physiological attributes, yield, nutrient uptake and oxidative status in maize hybrids. *Scientific Reports*, 9(1):3890, March 2019.

[125] S Mark Howden, Jean-Francois Soussana, Francesco N Tubiello, Netra Chhetri, Michael Dunlop, and Holger Meinke. Adapting agriculture to climate change. *Proceedings of the National Academy of Sciences*, 104(50):19691–19696, December 2007.

[126] Jane Southworth, J.C. Randolph, M. Habeck, O.C. Doering, R.A. Pfeifer, D.G. Rao, and J.J. Johnston. Consequences of future climate change and changing climate variability on maize yields in the midwestern United States. *Agriculture, Ecosystems & Environment*, 82(1-3):139–158, December 2000.

[127] Dengpan Xiao, Yongqing Qi, Yanjun Shen, Fulu Tao, Juana P. Moiwo, Jianfeng Liu, Rede Wang, He Zhang, and Fengshan Liu. Impact of warming climate and cultivar change on maize phenology in the last three decades in North China Plain. *Theoretical and Applied Climatology*, 124(3-4):653–661, May 2016.

[128] A. J. Challinor, J. Watson, D. B. Lobell, S. M. Howden, D. R. Smith, and N. Chhetri. A meta-analysis of crop yield under climate change and adaptation. *Nature Climate Change*, 4(4):287–291, 2014.

[129] William E Easterling. Adapting North American agriculture to climate change in review. *Agricultural and Forest Meteorology*, 80(1):1–53, June 1996.

[130] Ignacio Massigoge, Ana Carcedo, Jane Lingenfelser, Trevor Hefley, P.V. Vara Prasad, Dan Berning, Sara Lira, Carlos D. Messina, Charles W. Rice, and Ignacio Ciampitti. Maize planting date and maturity in the US central Great Plains: Exploring windows for maximizing yields. *European Journal of Agronomy*, 149:126905, 2023.

[131] Justin E. Bagley, Jesse Miller, and Carl J. Bernacchi. Biophysical impacts of climate-smart agriculture in the Midwest United States. *Plant, Cell & Environment*, 38(9):1913–1930, September 2015.

[132] Florian Zabel, Christoph Müller, Joshua Elliott, Sara Minoli, Jonas Jägermeyr, Julia M. Schneider, James A. Franke, Elisabeth Moyer, Marie Dury, Louis Francois, Christian Folberth, Wenfeng Liu, Thomas A.M. Pugh, Stefan Olin, Sam S. Rabin, Wolfram Mauser, Tobias Hank, Alex C. Ruane, and Senthold Asseng. Large potential for crop production adaptation depends on available future varieties. *Global Change Biology*, 27(16):3870–3882, August 2021.

[133] Boris Parent, Margot Leclere, Sébastien Lacube, Mikhail A. Semenov, Claude Welcker, Pierre Martre, and François Tardieu. Maize yields over Europe may increase in spite of climate change, with an appropriate use of the genetic variability of flowering time. *Proceedings of the National Academy of Sciences of the United States of America*, 115(42):10642–10647, 2018.

[134] Zunfu Lv, Feifei Li, and Guoquan Lu. Adjusting sowing date and cultivar shift improve maize adaption to climate change in China. *Mitigation and Adaptation Strategies for Global Change*, 25(1):87–106, January 2020.

[135] Peng Zhu, Qianlai Zhuang, Sotirios V. Archontoulis, Carl Bernacchi, and Christoph Müller. Dissecting the nonlinear response of maize yield to high temperature stress with model-data integration. *Global Change Biology*, 25(7):2470–2484, 2019.

[136] Dingrong Wu, Peijuan Wang, Chaoyang Jiang, Jianying Yang, Zhiguo Huo, and Qiang Yu. Measured Phenology Response of Unchanged Crop Varieties to Long-Term Historical Climate Change. *International Journal of Plant Production*, 13(1):47–58, March 2019.

[137] A. J. Challinor, A.-K. Koehler, J. Ramirez-Villegas, S. Whitfield, and B. Das. Current warming will reduce yields unless maize breeding and seed systems adapt immediately. *Nature Climate Change*, 6(10):954–958, October 2016.

[138] Brigitte Mueller, Mathias Hauser, Carley Iles, Ruksana Haque Rimi, Francis W. Zwiers, and Hui Wan. Lengthening of the growing season in wheat and maize producing regions. *Weather and Climate Extremes*, 9:47–56, 2015.

[139] Christopher A. Seifert and David B. Lobell. Response of double cropping suitability to climate change in the United States. *Environmental Research Letters*, 10(2), 2015.

[140] Jialu Xu, Jing Gao, Henrique Vinicius de Holanda, Luis F. Rodríguez, José Vicente Caixeta-Filho, Renhai Zhong, Hao Jiang, Haifeng Li, Zhenhong Du, Xuhui Wang, Shaowen Wang, K. C. Ting, Yibin Ying, and Tao Lin. Double cropping and cropland expansion boost grain production in Brazil. *Nature Food*, 2(4):264–273, April 2021.

[141] Deepak K. Ray, Nathaniel D. Mueller, Paul C. West, and Jonathan A. Foley. Yield Trends Are Insufficient to Double Global Crop Production by 2050. *PLoS ONE*, 8(6):e66428, June 2013.

[142] David Tilman, Christian Balzer, Jason Hill, and Belinda L. Befort. Global food demand and the sustainable intensification of agriculture. *Proceedings of the National Academy of Sciences of the United States of America*, 108(50):20260–20264, 2011.

[143] Crop Acreage Data. https://fsa.usda.gov/news-room/efoia/electronic-reading-room/frequently-requested-information/crop-acreage-data/index, 2023.

[144] Cause of Loss | RMA. https://www.rma.usda.gov/en/Information-Tools/Summary-of-Business/Cause-of-Loss, 2023.

[145] Moustafa T. Chahine. The hydrological cycle and its influence on climate. *Nature*, 359(6394):373–380, October 1992.

[146] Ruiqing Miao, Madhu Khanna, and Haixiao Huang. Responsiveness of Crop Yield and Acreage to Prices and Climate. *American Journal of Agricultural Economics*, 98(1):191–211, January 2016.

[147] Christopher N. Boyer, Eunchun Park, and Seong D. Yun. Corn and soybean prevented planting acres response to weather. *Applied Economic Perspectives and Policy*, 45(2):970–983, 2023.

[148] Patricio Grassini, James E Specht, Matthijs Tollenaar, Ignacio Ciampitti, and Kenneth G Cassman. High-yield maize–soybean cropping systems in the US Corn Belt. In *Crop Physiology*, pages 17–41. Elsevier, 2015.

[149] Balsher Singh Sidhu, Zia Mehrabi, Navin Ramankutty, and Milind Kandlikar. How can machine learning help in understanding the impact of climate change on crop yields? *Environmental Research Letters*, 18(2):024008, February 2023.

[150] Fabio Porto, Mariza Ferro, Eduardo Ogasawara, Thiago Moeda, and Claudio Barros. Machine Learning Approaches to Extreme Weather Events Forecast in Urban Areas: Challenges and Initial Results. *Supercomputing Frontiers and Innovations*, 9(1), March 2022.

[151] Scott M Lundberg and Su-In Lee. A Unified Approach to Interpreting Model Predictions. *Advances in neural information processing systems*, 30, 2017.

[152] Richard Seager, Nathan Lis, Jamie Feldman, Mingfang Ting, A. Park Williams, Jennifer Nakamura, Haibo Liu, and Naomi Henderson. Whither the 100th Meridian? The Once and Future Physical and Human Geography of America's Arid–Humid Divide. Part I: The Story So Far. *Earth Interactions*, 22(5):1–22, March 2018.

[153] John Newton. Crop progress and implications for 2015 prevented planting in corn and soybeans. *farmdoc daily*, 5(109), 2015.

[154] Soil Survey Staff. Gridded Soil Survey Geographic (gSSURGO) Database for the Conterminous United States, July 2020.

[155] Amy McNally, Kristi Arsenault, Sujay Kumar, Shraddhanand Shukla, Pete Peterson, Shugong Wang, Chris Funk, Christa D. Peters-Lidard, and James P. Verdin. A land data assimilation system for sub-Saharan Africa food and water security applications. *Scientific Data*, 4(1):170012, February 2017.

[156] NASA GSFC Hydrological Sciences Laboratory (HSL). FLDAS Noah Land Surface Model L4 Global Monthly 0.1 x 0.1 degree (MERRA-2 and CHIRPS) V001, 2018.

[157] Chris Funk, Pete Peterson, Martin Landsfeld, Diego Pedreros, James Verdin, Shraddhanand Shukla, Gregory Husak, James Rowland, Laura Harrison, Andrew Hoell, and Joel Michaelsen. The climate hazards infrared precipitation with stations—a new environmental record for monitoring extremes. *Scientific Data*, 2(1):150066, December 2015.

[158] Ronald Gelaro, Will McCarty, Max J. Suárez, Ricardo Todling, Andrea Molod, Lawrence Takacs, Cynthia A. Randles, Anton Darmenov, Michael G. Bosilovich, Rolf Reichle, Krzysztof Wargan, Lawrence Coy, Richard Cullather, Clara Draper, Santha Akella, Virginie Buchard, Austin Conaty, Arlindo M. Da Silva, Wei Gu, Gi-Kong Kim, Randal Koster, Robert Lucchesi, Dagmar Merkova, Jon Eric Nielsen, Gary Partyka, Steven Pawson, William Putman, Michele Rienecker, Siegfried D. Schubert, Meta Sienkiewicz, and Bin Zhao. The Modern-Era Retrospective Analysis for Research and Applications, Version 2 (MERRA-2). *Journal of Climate*, 30(14):5419–5454, July 2017.

[159] Xiaoge Xin, Tongwen Wu, Xueli Shi, Fang Zhang, Jianglong Li, Min Chu, Qianxia Liu, Jinghui Yan, Qiang Ma, and Min Wei. BCC BCC-CSM2MR model output prepared for CMIP6 ScenarioMIP ssp585, 2019.

[160] Aurore Voldoire. CNRM-CERFACS CNRM-CM6-1 model output prepared for CMIP6 ScenarioMIP ssp585, 2019.

[161] Aurore Voldoire. CNRM-CERFACS CNRM-ESM2-1 model output prepared for CMIP6 ScenarioMIP ssp585, 2019.

[162] Seiji Yukimoto, Tsuyoshi Koshiro, Hideaki Kawai, Naga Oshima, Kohei Yoshida, Shogo Urakawa, Hiroyuki Tsujino, Makoto Deushi, Taichu Tanaka, Masahiro Hosaka, Hiromasa Yoshimura, Eiki Shindo, Ryo Mizuta, Masayoshi Ishii, Atsushi Obata, and

Yukimasa Adachi. MRI MRI-ESM2.0 model output prepared for CMIP6 ScenarioMIP ssp585, 2019.

[163] Olivier Boucher, Sébastien Denvil, Guillaume Levavasseur, Anne Cozic, Arnaud Caubel, Marie-Alice Foujols, Yann Meurdesoif, Patricia Cadule, Marion Devilliers, Eliott Dupont, and Thibaut Lurton. IPSL IPSL-CM6A-LR model output prepared for CMIP6 ScenarioMIP ssp585, 2019.

[164] Diane Lambert. Zero-Inflated Poisson Regression, with an Application to Defects in Manufacturing. *Technometrics*, 34(1):1, February 1992.

[165] Cindy Xin Feng. A comparison of zero-inflated and hurdle models for modeling zero-inflated count data. *Journal of Statistical Distributions and Applications*, 8(1):8, December 2021.

[166] vincent d warmerdam, MBrouns, Stéphane Collot, Robert Kübler, Josko de Boer, pimhoeven, Francesco Bruzzesi, Arthur Paulino, Peter Verheijen, Maxime Borry, ktiamur, Kay Hoogland, Gaurav Sharma, Carlo Lepelaars, Gleb Levitski, Jan Keromnes, Sander van Dorsten, Stephen Anthony Rose, Tomas Borrella, David Masip, Frits Hermans, Cor, Rens, amrrs, Abo7atm, Damien Ready, Daniel Kulik, Eric Wong, and Fokko Driesprong. Koaning/scikit-lego: V0.6.16. Zenodo, October 2023.

[167] Leo Breiman. Random forests. *Machine learning*, 45:5–32, 2001.

[168] Scott M. Lundberg, Gabriel Erion, Hugh Chen, Alex DeGrave, Jordan M. Prutkin, Bala Nair, Ronit Katz, Jonathan Himmelfarb, Nisha Bansal, and Su-In Lee. From local explanations to global understanding with explainable AI for trees. *Nature Machine Intelligence*, 2(1):56–67, January 2020.

[169] NASA Jet Propulsion Laboratory (JPL) Tellus. JPL GRACE Mascon Ocean, Ice, and Hydrology Equivalent Water Height Release 06 Coastal Resolution Improvement (CRI) Filtered Version 1.0, 2018.

[170] Michael M. Watkins, David N. Wiese, Dah-Ning Yuan, Carmen Boening, and Felix W. Landerer. Improved methods for observing Earth's time variable mass distribution with GRACE using spherical cap mascons. *Journal of Geophysical Research: Solid Earth*, 120(4):2648–2671, April 2015.

[171] David N. Wiese, Felix W. Landerer, and Michael M. Watkins. Quantifying and reducing leakage errors in the JPL RL05M GRACE mascon solution. *Water Resources Research*, 52(9):7490–7502, September 2016.

[172] Felix W. Landerer, Frank M. Flechtner, Himanshu Save, Frank H. Webb, Tamara Bandikova, William I. Bertiger, Srinivas V. Bettadpur, Sung Hun Byun, Christoph Dahle, Henryk Dobslaw, Eugene Fahnestock, Nate Harvey, Zhigui Kang, Gerhard L. H. Kruizinga, Bryant D. Loomis, Christopher McCullough, Michael Murböck, Peter Nagel, Meegyeong Paik, Nadege Pie, Steve Poole, Dmitry Strekalov, Mark E.

Tamisiea, Furun Wang, Michael M. Watkins, Hui-Ying Wen, David N. Wiese, and Dah-Ning Yuan. Extending the Global Mass Change Data Record: GRACE Follow-On Instrument and Science Data Performance. *Geophysical Research Letters*, 47(12):e2020GL088306, June 2020.

[173] Ashraf Rateb, Bridget R. Scanlon, Donald R. Pool, Alexander Sun, Zizhan Zhang, Jianli Chen, Brian Clark, Claudia C. Faunt, Connor J. Haugh, Mary Hill, Christopher Hobza, Virginia L. McGuire, Meredith Reitz, Hannes Müller Schmied, Edwin H. Sutanudjaja, Sean Swenson, David Wiese, Youlong Xia, and Wesley Zell. Comparison of Groundwater Storage Changes From GRACE Satellites With Monitoring and Modeling of Major U.S. Aquifers. *Water Resources Research*, 56(12):e2020WR027556, December 2020.

[174] D. B. Egli and P. L. Cornelius. A Regional Analysis of the Response of Soybean Yield to Planting Date. *Agronomy Journal*, 101(2):330–335, March 2009.

[175] Guihua Chen and Pawel Wiatrak. Soybean Development and Yield Are Influenced by Planting Date and Environmental Conditions in the Southeastern Coastal Plain, United States. *Agronomy Journal*, 102(6):1731–1737, November 2010.

[176] Montserrat Salmeron, Edward E. Gbur, Fred M. Bourland, Normie W. Buehring, Larry Earnest, Felix B. Fritschi, Bobby R. Golden, Daniel Hathcoat, Josh Lofton, Travis D. Miller, Clark Neely, Grover Shannon, Theophilus K. Udeigwe, David A. Verbree, Earl D. Vories, William J. Wiebold, and Larry C. Purcell. Soybean Maturity Group Choices for Early and Late Plantings in the Midsouth. *Agronomy Journal*, 106(5):1893–1901, September 2014.

[177] Robert Schneider. Correlation of ground-water levels and air temperatures in the winter and spring in Minnesota. USGS Numbered Series, U.S. G.P.O., 1961.

[178] Timothy R. Green, Holm Kipka, Olaf David, and Gregory S. McMaster. Where is the USA Corn Belt, and how is it changing? *Science of The Total Environment*, 618:1613–1618, March 2018.

[179] Aaron Hrozencik. USDA ERS - Irrigation & Water Use. https://www.ers.usda.gov/topics/farm-practices-management/irrigation-water-use/, September 2023.

[180] John Baker and EGBERT SPAANS. Mechanisms of meltwater movement above and within frozen soil. In *International Symposium on Physics Chemistry and Ecology of Seasonally Froz*, 1997.

[181] Charles A Perry. *Significant Floods in the United States during the 20th Century: USGS Measures a Century of Floods*, volume 24. US Department of the Interior, US Geological Survey, 2000.

[182] William J. Sacks and Christopher J. Kucharik. Crop management and phenology trends in the U.S. Corn Belt: Impacts on yields, evapotranspiration and energy balance. *Agricultural and Forest Meteorology*, 151(7):882–894, 2011.

[183] Mohammad Shamsudduha and Richard G. Taylor. Groundwater storage dynamics in the world's large aquifer systems from GRACE: Uncertainty and role of extreme precipitation. *Earth System Dynamics*, 11(3):755–774, August 2020.

[184] The Subcommittee on Ground Water of the Advisory Committee on Water Information. A National Framework for Ground-Water Monitoring in the United States. Technical report, Advisory Committee on Water Information, June 2013.

[185] Marcia Bunger. Request for Information on Prevented Planting. *Federal Register: the daily journal of the United States Government*, 88(175):62524–62526, September 2023.

[186] Hossein Tabari. Climate change impact on flood and extreme precipitation increases with water availability. *Scientific Reports*, 10(1):13768, August 2020.

[187] P Sivanandhini and J Prakash. Crop Yield Prediction Analysis using Feed Forward and Recurrent Neural Network. *International Journal of Innovative Science and Research Technology*, 5(5), 2020.

[188] Gunnar Lischeid, Heidi Webber, Michael Sommer, Claas Nendel, and Frank Ewert. Machine learning in crop yield modelling: A powerful tool, but no surrogate for science. *Agricultural and Forest Meteorology*, 312:108698, January 2022.

APPENDIX

S1 Supplemental Materials for Chapter 2

S1.1 Functional forms for statistical models used in Figure 2.4a

Functional forms here correspond to the individual statistical model projections in Figure 2.4a, denoted by line number in the subplot. Table S1 provides a legend of the features used in the functional forms.

Table S1: Legend of features used in statistical model functional forms.

Feature	Definition
P	Total growing-season precipitation
P^2	Total squared growing-season precipitation
VPD	Total growing-season vapor-pressure deficit
VPD^2	Total squared growing-season vapor-pressure deficit
SM	Total growing-season soil moisture supply
SM^2	Squared total growing-season soil moisture supply
GDD	Total growing-season growing-degree days
HDD	Total growing-season high-degree days

Line 1:

$$\log(Y_{i,t}) = \alpha_i + \beta_P \cdot P_{i,t} + \beta_{P^2} \cdot P_{i,t}^2 + \beta_{VPD} \cdot VPD_{i,t} + \beta_{VPD^2} \cdot VPD_{i,t}^2 + \epsilon_{i,t}. \quad (6.1)$$

Line 2:

$$\log(Y_{i,t}) = \alpha_i + \beta_{VPD} \cdot VPD_{i,t} + \beta_{VPD^2} \cdot VPD_{i,t}^2 + \epsilon_{i,t}. \quad (6.2)$$

Line 3: Equation 2.7

Line 4:

$$\log(Y_{i,t}) = \alpha_i + \beta_{SM} \cdot SM_{i,t} + \beta_{SM^2} \cdot SM_{i,t}^2 + \epsilon_{i,t}. \quad (6.3)$$

Line 5: Equation 2.4

Line 6: Equation 2.3

Line 7:

$$\begin{aligned}\log(Y_{i,t}) &= \alpha_i + \beta_{GDD} \cdot GDD_{i,t} + \beta_{HDD} \cdot HDD_{i,t} + \\ &\beta_P \cdot P_{i,t} + \beta_{P^2} \cdot P_{i,t}^2 + \\ &\beta_{SM} \cdot SM_{i,t} + \beta_{SM^2} \cdot SM_{i,t}^2 + \epsilon_{i,t}. \quad (6.4)\end{aligned}$$

Line 8:

$$\begin{aligned}\log(Y_{i,t}) &= \alpha_i + \beta_{GDD} \cdot GDD_{i,t} + \beta_{HDD} \cdot HDD_{i,t} + \\ &\beta_P \cdot P_{i,t} + \beta_{P^2} \cdot P_{i,t}^2 + \\ &\beta_{VPD} \cdot VPD_{i,t} + \beta_{VPD^2} \cdot VPD_{i,t}^2 + \\ &\beta_{SM} \cdot SM_{i,t} + \beta_{SM^2} \cdot SM_{i,t}^2 + \epsilon_{i,t}. \quad (6.5)\end{aligned}$$

Line 9:

$$\begin{aligned}\log(Y_{i,t}) &= \alpha_i + \beta_{GDD} \cdot GDD_{i,t} + \beta_{HDD} \cdot HDD_{i,t} + \\ &\beta_P \cdot P_{i,t} + \beta_{P^2} \cdot P_{i,t}^2 + \\ &\beta_{VPD} \cdot VPD_{i,t} + \beta_{VPD^2} \cdot VPD_{i,t}^2 + \epsilon_{i,t}. \quad (6.6)\end{aligned}$$

Process-based model	Within R^2	Scenario (°C)	Simulation (%/K)	Model (%/K)	Factor
CARAIB	0.67 (± 0.00)	+2	-4.9	-8.8	1.8
		+4	-4.94	-10.06	2.04
		+6	-5.36	-11.43	2.13
EPIC-TAMU	0.53 (± 0.00)	+2	-3.45	-11.69	3.39
		+4	-4.51	-16.61	3.68
		+6	-5.08	-21.95	4.32
GEPIC	0.60 (± 0.00)	+2	-5.88	-12.72	2.16
		+4	-5.64	-16.21	2.87
		+6	-5.73	-20.05	3.5
LPJ-GUESS	0.26 (± 0.00)	+2	-5.95	0.55	-0.09
		+4	-4.88	-1.7	0.35
		+6	-4.69	-4.29	0.91
LPJmL	0.51 (± 0.00)	+2	-3.92	-7.57	1.93
		+4	-4.85	-10.73	2.21
		+6	-5.17	-14.18	2.75
LPJmL (ESM-based)	0.55 (± 0.00)	+2	-4.42	-11.61	2.63
		+4	-6.62	-12.72	1.92
		+6	-6.28	-14.95	2.38
pDSSAT	0.34 (± 0.00)	+2	-7.94	-6.17	0.78
		+4	-10.53	-9.59	0.91
		+6	-13.38	-13.32	1
PEPIC	0.50 (± 0.00)	+2	-2.48	-9.42	3.8
		+4	-3.64	-13.58	3.73
		+6	-4.63	-18.16	3.92

Table S2: Summary statistics for the TP statistical models in this work trained and tested on separate simulated yield datasets. Column 1 (leftmost) denotes the process-based maize model that produced simulated yield train and test sets. Columns 2–3 show the historical withiin R^2 values for the TP statistical models with a piecewise linear temperature responses and stepwise temperature response, respectively. Columns 4–7 columns correspond to tests at increasing warming levels noted by the warming scenario in the fourth column. The fifth column shows the target yield change at that warming level, given in units of %/K, assuming compounding percentage losses. The sixth column shows the projected yield change at that warming level for the TP models, also through units of compound %/K impacts. The seventh column shows the ratio of the projected to simulated yield changes as a metric of the factor projection error. A factor of 1 indicates perfect projection accuracy; a factor of 2 indicates overprojected impacts by double. The "LPJmL (ESM-based)" row corresponds to tests under the ESM-based scenario, RCP8.5; warming levels are determined based on the thirty-year running mean temperature in the Corn Belt.

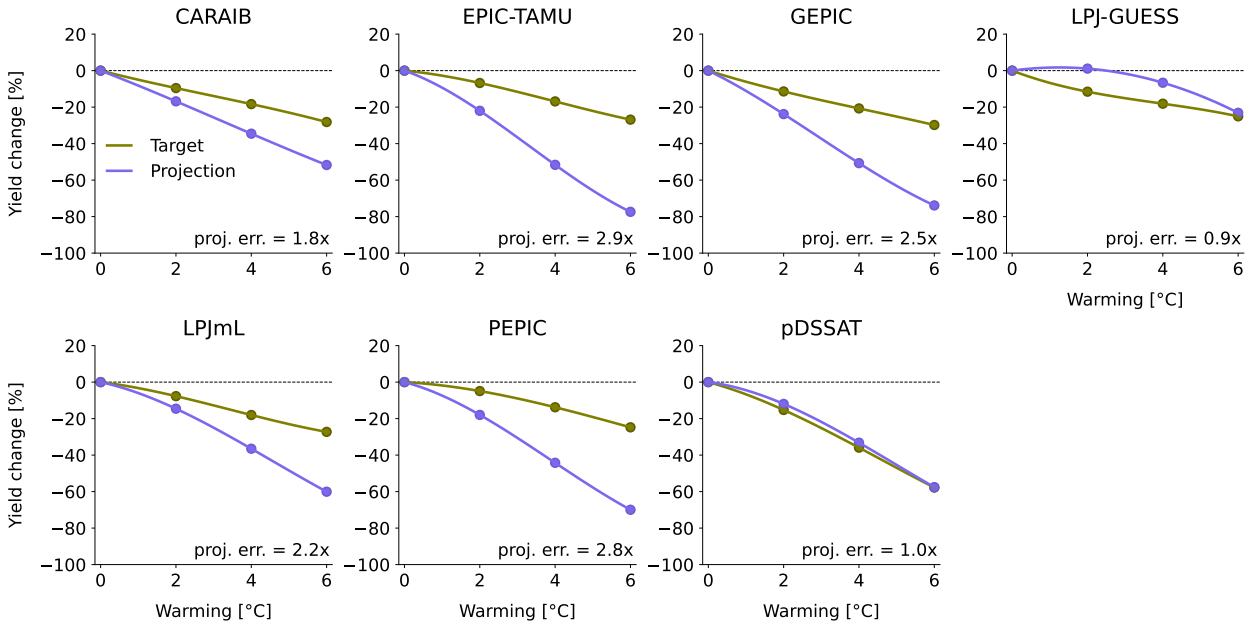

Figure S1: TP statistical model projections across all seven simulated yield datasets under uniform warming scenarios, as in Figure 2.1a. Green lines show target yield changes and purple lines show projections of the respective TP statistical model trained under historical conditions. Titles correspond to the process-based model used in each case to produce the simulated training set. Text values in each panel show the fractional projection error under warming of 6 °C (bottom right of each subplot). TP statistical models overproject target yield losses by factors of 1.8–2.9 in five of the seven simulated yield datasets.

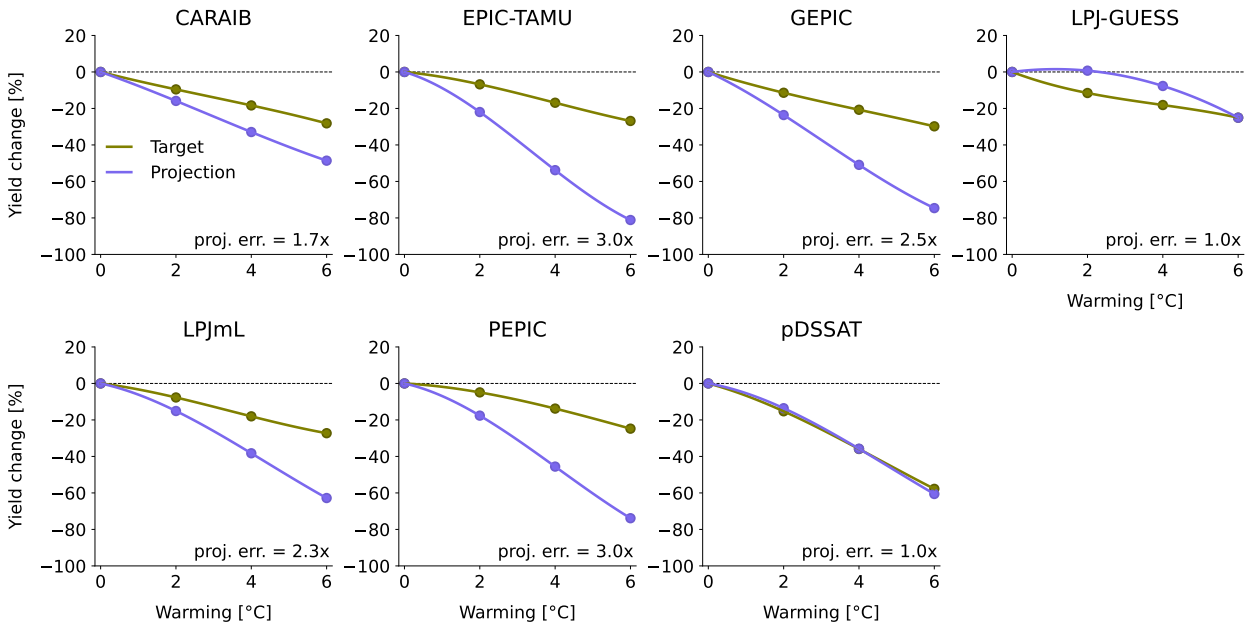

Figure S2: As in Figure S1, but for TP statistical models with stepwise temperature responses (equations shown in Methods). Results are similar to the piecewise linear TP model findings.

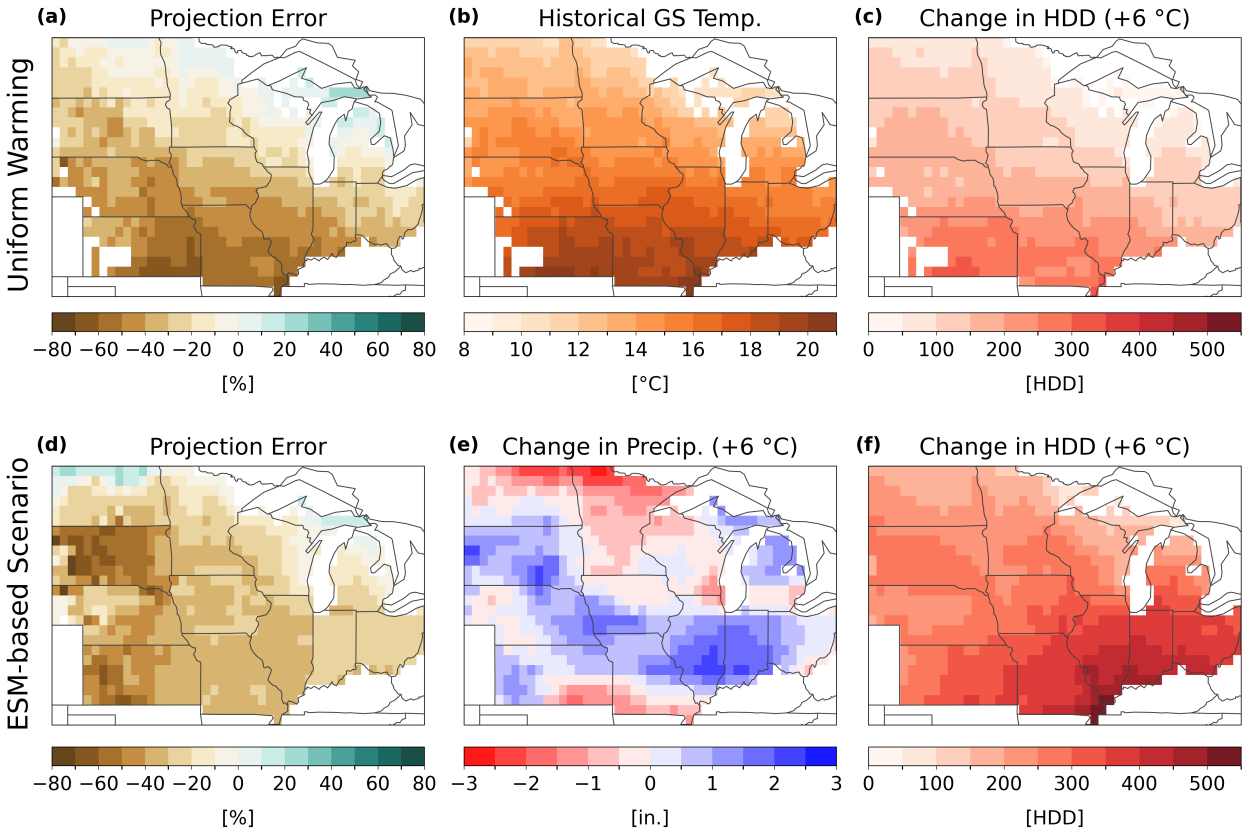

Figure S3: Spatial patterns of projection error for the TP statistical models along with related weather conditions. The top row corresponds to projections for a TP model trained and tested on yields by LPJmL under uniform warming scenarios. Top left shows the average projection error under warming of six degrees (same as inset map of Figure 2.1a). Top middle shows the average baseline (1981–2010) growing-season temperature. Top right shows the average change in HDDs under warming of +6 °C. The bottom row corresponds to projections for a TP model trained and tested on yields by LPJmL under the ESM-based scenario (RCP8.5), analyzed at a mean growing-season warming of +6 °C (2067–2096). Bottom left shows the average projection error (same as inset map of Figure 2.1b). Bottom middle shows the average change in precipitation. Bottom right shows the average change in HDDs. Projection error in the uniform warming scenario shows a correlation to baseline temperatures and the change in HDDs. Precipitation changes appear to influence projection error in the ESM-based scenario.

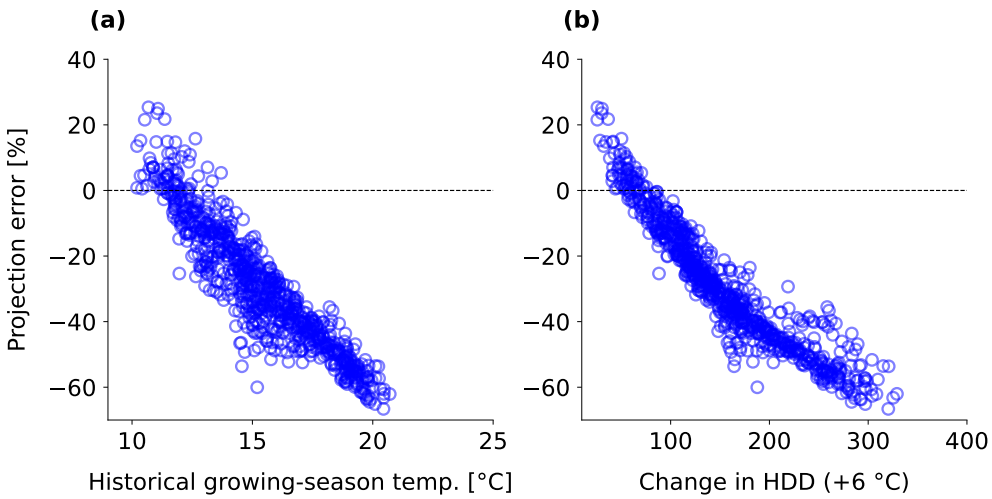

Figure S4: Projection error and temperature conditions for the TP statistical model trained and tested on yields by LPJmL under uniform warming scenarios. (a) Scatter plot shows the average projection error in each gridcell against the respective average historical growing-season temperature. (b) Scatter plot shows the average projection error in each gridcell against the respective average increased in HDDs under +6 °C. Projection error under warming is strongly associated with HDD increases, which correlates with baseline temperatures.

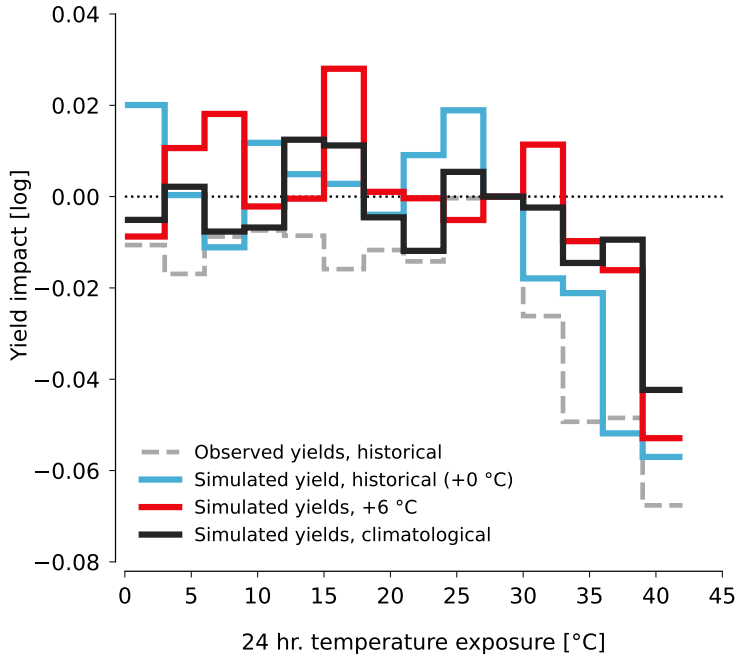

Figure S5: Statistical model temperature responses, in the same fashion as Figure 2.2a, for the stepwise TP model trained on yields by LPJmL under uniform warming scenarios. Lines show the impact on yields of a day of at each temperature, for models trained on simulated yields under historical weather (purple), +6 °C warming (orange), and all training data (+0, +2, +4, and +6 °C, green). The grey line shows the response of a similar multi-bin model trained on U.S. maize observations. As with the piecewise linear temperature response, the stepwise response also shows decreasing sensitivity to high temperatures when trained on variations within the +6 °C climate state, and even less sensivity when trained on variations across climate states.

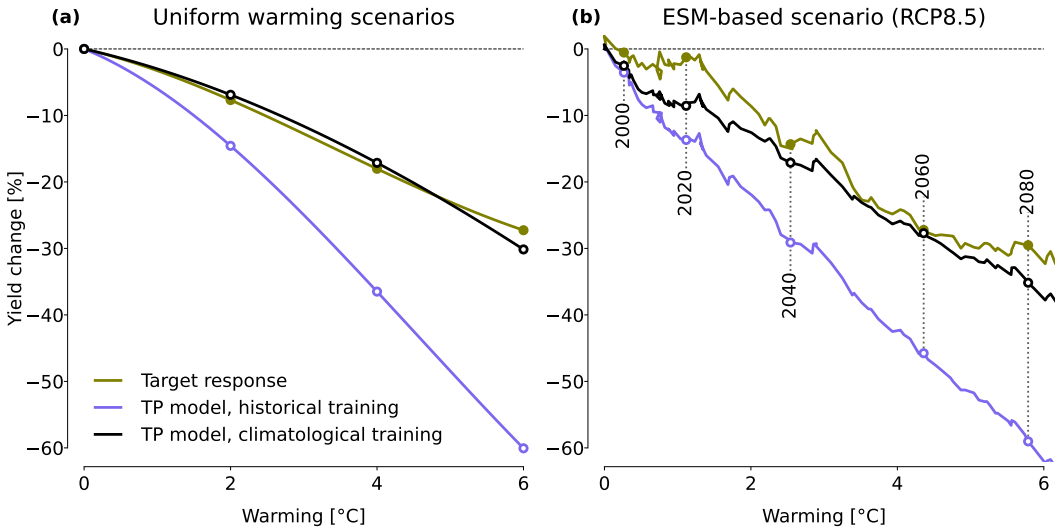

Figure S6: Same format as line plots in Figure 2.1, now for projections from TP statistical models trained across all climate states (historical, +2 °C, +4 °C, +6 °C). **(a)** Line plots show yield changes under uniform warming scenarios. The solid green line shows the target yield response and the solid blue line shows the projection from a TP statistical model trained under historical conditions (same as line plot in Figure 2.1a). The dashed blue line shows the projection from a TP model trained on variations across all warming scenarios, referred to as the climatological TP model. **(b)** Same format as (a) for results under the ESM-based scenario, with vertical dashed lines indicating the mean warming at vicennial markers. Climatological TP models project more accurate yield changes under warming relative to historically trained models. This is to be expected, however, as the climatological models are trained on data across all warming levels, so their projections are all in-sample.

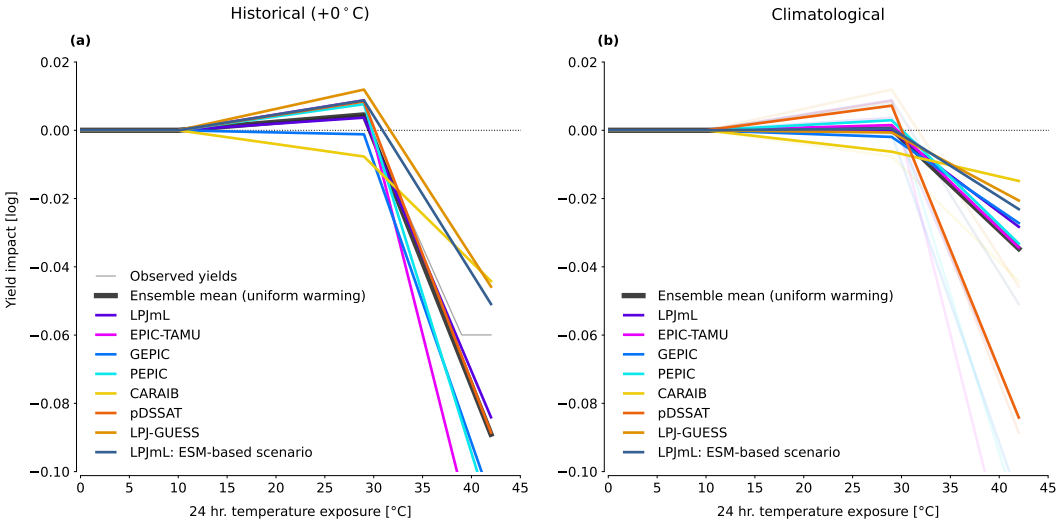

Figure S7: Temperature responses for TP statistical models across all seven simulated yield datasets under uniform warming scenarios, in the same format as Figure 2.2 (which showed only LPJmL). **(a)** Colored lines represent temperature responses for TP statistical models trained on different simulated yields (CARAIB, EPIC-TAMU, GEPIC, LPJ-GUESS, LPJmL, pDSSAT, PEPIC) under historical conditions. The gray line The gray line corresponds to a similar temperature-precipitation statistical model from the literature trained on observed U.S. maize yield variations within historical conditions [10], for comparison; note that this model is slightly different in its flattened response for temperatures above 39 °C. **(b)** Same layout as (a), now showing TP statistical models trained on varitions across climate states. Nearly all TP statistical models show a weakening sensitivity to high temperatures (i.e. HDDs) when trained across climate states relative to historical responses; this misalignment contributes to statistical model projection error under warming.

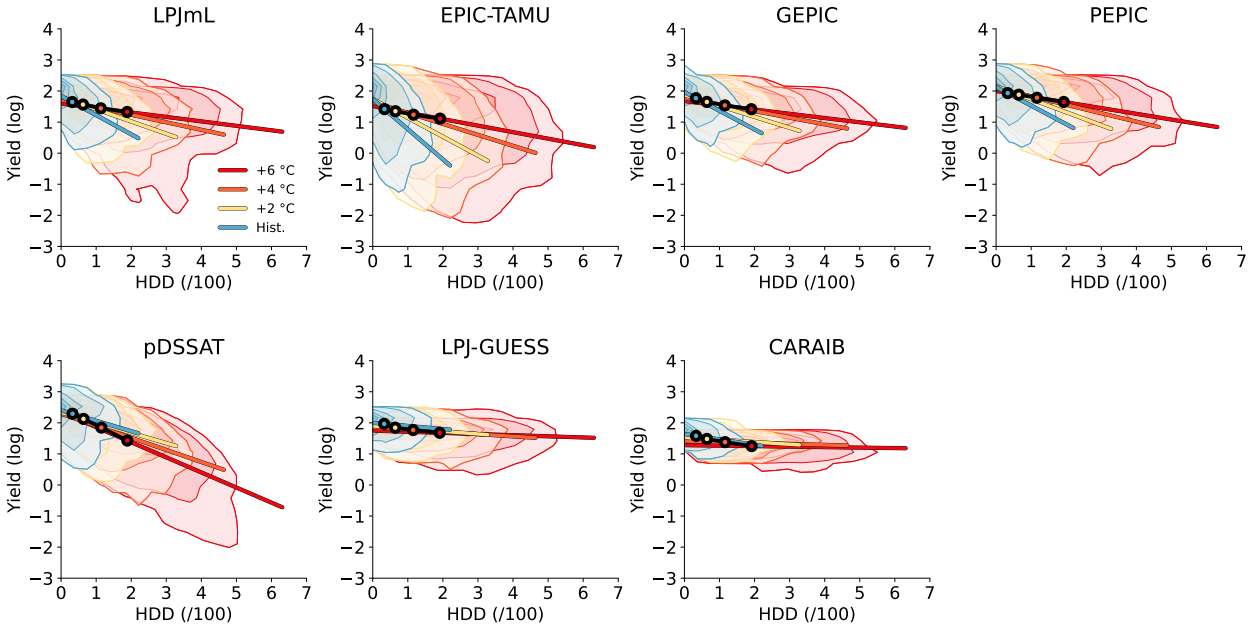

Figure S8: Yield-HDD associations across all seven simulated yield datasets under uniform warming scenarios, in the same format as Figure 2.3a (which showed only LPJmL). Each panel corresponds to simulated yields by a different process-based model. Colored contours show the distribution of growing-season cumulative HDDs and simulated yields under uniform warming scenarios. Solid colored lines show the linear association within each scenario. Colored dots outlined in black show the mean yield and HDD value in each scenario, with the connecting black line representing the climatological relationship. Simulated yields generally show changing yield-HDD associations under warming scenarios.

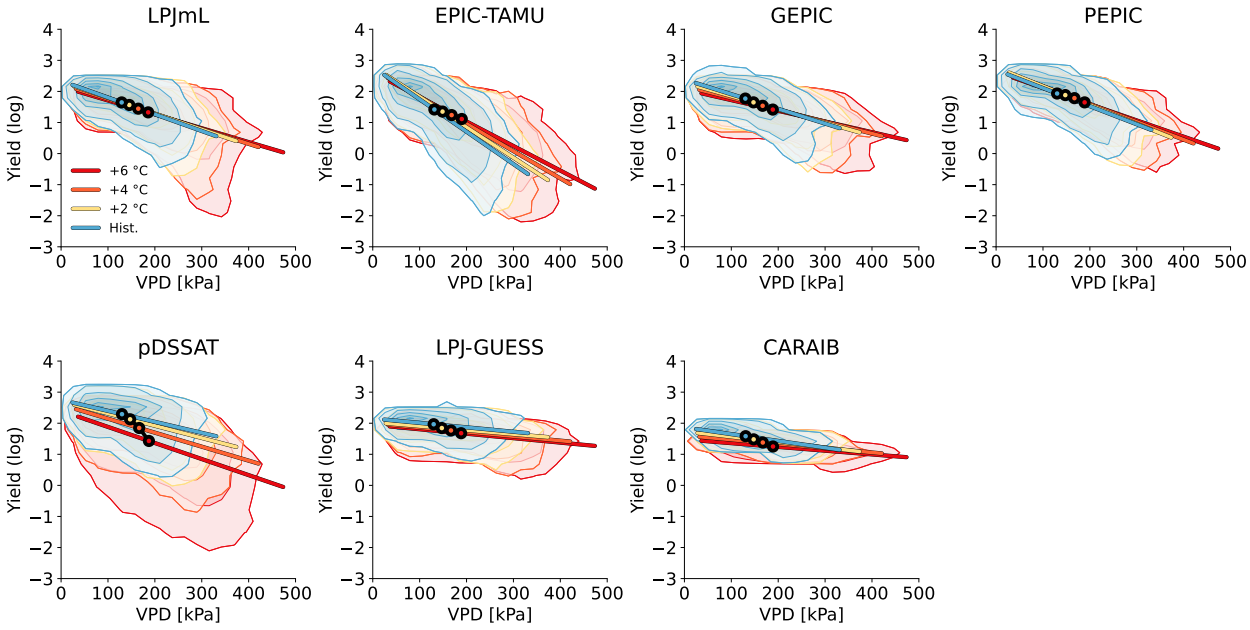

Figure S9: As in Figure S8, but for yield-VPD associations. Yield relationships to VPDs are generally roughly consistent between historical and climate states.

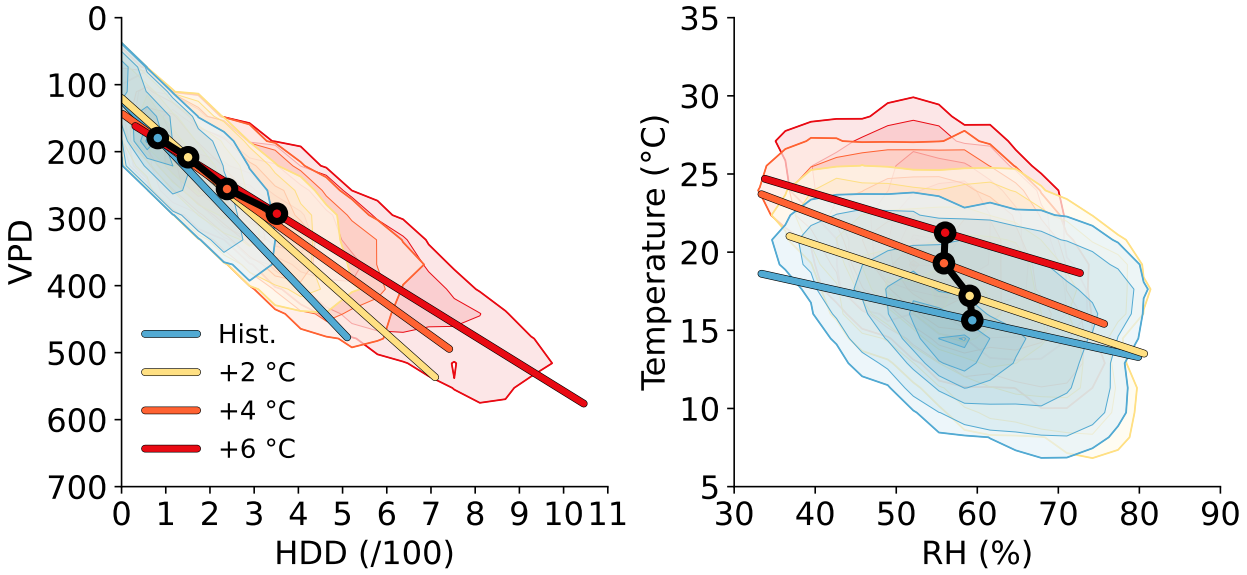

Figure S10: VPD, HDD, and humidity associations under the ESM-based scenario. **(a)** Colored contours show the distribution of growing-season cumulative VPD [kPa] and HDD values, separated by the mean growing-season warming level (corresponding years shown in Figure 2.1). Solid colored lines show the linear association within each warming level. Colored dots with black outlines show the mean value in each warming level, with the connect solid black line representing association across climate states. **(b)** Same format as (a), but not showing growing-season mean temperature against growing-season mean relative humidity. Like the uniform warming scenarios, the realistic warming scenario also shows changing heat-moisture associations as growing-season temperature increases.

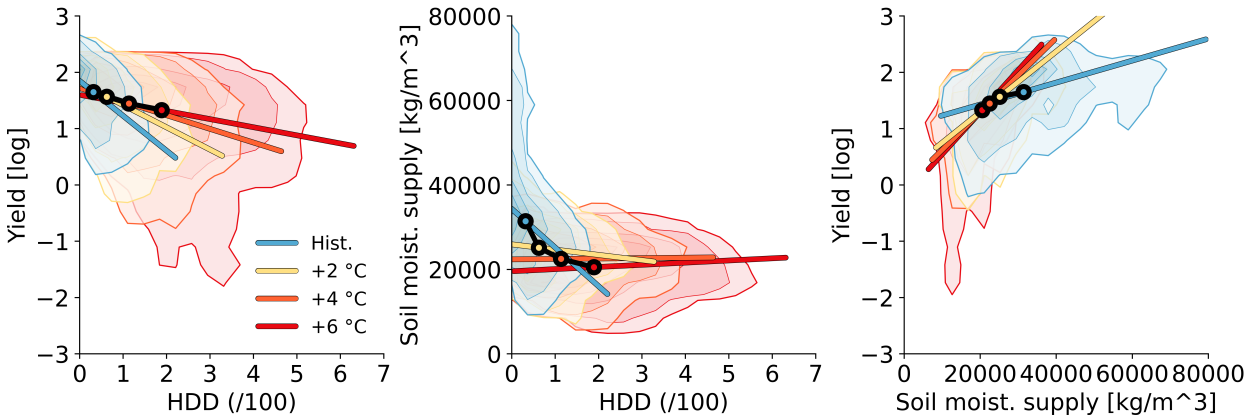

Figure S11: Yield, HDD, and soil moisture supply associations under uniform warming scenarios, in the same fashion as Figure 2.3. Like with VPD, associations between high temperatures and soil moisture supply differ between historical and climate states. Yield associations with soil moisture are less stable than the association with VPD. However, the relationship is roughly similar between historical and climate states, causing statistical models based on soil moisture to project yield changes more accurate than TP statistical models.

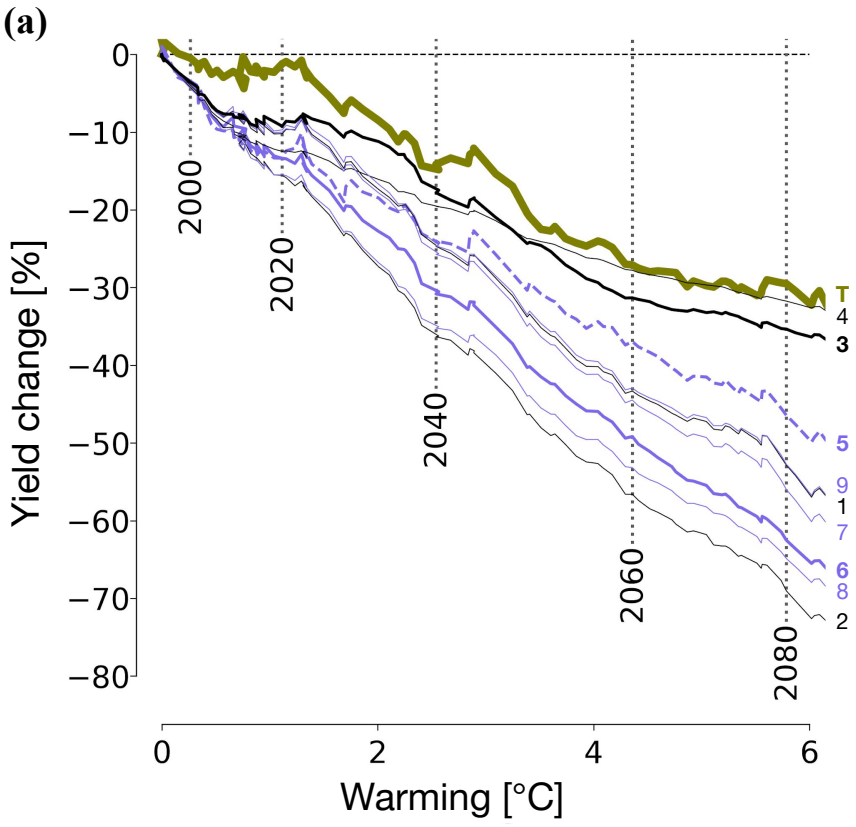

Figure S12: Statistical model projections in the ESM-based scenario (RCP 8.5), in the same fashion as Figure 2.4a.

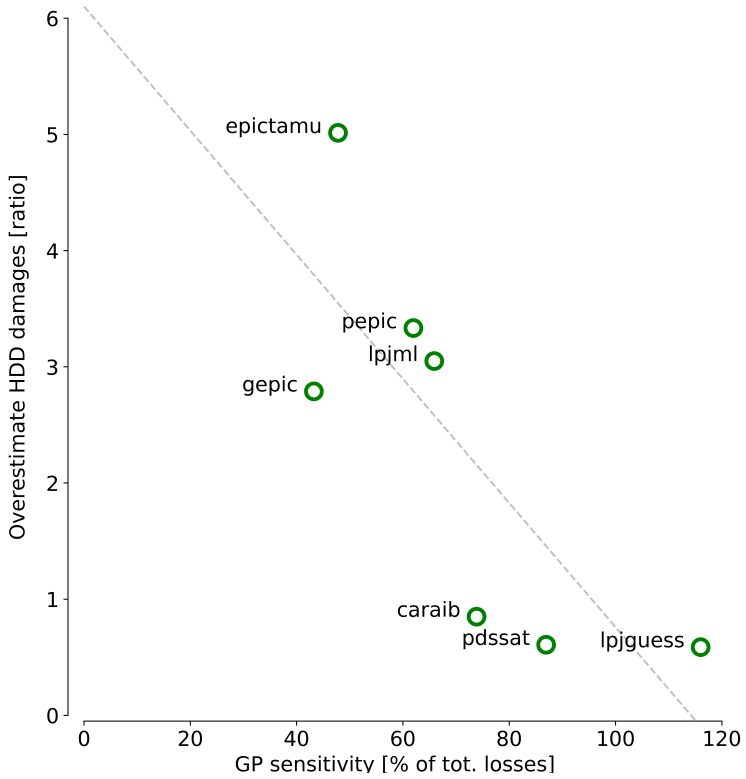

Figure S13: Comparisons of overestimated temperature damages and process-based-model sensitivities to water supply and growing-period shortening. Scatter plot shows the overestimated HDD damages for respective TP statitsical models trained on each of the simulated yield datasets under uniform warming (+6 °C), plotted against the yield sensitivity to growing period shortening for the underlying process-based models. Sensitivities to the growing period represent the percentage portion of yield losses under the +6 °C that can be attributed to growing period shortening (i.e. accelerated maturity). Overestimated HDD damages show a positive relationship to water sensitivity, which in turn shows a negative relationship to growing-period sensitivity. Thus, it appears yield sensitivities under increased temperatures in the process-based models can be approximately broken down into two responses: sensitivity to water stress and sensitivity to growing period shortening. For water-sensitive models, the TP statistical model cannot capture the underlying behavior, and thus overprojects yield damages based on historical hot-dry correlations. For GP-sensitive yields, the TP statistical model can mostly capture target yield losses because the HDD feature acts as a proxy for growing period shortening. An ideal statistical model with features related to water-sensitive and growing-period responses may accurately project yield responses in warming scenarios for all simulated yield datasets in the ensemble.

S2 Supplemental Materials for Chapter 3

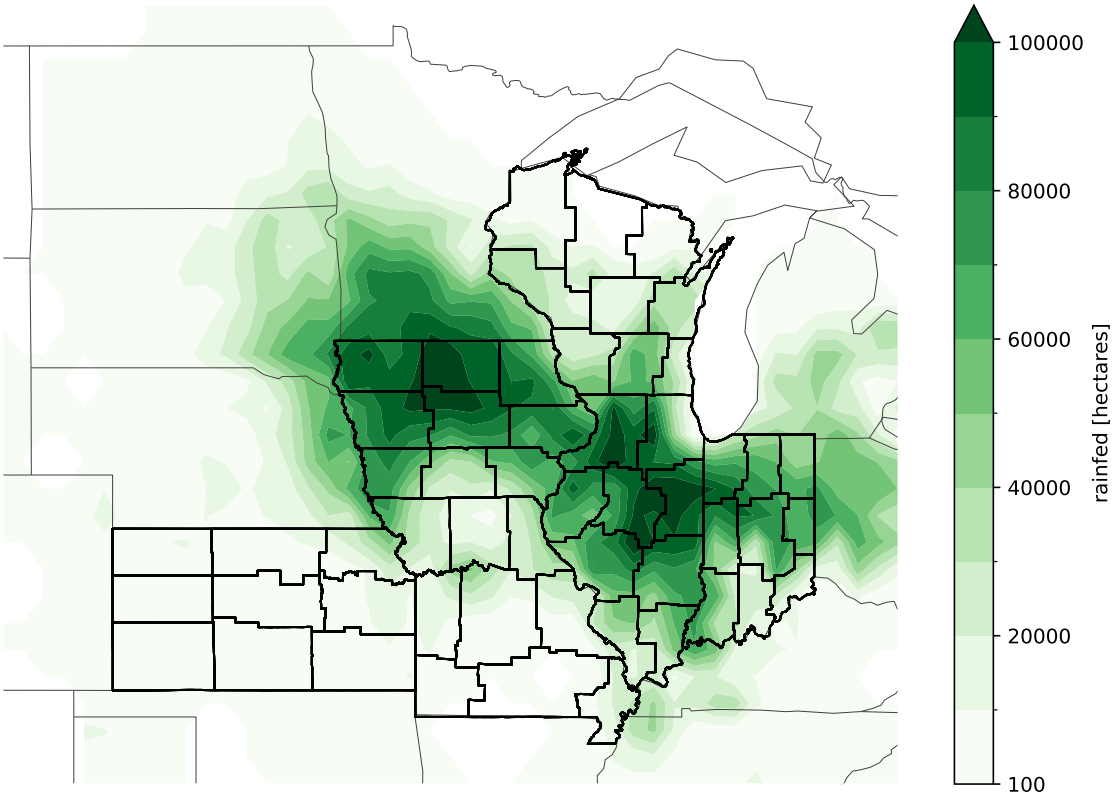

Figure S14: A map showing rainfed maize cultivation areas across the Corn Belt, taken from the MIRCA2000 product [71]. Bold borders outline the agricultural districts in our study. The six states included (KS, IL, IN, IA, MO, and WI) account for 50% of U.S. Corn Production.

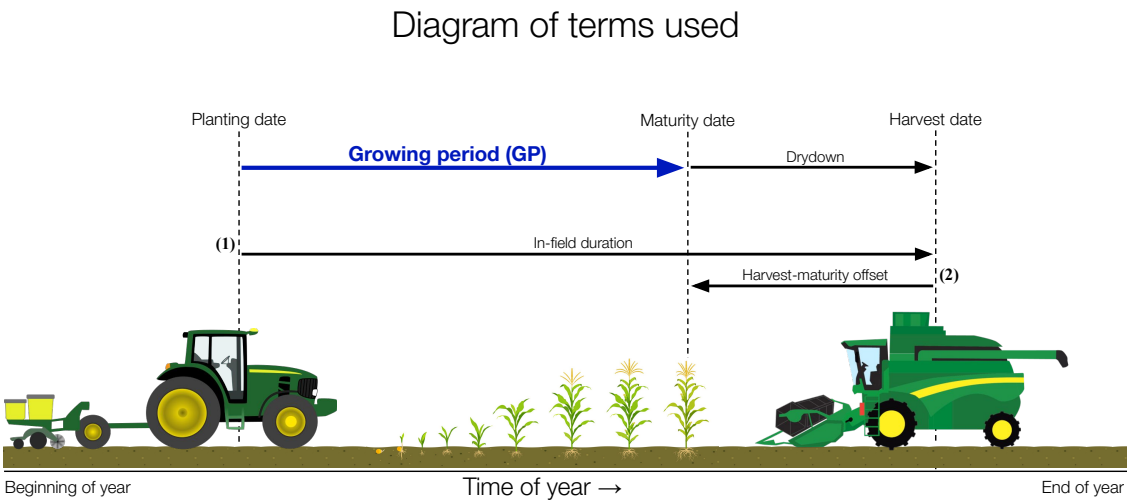

Figure S15: A diagram displaying the definition of maturity duration and its calculation (not to scale). Maturity duration is defined as the number of days from the sowing date to the approximate maturity date. It is calculated by: **(1)** taking district-level durations between sowing and harvest date (i.e. in-field duration), then **(2)** subtracting state-level offsets between harvest and maturity dates. Process-based models that tune management and cultivars based on state-level records can miss considerable in-state heterogeneity.

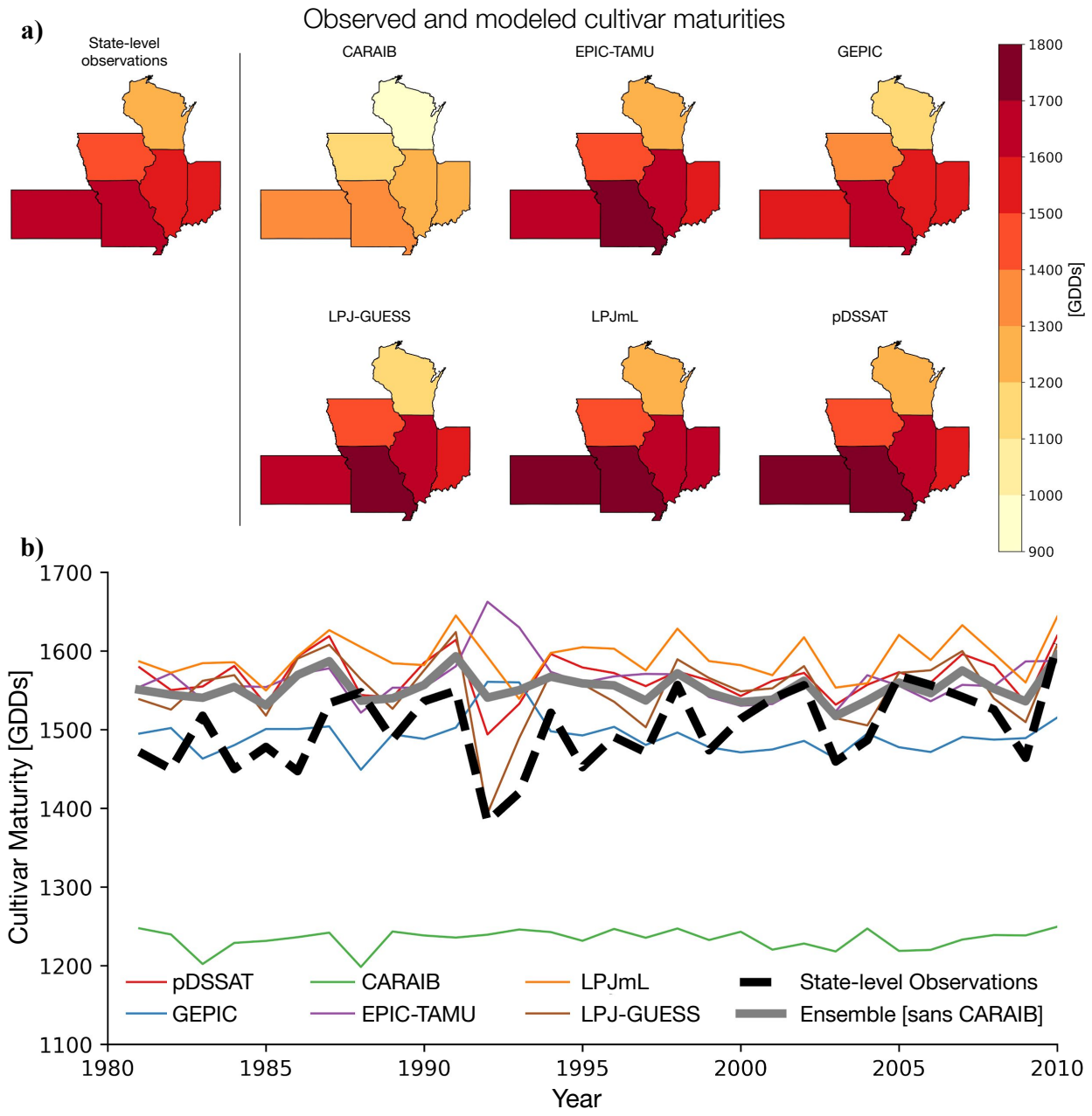

Figure S16: Comparison of observed and modeled historical cultivar maturities. **(a)** Map subplots show average historical maize cultivar maturities for observations, calculated from state-level crop calendars, and each process-based model considered in the ensemble. **(b)** Line plots show the historical timeseries of regional average cultivar maturities for observations and models. Models show slightly later maturities than observations suggest, however to relatively smaller proportion than growing periods, due in part to less heat accumulation in the differing growing-period segments.

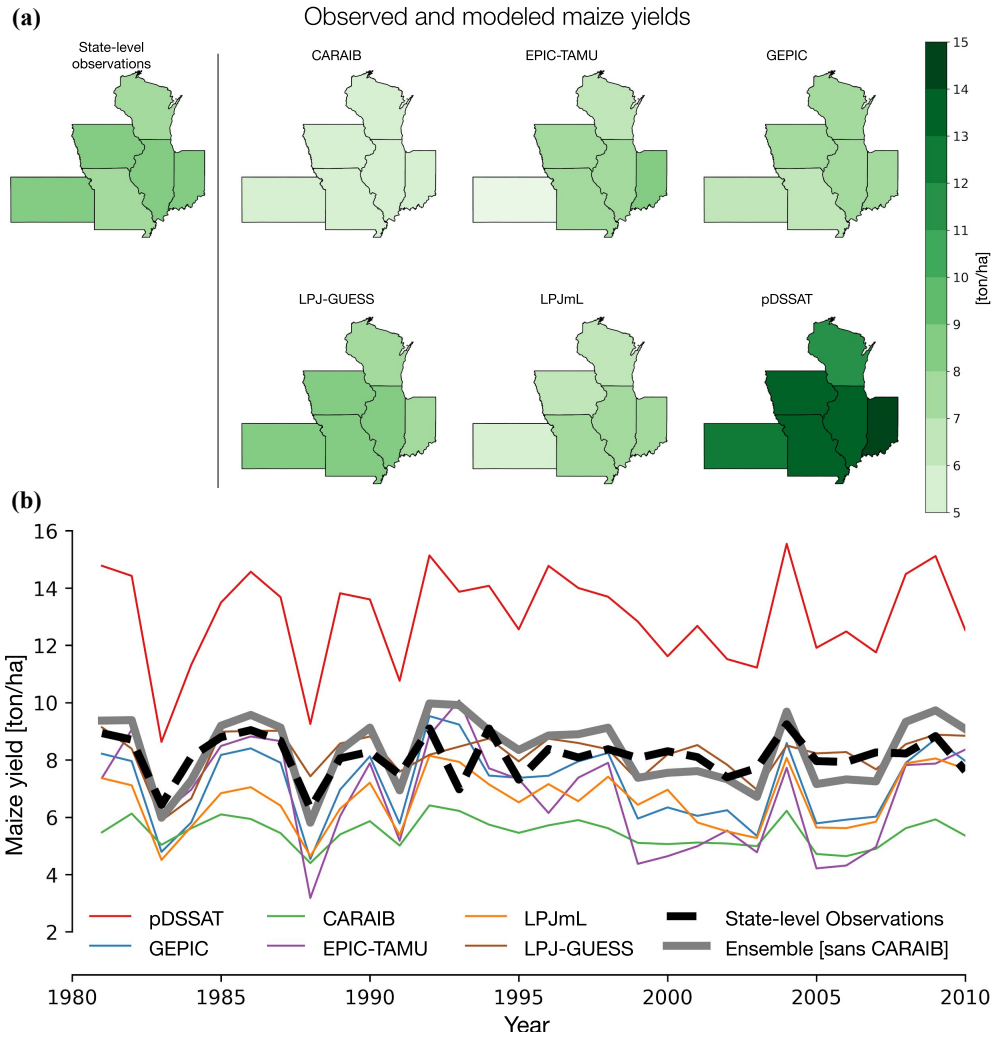

Figure S17: Comparisons of multi-year yield values between models and observations. **(a)** Map subplots show average historical maize yields for observations, taken from state-level reports, and each process-based model considered in the ensemble. **(b)** Line plots show the historical timeseries of average yields for observations and models. Ensemble mean yield values are calculated excluding values from CARAIB, which did not participate in the protocol to tune historical growing periods. Model yields align with state-level observations on average.

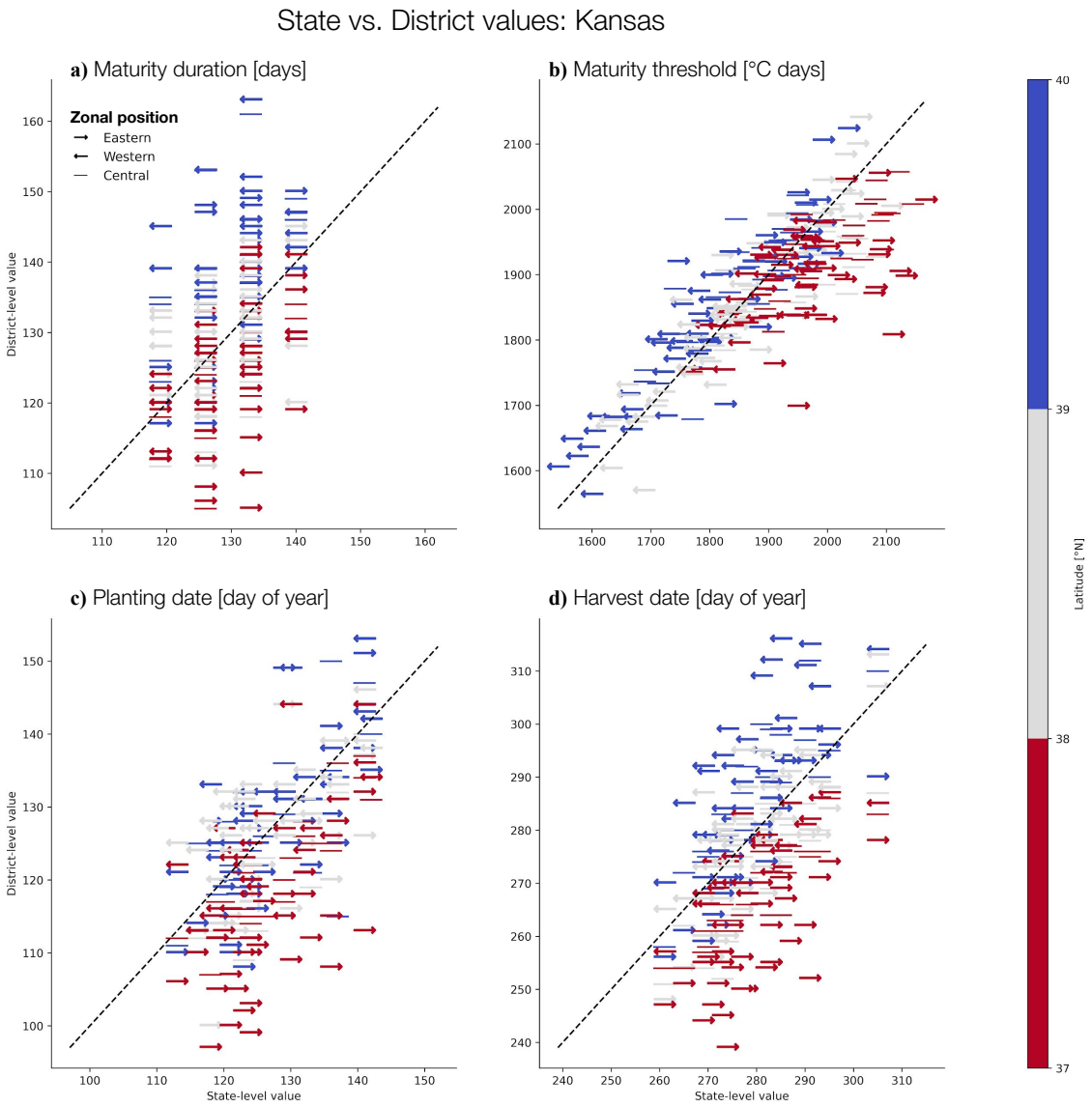

Figure S18: Comparison between district-level and state-level values for **(a)** maturity duration, **(b)** calculated maturity threshold, **(c)** sowing date, and **(d)** harvest date for the state of Kansas. Points are colored by the centroid latitude of their corresponding district and shaped according to their zonal position within the state (Eastern, Western, and Central). The dashed black line shows the 1:1 line.

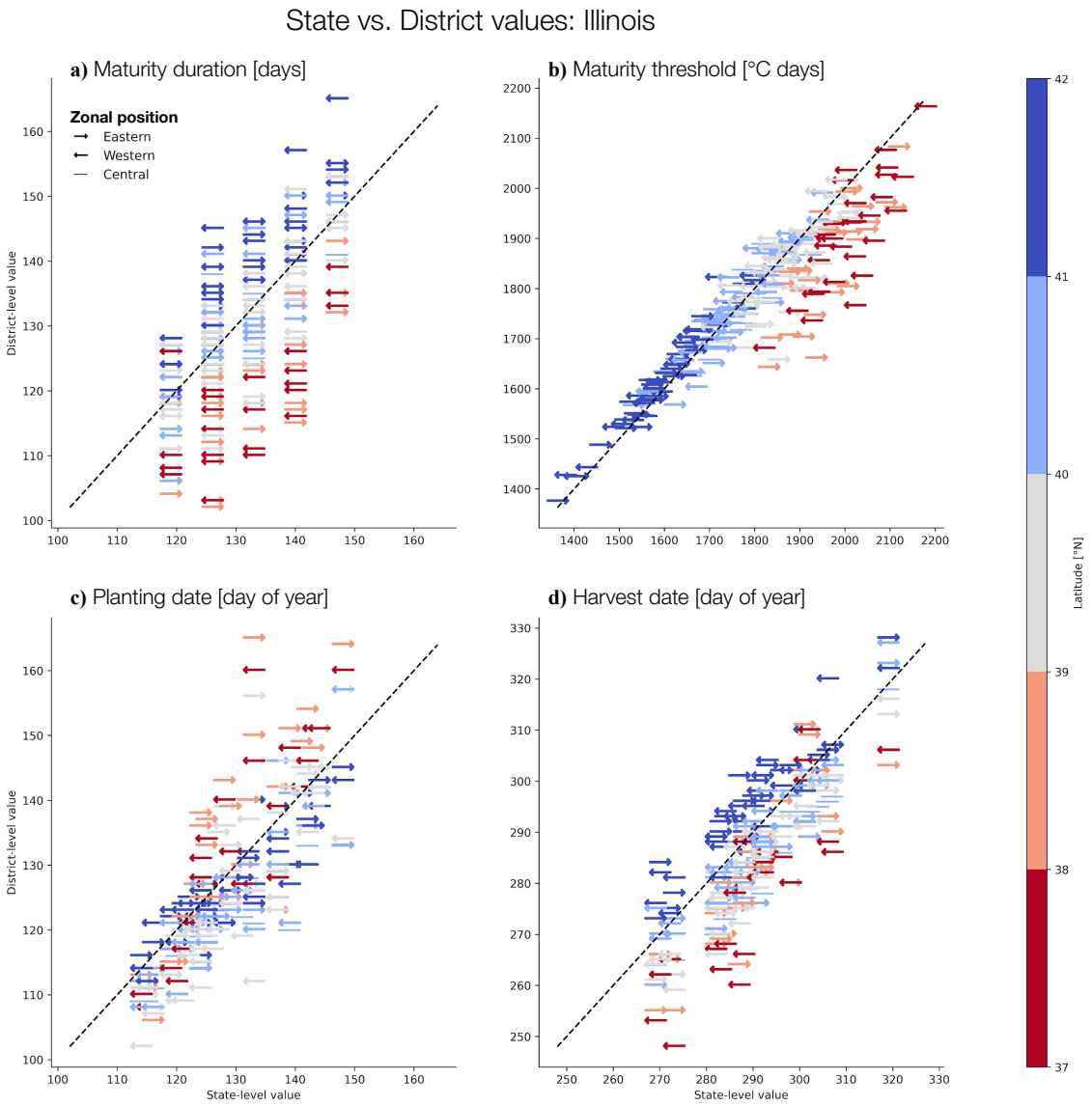

Figure S19: Same as Figure S18, but for Illinois.

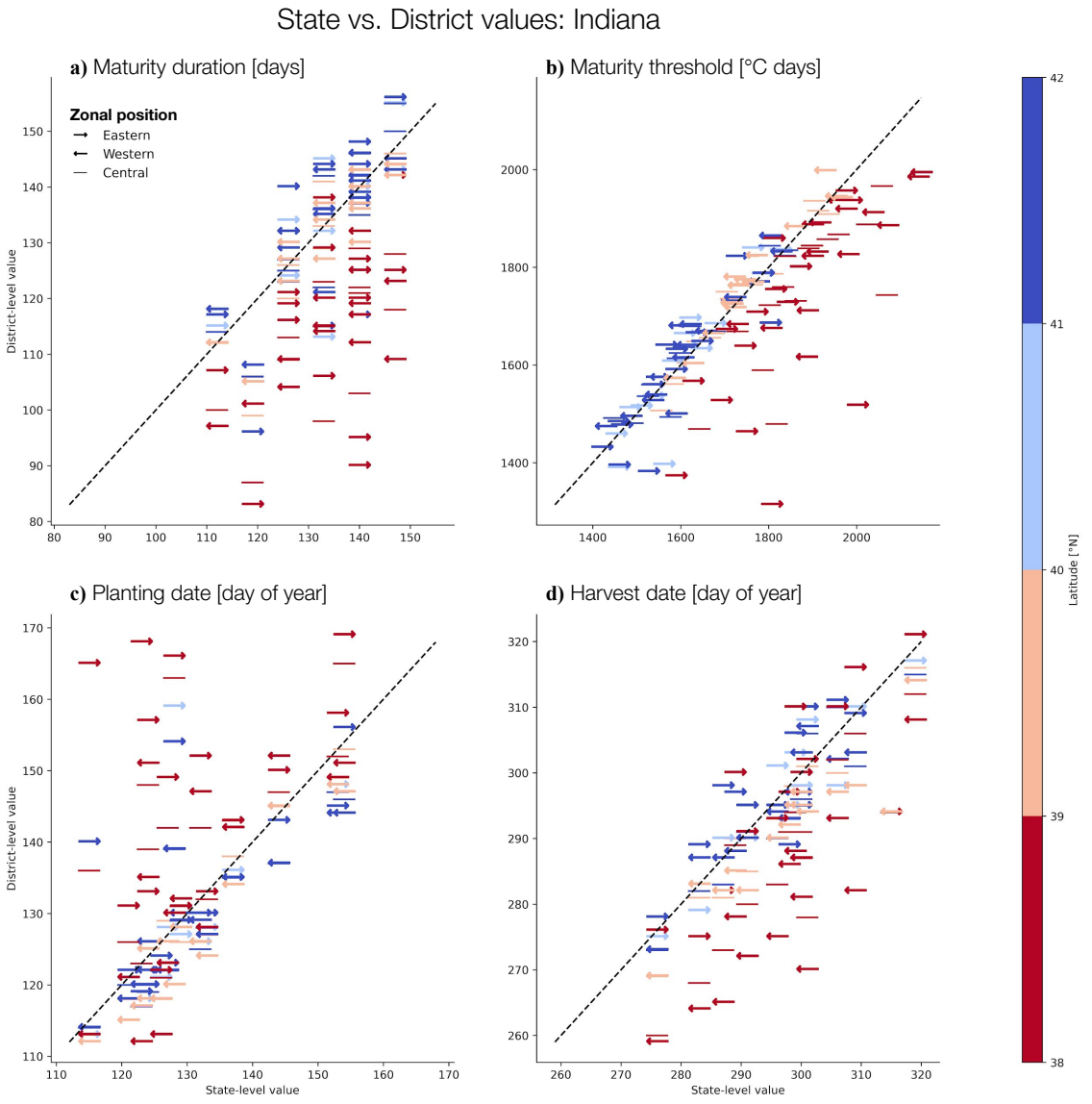

Figure S20: Same as Figure S18, but for Indiana.

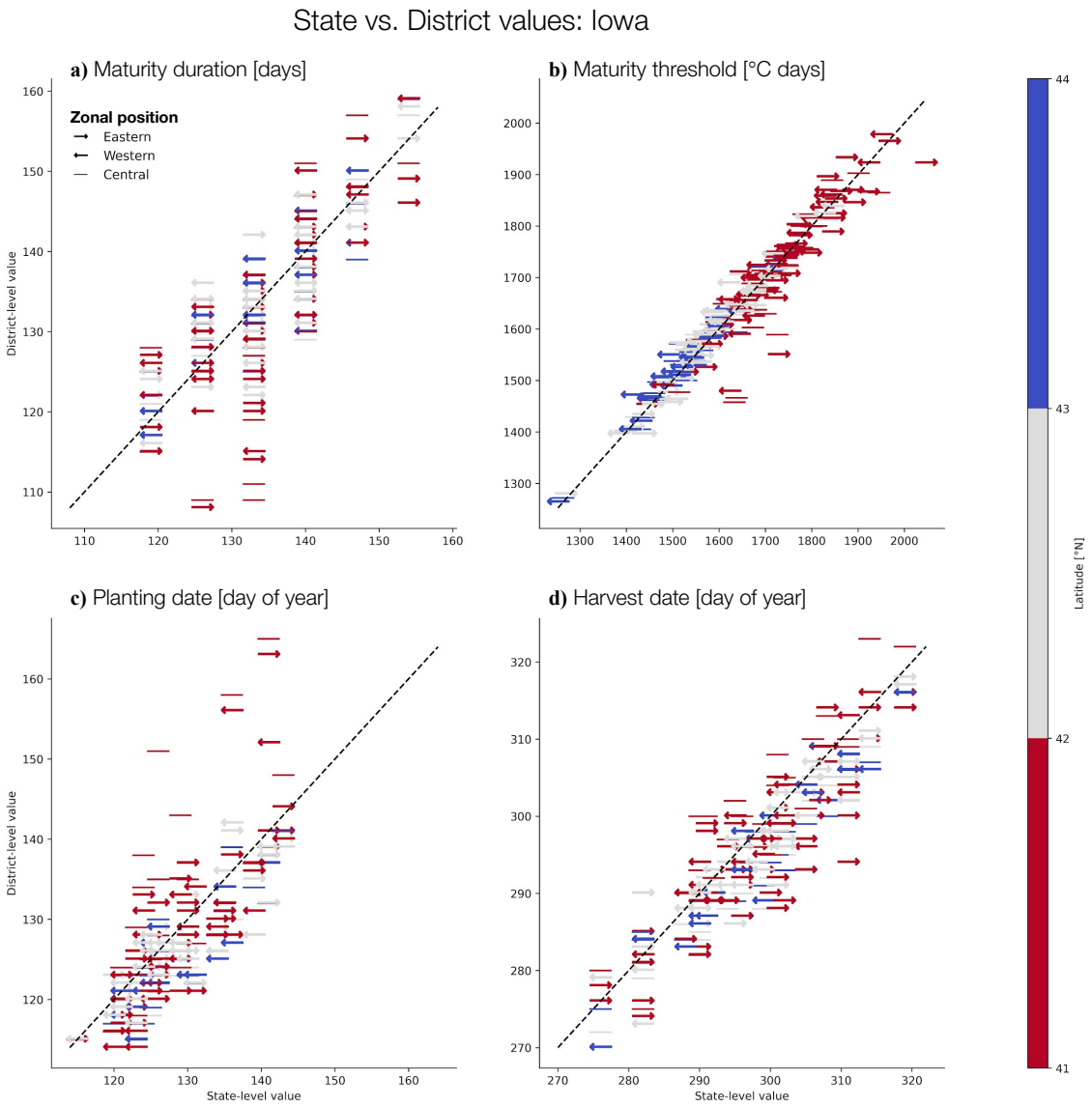

Figure S21: Same as Figure S18, but for Iowa.

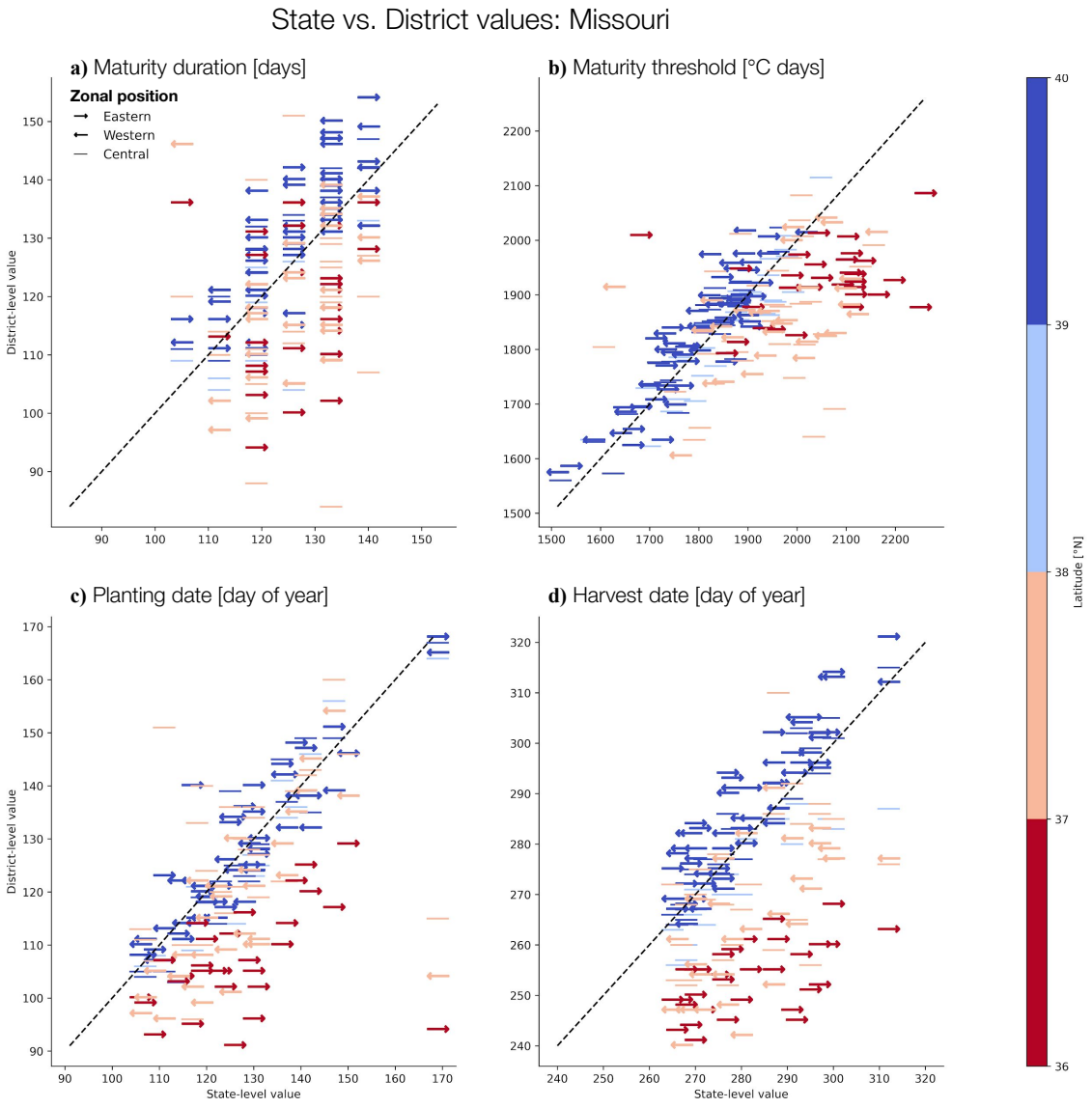

Figure S22: Same as Figure S18, but for Missouri.

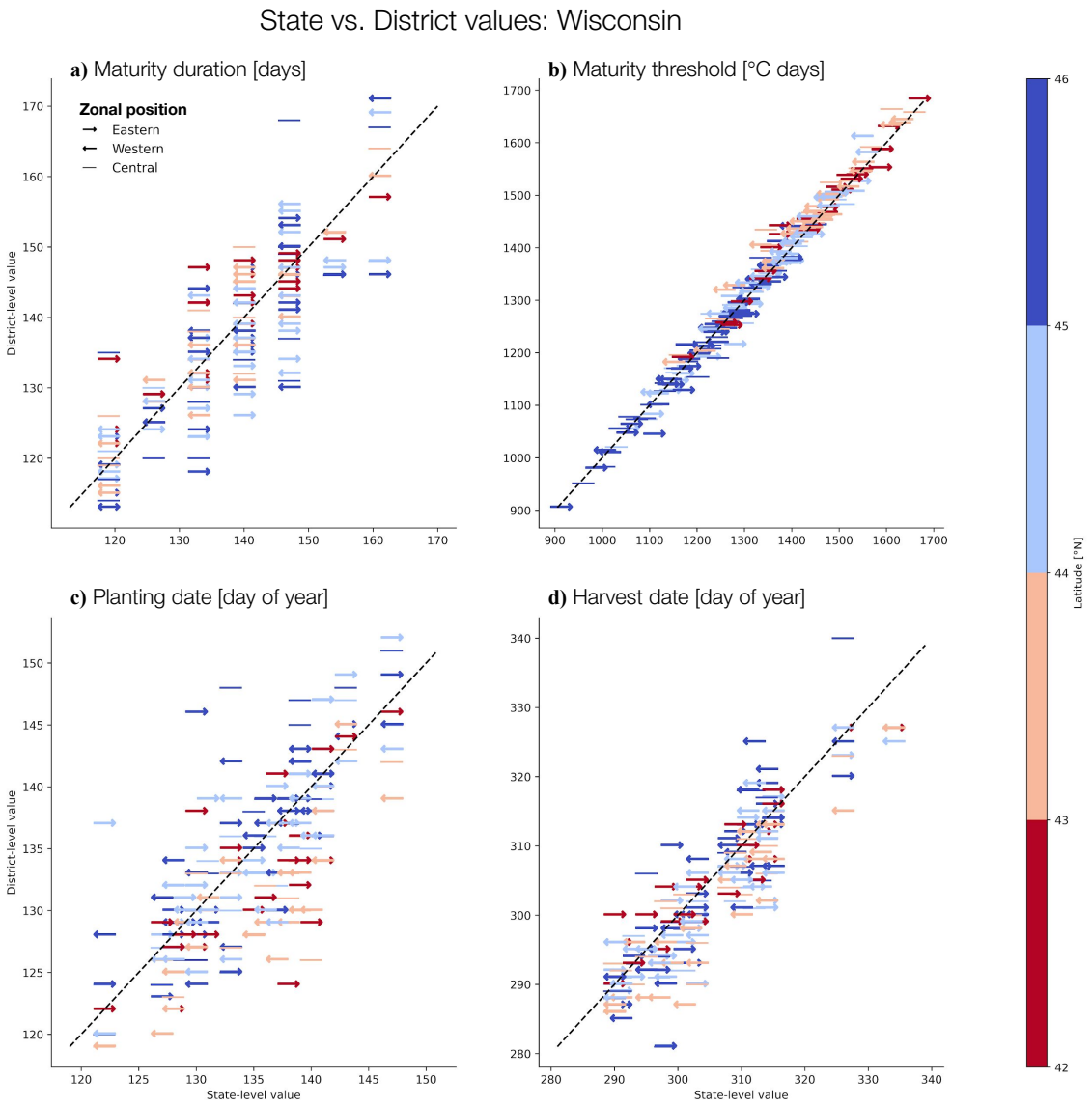

Figure S23: Same as Figure S18, but for Wisconsin.

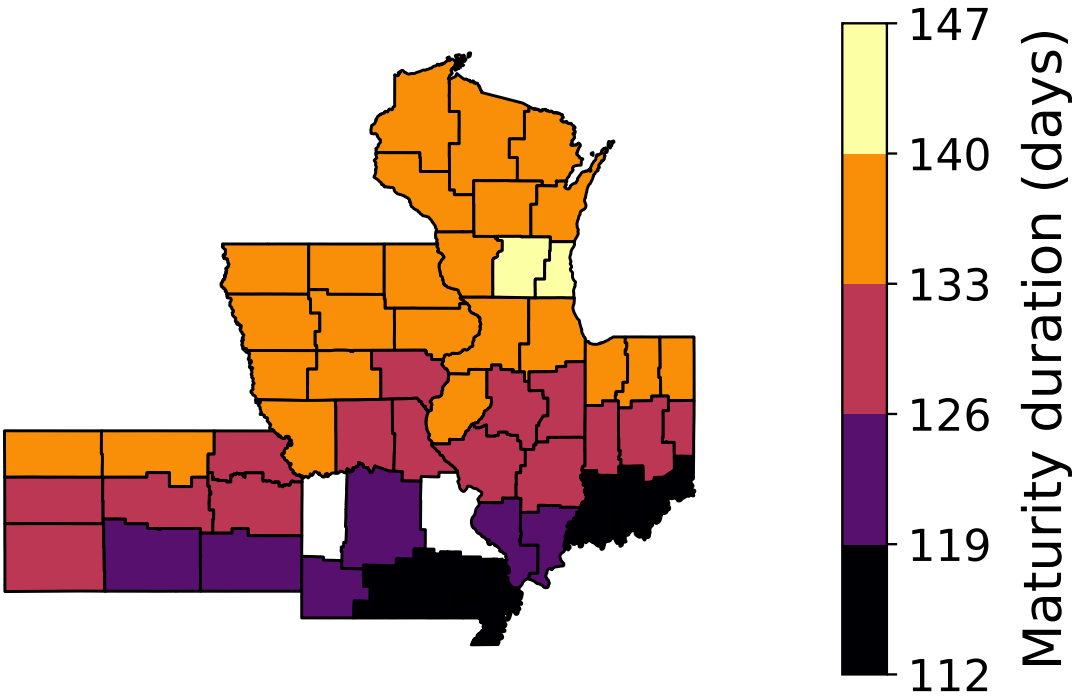

Figure S24: Spatial pattern of average historical growing periods in the Corn Belt. 112 days corresponds to 16 weeks, and 147 days corresponds to 21 weeks. Most states show a north-south gradient spanning roughly two weeks, with more similar values among districts in Iowa and Wisconsin.

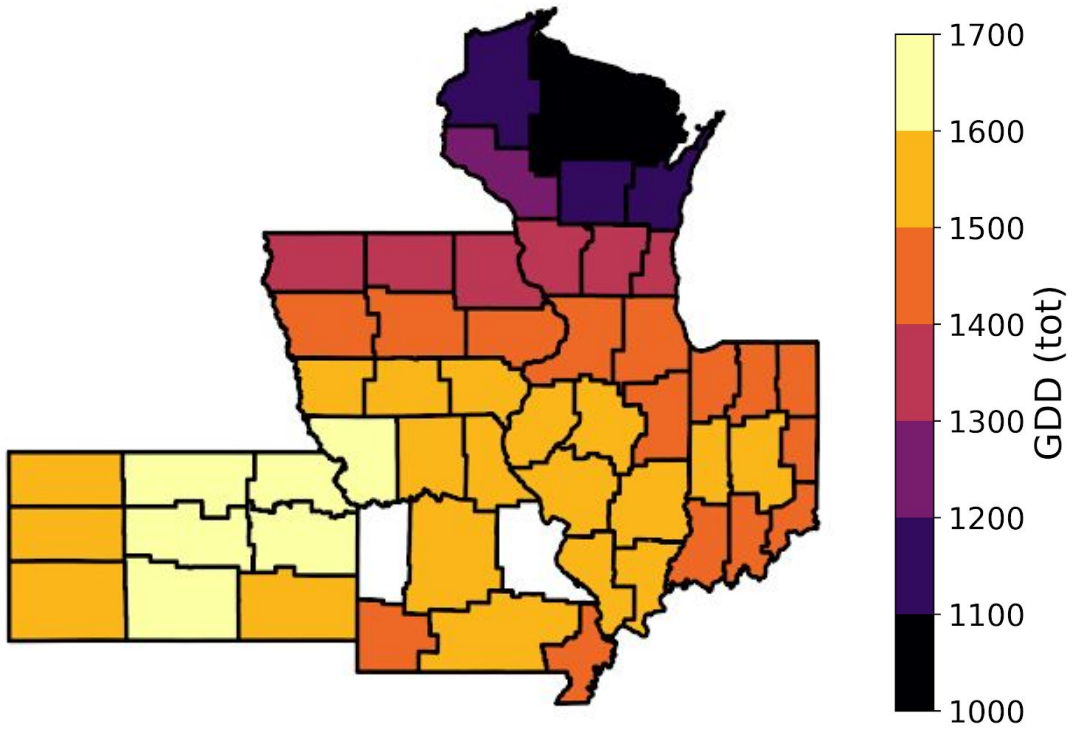

Figure S25: The spatial pattern of average historical growing-season GDDs in the Corn Belt. Cumulative GDDs are calculated across a fixed growing season (Mar 1–Aug 31) for each district and year. Heat availability in the Corn Belt shows a SW-NE gradient, with the largest availability of heat units in Kansas and Missouri, and the smallest availability in Wisconsin.

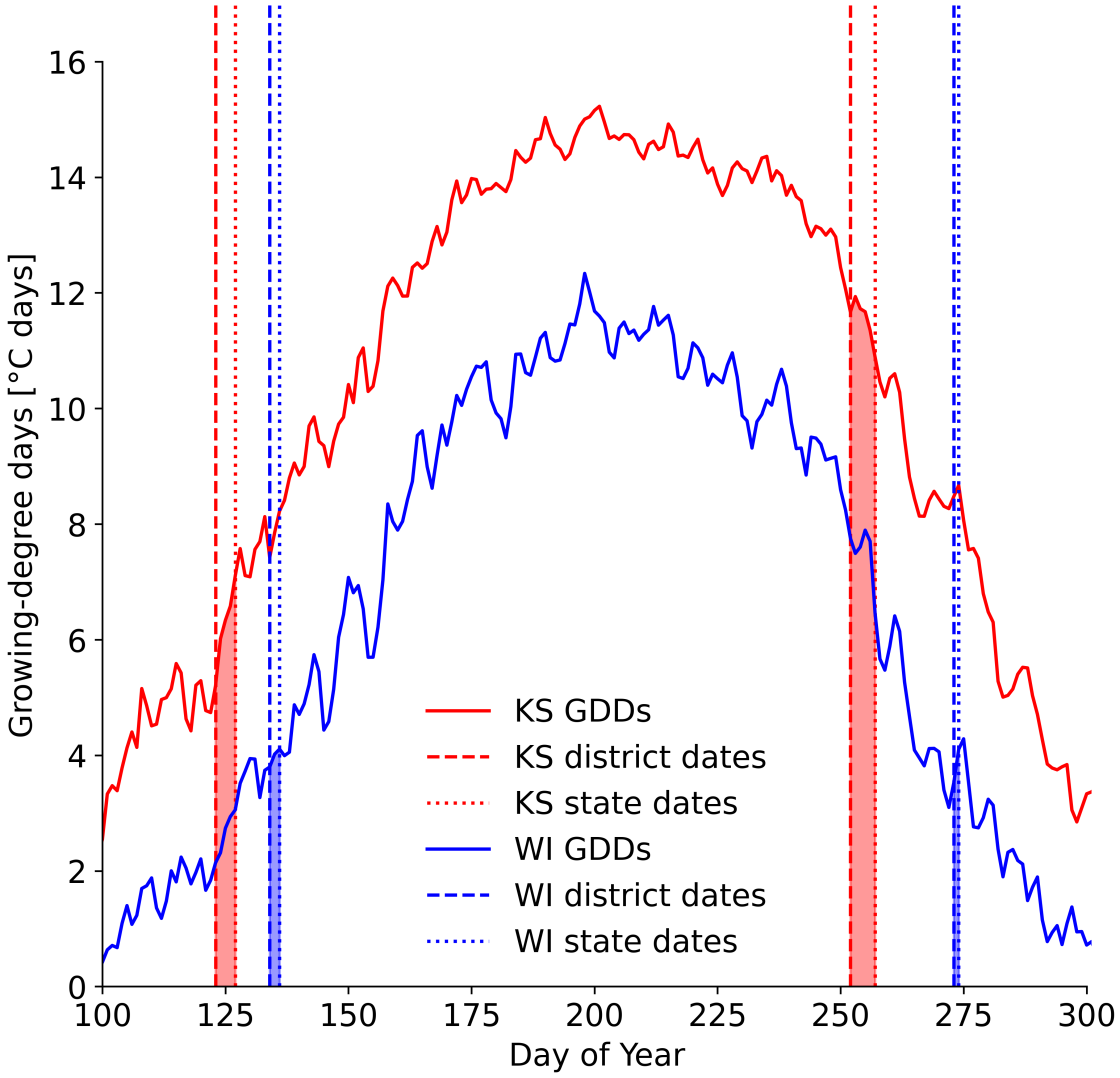

Figure S26: Comparison of differences in growing-degree days (GDDs) between Southern and Northern states. Line plots show the time series of average daily GDDs, for the period 1981–2010, within Kansas (KS, red) and Wisconsin (WI, blue). District-level sowing and maturity dates are shown by vertical dashed lines, and state-level dates are shown by vertical dotted lines. The shaded areas show the difference in accumulated GDDs between district- or state-level dates. Relative to Kansas, Wisconsin experiences lower daily GDD values and smaller differences between district- and state-level dates. Thus, Wisconsin has relatively smaller differences between calculated maturity thresholds (total accumulated GDD to maturity) based on district- and state-level dates.

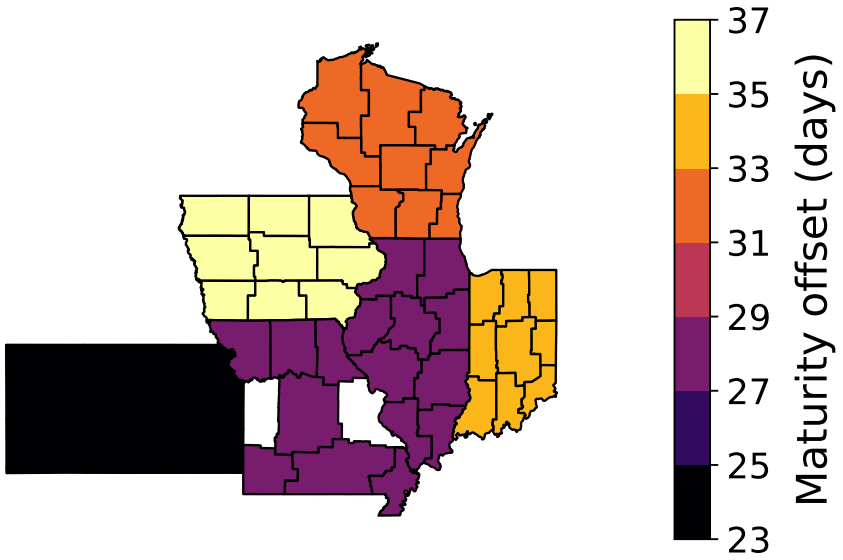

Figure S27: Mean offsets between maturity and harvest dates in state-level USDA observations for the period 1981–2010.

S3 Supplemental Materials for Chapter 4

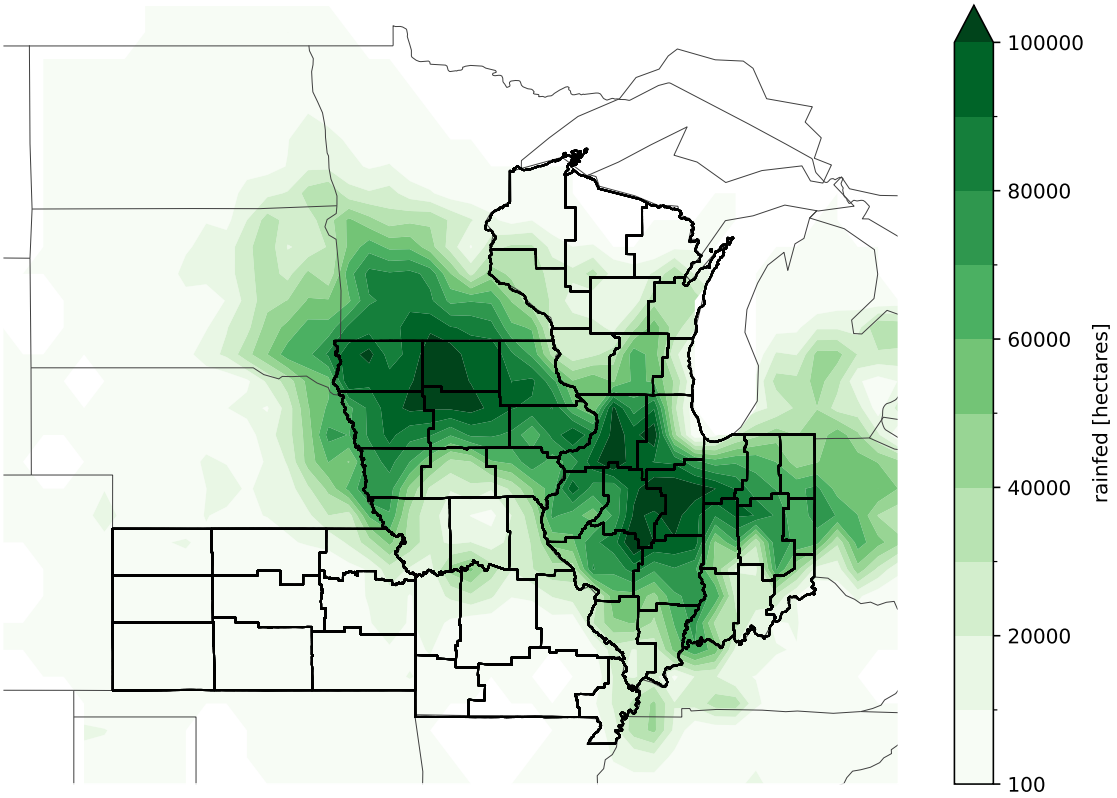

Figure S28: A map showing rainfed maize cultivation areas across the Corn Belt, taken from the MIRCA2000 product [71]. Bold borders outline the agricultural districts in our study. The six states included (KS, IL, IN, IA, MO, and WI) account for 50% of U.S. Corn Production.

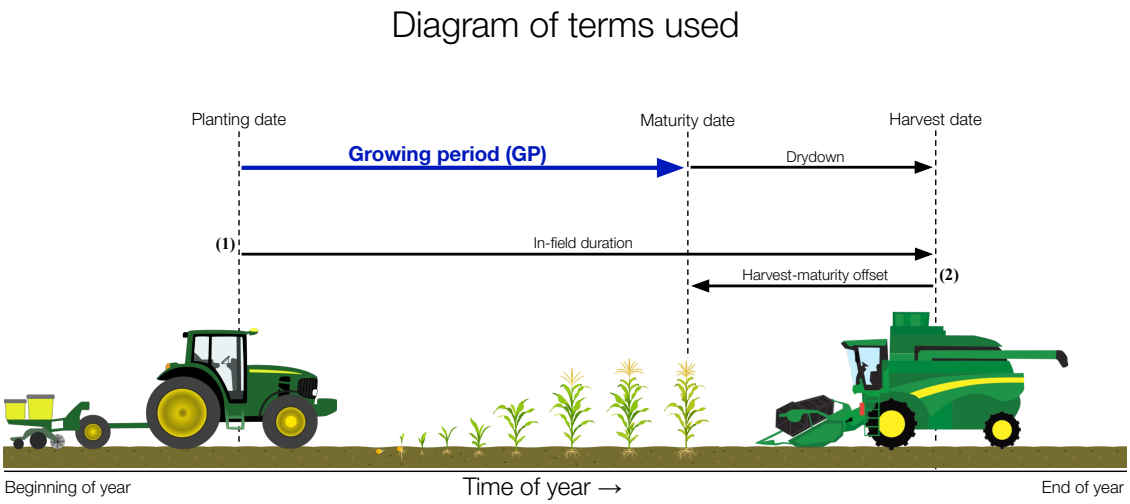

Figure S29: A diagram displaying the definition of maturity duration and its calculation (not to scale). Maturity duration is defined as the number of days from the sowing date to the approximate maturity date. It is calculated by: **(1)** taking district-level durations between sowing and harvest date (i.e. in-field duration), then **(2)** subtracting state-level offsets between harvest and maturity dates. Process-based models that tune management and cultivars based on state-level records can miss considerable in-state heterogeneity.

Model	Hist. mean yield [ton/ha]	MD change (+6 °C) [%]	Yield change (+6 °C) [%]	Maturity related impacts [% of total yield change]
CARAIB	5.5	24	27	75
EPIC-TAMU	6.9	32	29	33
GEPIC	7.3	30	30	53
LPJ-GUESS	8.1	28	25	100*
LPJmL	6.8	29	26	55
pDSSAT	13.2	29	55	87

Table S3: Mean yield, growing period, and maturity statistics for models in the GGCMI Phase 2 ensemble. * 100% of yield losses for LPJ-GUESS are due to growing period shortening based on our calculations, as growing period adaptations boost yields above baseline levels.

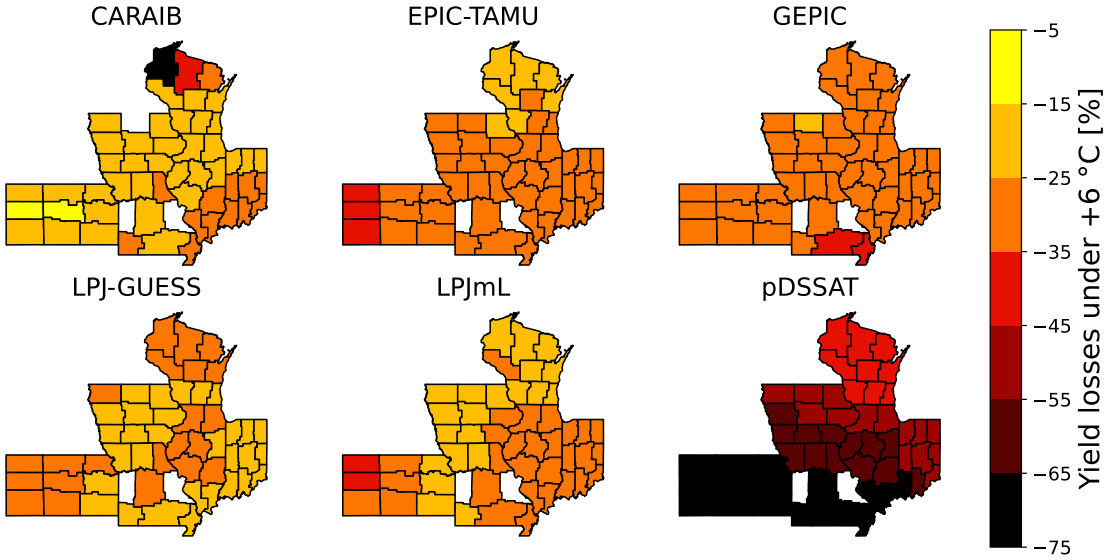

Figure S30: Mean yield losses under high Corn Belt warming across the GGCMI models. Maps show the change in 30-year mean yields from the baseline historical scenario to a uniform +6 °C perturbation scenario without cultivar adaptation. Losses in Illinois, Indiana, and Missouri, for example, are generally greater than losses in Iowa and Wisconsin. CARAIB shows relatively largest losses for northern Wisconsin. However, this is potentially due to issues with model output, as evidenced by missing data in northern Iowa.

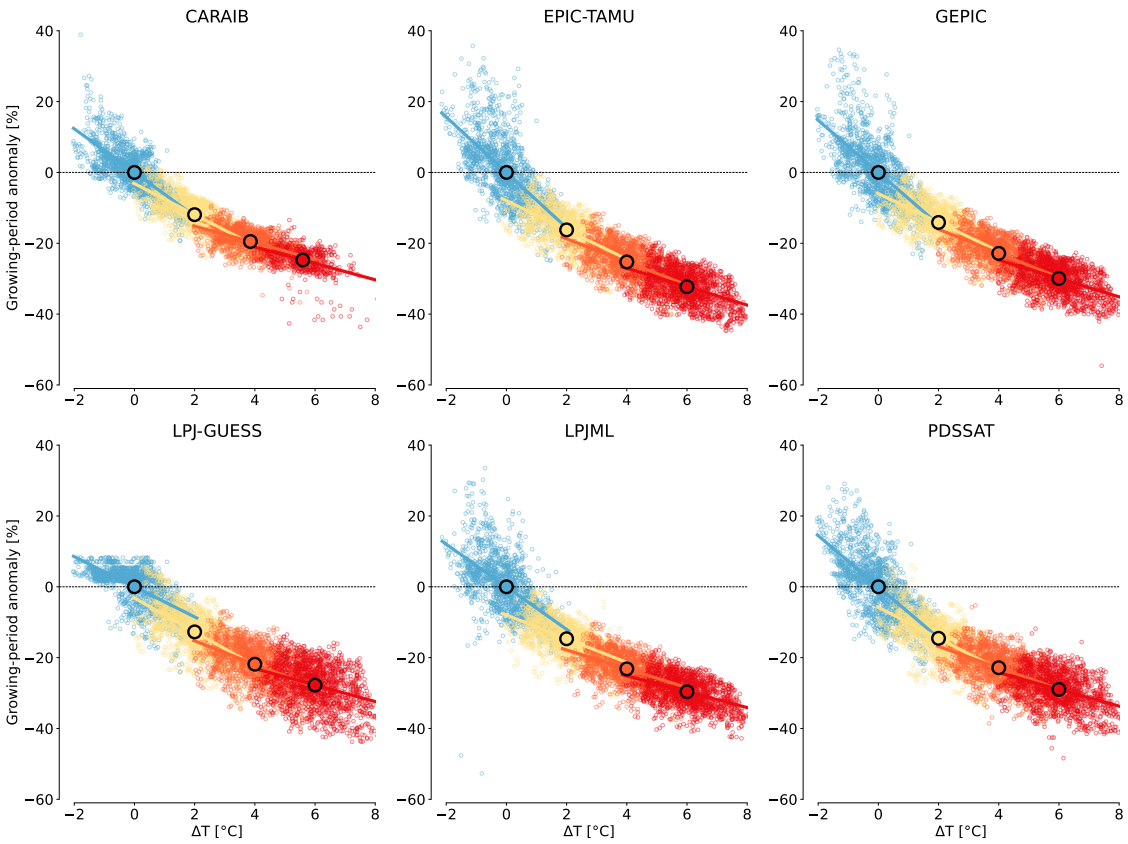

Figure S31: Growing period anomalies in the GGCMI models across warming scenarios. Scatter plots show maturity duration anomalies against growing-season temperature anomalies, both relative to historical mean values. Colors indicate model outputs across warming scenarios, from historical (blue), +2 °C (yellow), +4 °C (orange), and +6 °C (red) uniform warming. Solid colored lines show the linear behavior within each warming scenario, and large colored dots show the mean anomaly values within each scenario. GGCMI models show similar responses of maturity duration to temperature, with nonlinear losses appearing under high-warming scenarios.

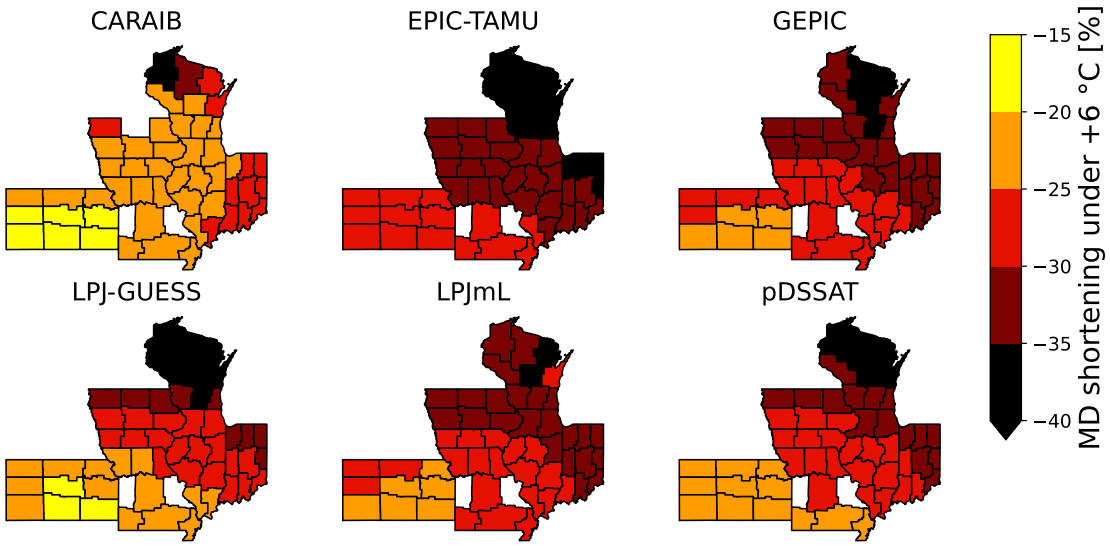

Figure S32: Mean growing period changes under high Corn Belt warming across the GGCMI models. Maps show the change in 30-year mean MD from the baseline historical scenario to a uniform +6 °C perturbation scenario without cultivar adaptation. MD changes show similar magnitude and spatial patterns across the ensemble, suggesting maturation processes are similarly rooted in the concept of heat unit accumulation

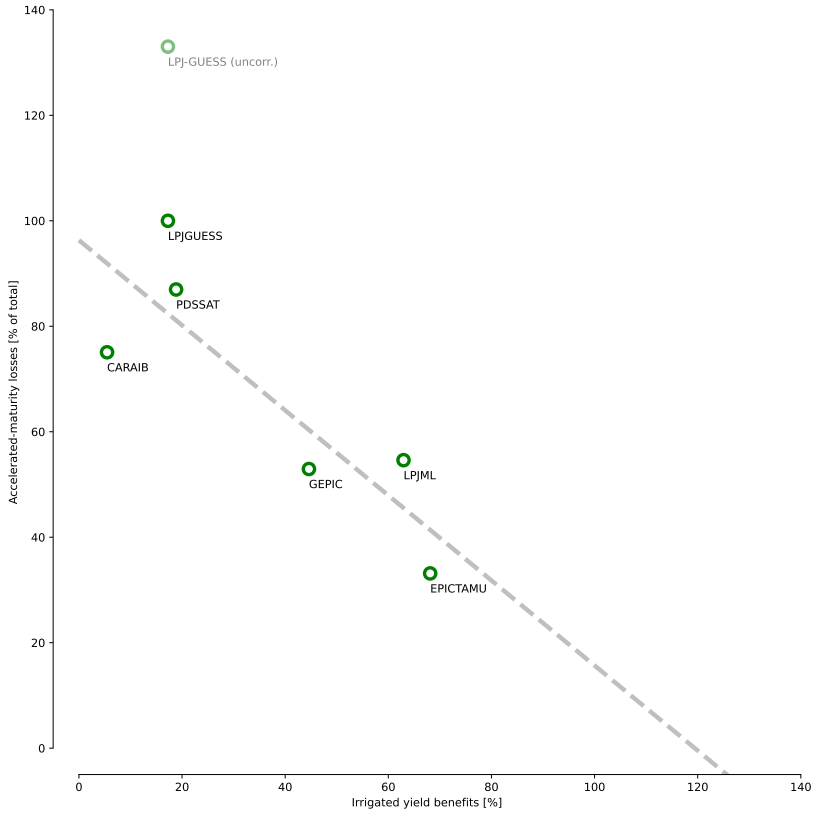

Figure S33: Comparing yield sensitivity to accelerated phenology against yield sensitivity to water stress. Scatter plot shows the portion of total yield losses under warming attributed to accelerated phenology against yield sensitivity to water stress. Yield losses due to accelerated phenology are determined by comparing yield changes under +6 °C perturbations between non-adaption and cultivar-adaptation scenarios. Water stress sensitivity values are calculated by comparing historical yield levels between rainfed and irrigated farming practices. Models with higher sensitivity to water stress show smaller portions of yield losses due to accelerated phenology, suggesting model responses to temperature increases can be roughly separated into causes of water stress and accelerated phenology.

S4 Supplemental Materials for Chapter 5

Table S4: USDA Risk Management Agency Stage Codes and Descriptions used to obtain prevented planting data. The full list of all codes, descriptions, and years activated can be found at the USDA RMA Cause of Loss website

RMA Stage Code	Code Description
H3	Prevented Planting Option 3 - Harvested Acres
NP	Prevented Planting - Insured Crop NOT Planted
P1	Prevented Planting Option 1
P2	Prevented Planting Option 2
P3	Prevented Planting Option 3
P4	Prevented Planting Option 4
PF	Prevented Planting - Unplanted Acreage with 5% buyup option
PL	Preliminary Loss Payment (GRP): Prevented Planting Endorsement (Qualifying Crop)
PT	Prevented Planting - Insured Crop Planted (Unplanted Acreage with 10% buy up option 1998)
PU	Prevented Planting - Uninsured Loss
U3	Prevented Planting Option 3 - Unharvested Acreage

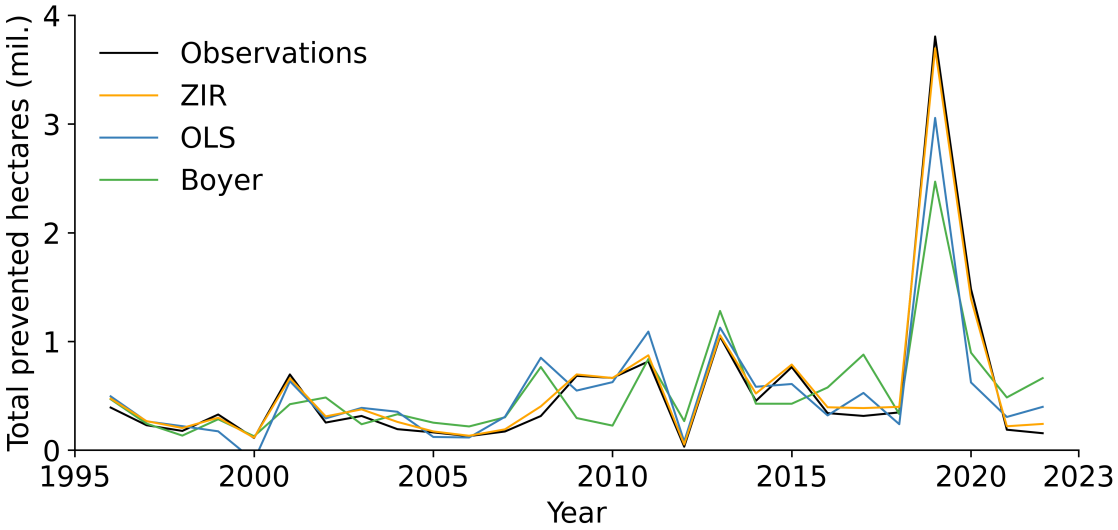

Figure S34: Historical performance of different model formulations. The line plot shows observed and predicted time series of total historical prevented acres for maize due to excess moisture/precipitation. Observations are shown in black. Predictions from the ZIR model used in this study are shown in orange. Predictions from a linear model, using the same feature set as the ZIR model, are shown in purple. Predictions from a linear model using the Boyer et al. (2023) [147] feature set are shown in green. The ZIR model can predict historical prevented planting acreage with greater proficiency than more traditional linear model structures, particularly in predicting the 2019 extreme.

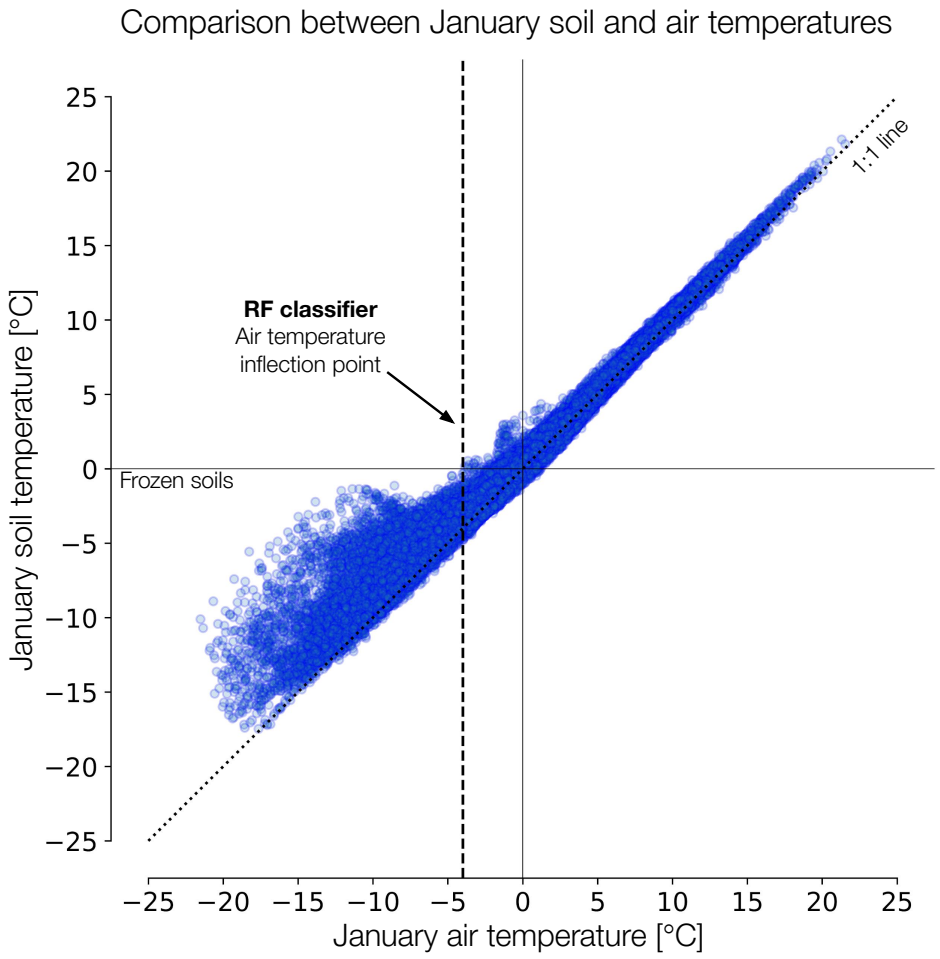

Figure S35: Mean January air and soil temperatures from FLDAS across the historical sample. The scatter plot shows January air temperature values against their corresponding soil temperature values for all county-year combinations in the historical sample. Points lying below zero on the Y-axis correspond to theoretically frozen soils. The dotted line shows a 1:1 relationship. The vertical dashed line denotes the inflection point of the Random Forest classifier's response to January air temperatures (approximately -4 °C). The model predicts air temperatures below this point to increase the likelihood of prevented planting occurrences. This air temperature value also corresponds to the freezing point for soil temperatures in FLDAS. Although the RF classifier does not take in information about soil temperatures directly, it may be inferring the freezing point of soils through its air-temperature response.

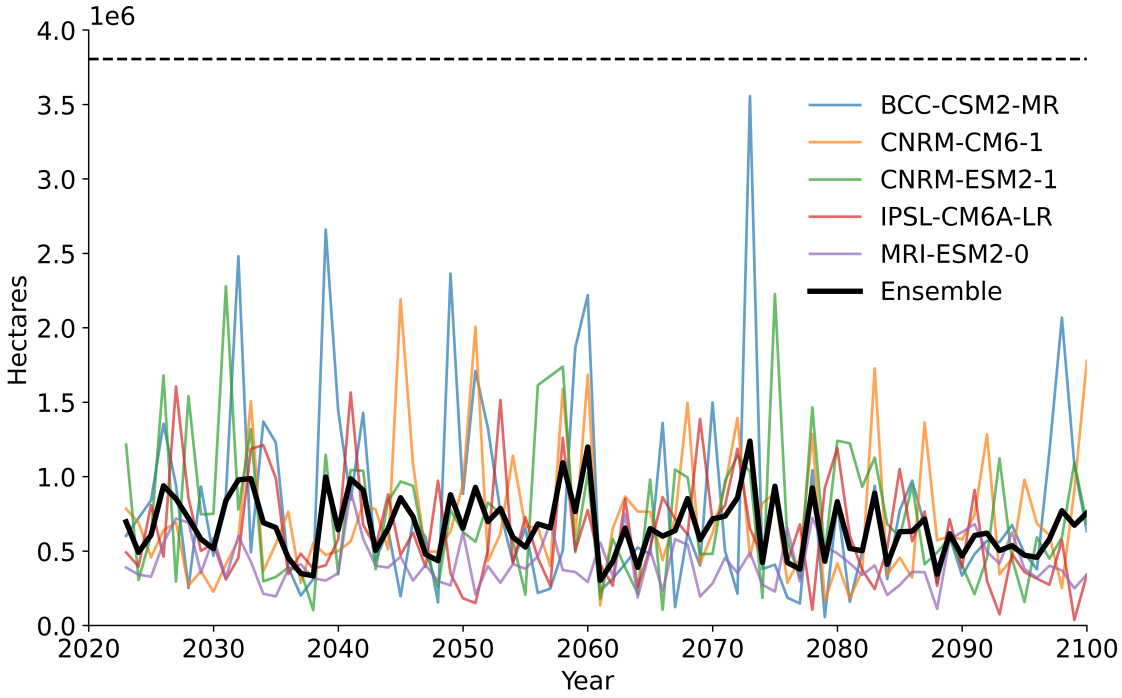

Figure S36: Projections of annual prevented planting acreage under climate change. Line plots show projections from the ZIR model for the total U.S. prevented planting area, assuming planned maize acreage constant from the 2012–2022 mean value for each county. Thin colored lines show projections corresponding to the SSP-585 scenario as modeled by each CMIP6 model. The thick black line shows the ensemble mean. The horizontal dashed line shows the total prevented area in 2019 for reference. No future projection meets or exceeds the 2019 extreme value. However, projections exceed 1 million hectares of prevented planting more frequently than the historical record.